Appendix Q
Characterization of Lake Erie Ice

ERDC/CRREL TR-16-5

US Army Corps
of Engineers®
Engineer Research and
Development Center

ERDC
INNOVATIVE SOLUTIONS
for a safer, better world

Characterization of the Lake Erie Ice Cover

Steven F. Daly

April 2016

Cold Regions Research
and Engineering Laboratory

The U.S. Army Engineer Research and Development Center (ERDC) solves the nation's toughest engineering and environmental challenges. ERDC develops innovative solutions in civil and military engineering, geospatial sciences, water resources, and environmental sciences for the Army, the Department of Defense, civilian agencies, and our nation's public good. Find out more at www.erdc.usace.army.mil.

To search for other technical reports published by ERDC, visit the ERDC online library at http://acwc.sdp.sirsi.net/client/default.

ERDC/CRREL TR-16-5
April 2016

Characterization of the Lake Erie Ice Cover

Steven F. Daly

U.S. Army Engineer Research and Development Center (ERDC)
Cold Regions Research and Engineering Laboratory (CRREL)
72 Lyme Road
Hanover, NH 03755-1290

Final Report

Prepared for Lake Erie Energy Development Corporation (LEEDCo), Cleveland, OH

Under CRADA-14-CRL-04-0, “Impacts of Ice on Offshore Wind Turbines in Lake Erie”

Abstract

The developing offshore wind energy industry in Northern Ohio is looking to place wind turbines in Lake Erie. The floating lake ice that forms in Lake Erie each winter is a very important consideration for the design of the wind-turbine towers and for the foundations sited in the lake.

This report uses historical meteorological and surface-ice thickness observations, 41 years of ice chart information, and lake-bed surveys of ice scours to estimate the characteristics of the Lake Erie ice cover important to the design of offshore wind-turbine towers. These characteristics include the expected thickness of the ice cover due to thermal growth, the historical spatial and temporal distribution of the ice cover throughout the winter season; and the estimated consolidated layer thickness and maximum keel depths of ice ridges formed in the lake. The report also describes the results of an innovative satellite-based synthetic aperture radar survey that included multi-temporal acquisitions of the lake ice cover during the winter of 2014–15. A stationary linear feature was evident in a time series of three spatially overlapping images, suggesting a grounded ice ridge. At that time of this publication, this is the first satellite-based evidence of ice ridges in Lake Erie.

Contents

Illustrations

Figures

Tables

Preface

This study was conducted for the Lake Erie Energy Development Corporation (LEEDCo) under Cooperative Research and Development Agreement (CRADA) CRADA-14-CRL-04-0, "Impacts of Ice on Offshore Wind Turbines in Lake Erie."

The work was performed by Dr. Steven F. Daly (Terrain and Ice Engineering Group, Stephen Newman, Chief), U.S. Army Engineer Research and Development Center, Cold Regions Research and Engineering Laboratory (ERDC-CRREL). At the time of publication, Timothy Pangburn was Director of the Remote Sensing and Geographic Information Systems Center of Expertise (RS/GIS CX), ERDC-CRREL. The Deputy Director of ERDC-CRREL was Dr. Lance Hansen, and the Director was Dr. Robert Davis.

Dr. Elias J. Deeb scheduled the satellite acquisitions, conducted the analysis of the satellite data, and contributed to Chapter 4. Dr. Meredith Carr assisted with the analysis of the Lake Erie ice-thickness data. Timothy B. Baldwin conducted the GIS analysis and produced all the maps included in this report. John J. Gagnon acquired and analyzed the meteorology data. All four contributors are with ERDC-CRREL. The kind assistance of Anne H. Clites, Physical Scientist, NOAA Great Lakes Environmental Research Laboratory, Ann Arbor, MI, is gratefully acknowledged.

COL Bryan S. Green was the Commander of ERDC, and Dr. Jeffery P. Holland was the Director.

Acronyms and Abbreviations

AFDD	Accumulated Freezing Degree-Days
CIS	Canadian Ice Service
CRADA	Cooperative Research and Development Agreement
CRREL	U.S. Army Cold Regions Research and Engineering Laboratory
CSR	Canadian Seabed Research
ERDC	Engineer Research and Development Center
GIS	Geographic Information System
GLERL	Great Lakes Environmental Research Laboratory
LEEDCo	Lake Erie Electrical Development Corporation
NCDC	National Climatic Data Center
NIC	National Ice Center
NOAA	National Oceanic and Atmospheric Administration
NRCS	National Resources Conservation Service
NWS	National Weather Service
RS/GIS CX	Remote Sensing and Geographic Information Systems Center of Expertise
SAR	Synthetic Aperture Radar
USACE	U.S. Army Corps of Engineers
USGS	U.S. Geological Survey

Unit Conversion Factors

Multiply	By	To Obtain
degrees (angle)	0.01745329	radians
degrees Fahrenheit	(F-32)/1.8	degrees Celsius
feet	0.3048	meters
miles (U.S. statute)	1,609.347	meters

1 Introduction

1.1 Background

The Lake Erie Energy Development Corporation (LEEDCo) is leading the way towards large-scale wind development of Lake Erie with the Ice-breaker demonstration project. The project is to be located in Lake Erie 6–8 miles offshore of Cleveland, Ohio. It will consist of five to nine turbines in approximately 60 ft of water. The floating lake ice that forms in Lake Erie each winter is a very important consideration for the design of the wind turbine towers and for the foundations sited in the lake. The ice cover has the potential to produce two different types of loading on the turbine tower. First, surface ice formed through heat transfer from the Lake Erie surface to the atmosphere can grow to be several feet thick. When driven by the winds and currents, this ice can cause steady and periodic loads on the wind-turbine tower. The second type of loading can come from ice ridges, which are formed when moving surface ice collides with stationary ice, causing the ice to pile up. The section of the ridge below the surface, called the *keel*, can extend downwards 30 m and more and can create ice gouges (or scours). The interstitial water between the ice pieces of the keel can freeze due to heat transfer to the atmosphere, creating a *consolidated layer* in the ridge. The potential ice load from a moving ice ridge colliding with a wind turbine tower can be very significant. The towers and their foundations must be designed to resist these loads. To estimate these loads, it is necessary to characterize the ice cover expected to form on Lake Erie. Therefore, this report characterizes the aspects of the Lake Erie ice cover that are important with regard to the ice loading.

1.2 Objectives

This report has four overall objectives. The first is to estimate the likely range of thickness of the surface ice that can form each winter in Lake Erie through thermal growth. The second is analyze 41 years of available ice records to describe where the ice is likely to form and when the ice is likely to be in place during the winter season. The next two objectives are concerned with ice ridge formation in the lake. There is ample indirect evidence of ice-ridge formation in Lake Erie, based on the ice scours that have been observed in the lake bed. However, there is little direct evidence of ice-ridge formation. Therefore, the third objective is to determine the

potential for using remote sensing using satellite-based synthetic aperture radar (SAR) to detect ice ridges. The fourth and final objective is to estimate the likely thicknesses of the consolidated layers and keel depths of ice ridges in Lake Erie.

1.3 Approach

Chapter 2 characterizes the thickness of the surface ice that forms through heat transfer from the Lake Erie surface to the atmosphere. This analysis used 21 meteorological stations with at least 10 years of data and then, based on the Stefan equation calibrated using ice-thickness observations, developed a model of the thermally grown ice thickness of Lake Erie as a function of the meteorological conditions. The extreme values of the annual maximum thermal ice-growth thickness were then estimated based on an extreme-value analysis of the winter conditions recorded at each meteorological station. The result is an estimate of the likelihood of a given annual maximum surface-ice thickness in each winter season.

Chapter 3 describes the spatial and temporal extent of the Lake Erie surface ice each winter. This analysis was based on 41 years of ice charts of the Lake Erie ice cover that were prepared by the Canadian Ice Service (CIS) and the National Ice Center (NIC) (NIC 2015). The geographic information system (GIS) analysis based on these records resulted in 41 years of gridded daily ice-cover information with a roughly 2 km grid cell size. The ice cover distribution of Lake Erie is strongly influenced by the lake bathymetry and the wintertime meteorological conditions, particularly the duration and magnitude of the subfreezing air temperatures and the overall wind direction and speed. These are briefly described to provide a context for the ice cover results. The gridded daily ice-cover information was used to explore the overall relationship between the maximum ice cover extent and the maximum accumulated freezing degree-days (AFDD) each winter. Next, the chapter describes the variability of the ice cover of the entire lake throughout the winter season and from year-to-year. Finally, the chapter presents maps displaying the earliest, average, and latest dates of the first and last ice each winter for each grid cell and the minimum, average, and maximum duration of ice for each grid cell.

Chapter 4 describes using satellite-based SAR to detect ice ridges. The U.S. Army Cold Regions Research and Engineering Lab (CRREL) tasked a commercial radar satellite (TerraSAR-X) to acquire imagery over Lake Erie

during February and March 2015. Based on the time series of satellite images acquired offshore Erie, PA, a linear feature potentially representing an ice ridge was immediately apparent in each of the images. Over the 33-day period that spanned the three satellite acquisitions, this location of this feature did not move while ice surrounding this linear feature had moved.

Chapter 5 estimates the consolidated layer thickness and maximum keel depths of ice ridges formed in Lake Erie. There is conclusive evidence that ice ridges form in Lake Erie and that their keels can be 25 m deep or more. Most of the evidence is indirect and consists of ice scours in the lake bed that were created by the keels of ice ridges in contact with the bed. The available lake bed survey information was analyzed in Chapter 5 to provide water depth information on 210 ice scours. Based on the historical ice-cover duration (described in Chapter 3) and meteorological conditions (described in Chapter 2), Chapter 5 characterized the thickness of the consolidated layers of ice ridges. An estimate of the maximum keel depths of the ice ridges in Lake Erie was developed in Chapter 5 based on a relationship between the surface ice thickness and the maximum possible keel depths that have been observed for ocean ice ridges. This study modified the relationship to account for the difference is strength between sea ice and the freshwater ice of Lake Erie. The relationship was further tuned by comparing the results to the water depths in which the ice scour depths were observed. The water depth provides information on the approximate depth of the bottom of the ice-ridge keels that created the scours, given that the actual scour indentation into the bed were usually much less than 1 m. The likely range of the ice ridge keel depth was then characterized based on this approach.

2 Surface-Ice Thickness

2.1 Introduction

This chapter presents estimates of the extreme values of the thermally grown surface-ice thickness based on the Lake Erie meteorological conditions. The analysis used 21 meteorological stations—located in all the states surrounding Lake Erie (Michigan, Ohio, Pennsylvania, and New York) and in the Canadian Province of Ontario—that are still producing information and that provide at least ten years of data. This study calculated the AFDD for each station over its period of record and then analyzed the available Lake Erie ice-thickness measurements. Each measurement location was matched with the closest meteorological station where AFDD were available on the dates the measurements were made. Subsequently, a model, based on the Stefan equation, of the thermally grown ice thickness of Lake Erie as a function of the AFDD was then developed. Extreme values of the annual maximum thermal ice-growth thickness were estimated based on an extreme-value analysis of the annual maximum series of the AFDD recorded at each station. The result was an estimate of the likelihood of a given annual maximum surface-ice thickness. Finally, this chapter presents the extreme-value analysis of the annual maximum surface-ice thickness for Lake Erie in the vicinity of Cleveland, OH. This is the proposed location for the LEEDCo offshore wind turbine towers.

2.2 Estimating the accumulated freezing degree-days

Information on the winter conditions in the Lake Erie region was provided by The National Oceanic and Atmospheric Administration's (NOAA) Global Summary of the Day data set from the National Climatic Data Center (NCDC) (NOAA 2015). This data set uses meteorological information collected at first-order National Weather Service (NWS) stations. All the stations within 82 km (50 miles) of the shoreline of Lake Erie (Figure 1), about 96 stations, were reviewed in this study for length of record and completeness. The first step in the analysis was to use recorded air temperature to estimate the AFDD for each station for each year that information was available.

Figure 1. Meteorological stations in the NCDC database in the vicinity of Lake Erie.

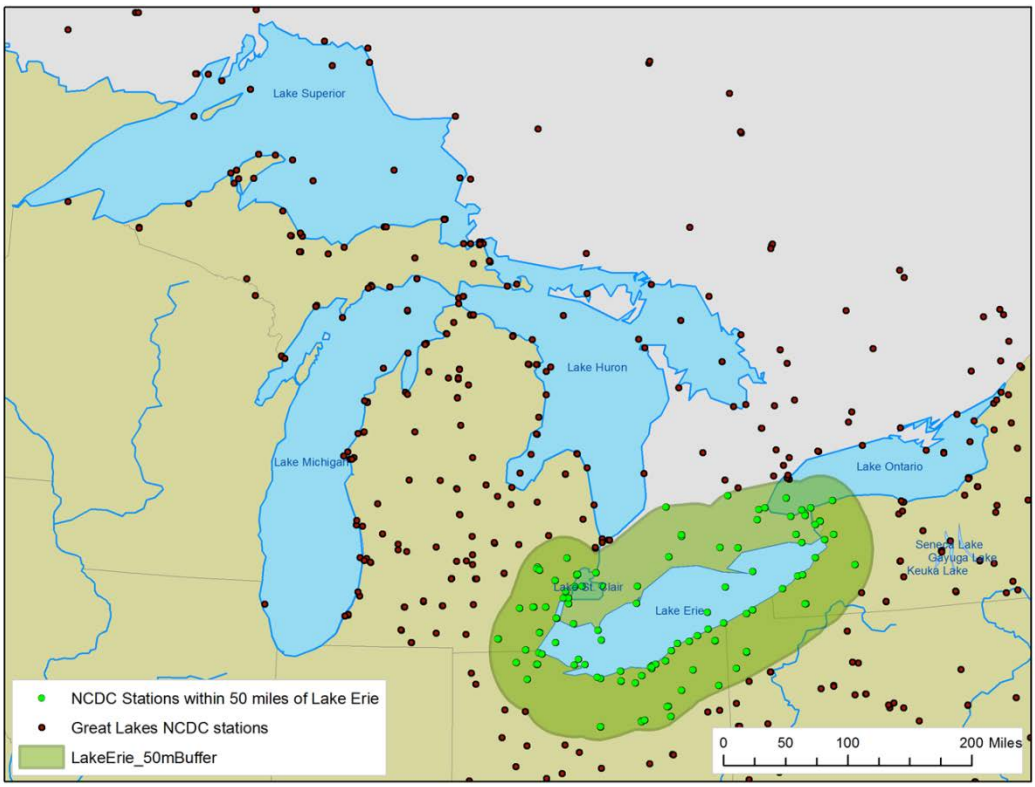

To start the analysis, the average daily air temperature was estimated over each station's period of record based on the daily maximum and minimum air temperatures. If either a maximum or minimum was missing, then the average temperature was considered missing for that day.

The AFDD were estimated for the period of record for each station based on the estimated average daily air temperature. The AFDD for each station was set to zero on the first day of August of each year and was allowed to accumulate from that point onward. The AFDD on any day of the winter season, $AFDD_n$, represents the accumulated difference between freezing and the average daily temperature since 1 August.

$$AFDD_n = \sum_{i=1}^{n} \left(T_m - T_i\right) \quad \text{for} \quad \left(T_m - T_i\right) > 0 \tag{1}$$

where

n = the number of days since 1 August;
T_i = the average daily temperature on day i; and
T_m = the ice/water equilibrium temperature (0°C).

Note that if the average daily temperature is greater than T_m, the difference is ignored and the AFDD does not change for that day.

The annual maximum AFDD, $AFDD_{max}$, for each winter was then found as the maximum of the AFDD accumulated over the course of the winter season. Generally, the annual maximum AFDD was reached in March or April. If daily average temperature was missing for more than 7 days over the course of the winter, $AFDD_{max}$ was set to "missing" for the entire winter season.

Each station was placed into one of four groups based on the AFDD record:

Group A stations had at least 10 years of data and were operating through 2014. In this group, $AFDD_{\max}$ was estimated in over 91% of the years for which the stations were operational. There were 21 stations in Group A.

Group B stations had less than 10 years of data and were also operating through 2014. There were 18 stations in Group B.

Group C stations had more than 10 years of data and had stopped producing data before 2014. There were 10 stations in Group C.

Group D stations had less than 10 years of data and had stopped producing data before 2014. There were 19 stations in Group D.

Figure 2 shows the locations of the stations around Lake Erie. After reviewing the results, this study used only the stations included in Group A (Table 1). Table 1 also lists the average annual maximum, $\overline{AFDD}_{\max}$, found by averaging $AFDD_{max}$ over all the years in the period of record, for each station (Figure 3). The average annual maximum AFDD is fairly consistent for all the stations near Lake Erie.

The average annual maximum for Lake Erie as a whole was found by averaging $AFDD_{max}$ for all the stations each winter. Figure 4 shows the time series of these results along with the annual range of the AFDD values, determined as the standard deviation around the mean each winter.

Figure 2. Meteorological stations around Lake Erie. The study included only the stations in Group A.

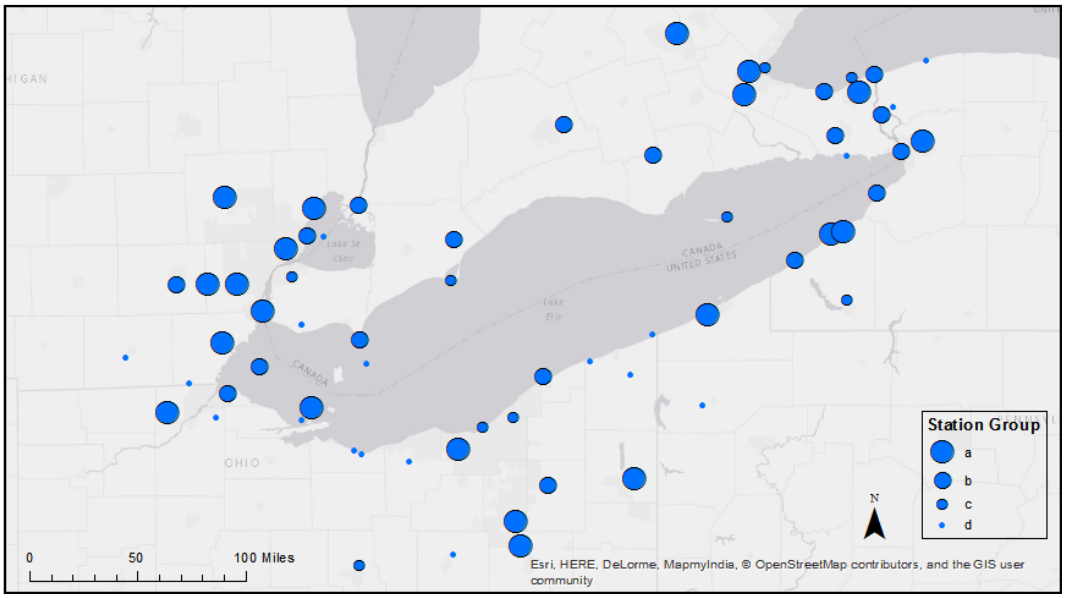

Table 1. Stations used to estimate AFDD for Lake Erie.

State/ Province	Station	Start Year	Final Year	Years with Data	$\overline{AFDD}_{max}$ (°C-Days)	$\overline{AFDD}_{max}$ (°F-Days)
MI	SELFRIDGE_ANGB	1961	2014	54	392	706
NY	GREATER_BUFFALO_INT	1961	2014	52	418	753
OH	YOUNGSTOWN_MUNI	1961	2014	45	371	668
MI	DETROIT_CITY	1974	2014	41	324	584
MI	DETROIT_METROPOLITA	1974	2014	41	374	673
OH	AKRON_AKRON-CANTON	1974	2014	41	335	603
OH	CLEVELAND	1974	2014	41	308	554
OH	TOLEDO_EXPRESS	1974	2014	41	386	694
PA	ERIE_INTL_AIRPORT	1974	2014	41	318	572
MI	WILLOW_RUN	1974	2014	26	415	747
MI	OAKLAND_CO_INTL	1976	2014	24	446	804
ON	NIAGARA_DISTRICT	1985	2014	30	339	610
NY	DUNKIRK	1987	2014	24	285	513
OH	SOUTH_BASS_ISLAND	1987	2014	16	287	517
ON	HAMILTON_AIRPORT	1994	2014	21	477	859
ON	KITCHENER_WATERLOO	1994	2014	21	572	1030
MI	GROSSE_ILE_MUNI	1999	2014	15	296	533
MI	CUSTER	2000	2014	15	332	597
NY	CHAUTAUQUA_CO_DUNKIR	2000	2014	15	334	600
OH	AKRON_FULTON_INTL	2001	2014	13	333	600
ON	HAMILTON_RBG_CS	2005	2014	10	472	850

Figure 3. The average annual maximum AFDD for each station.

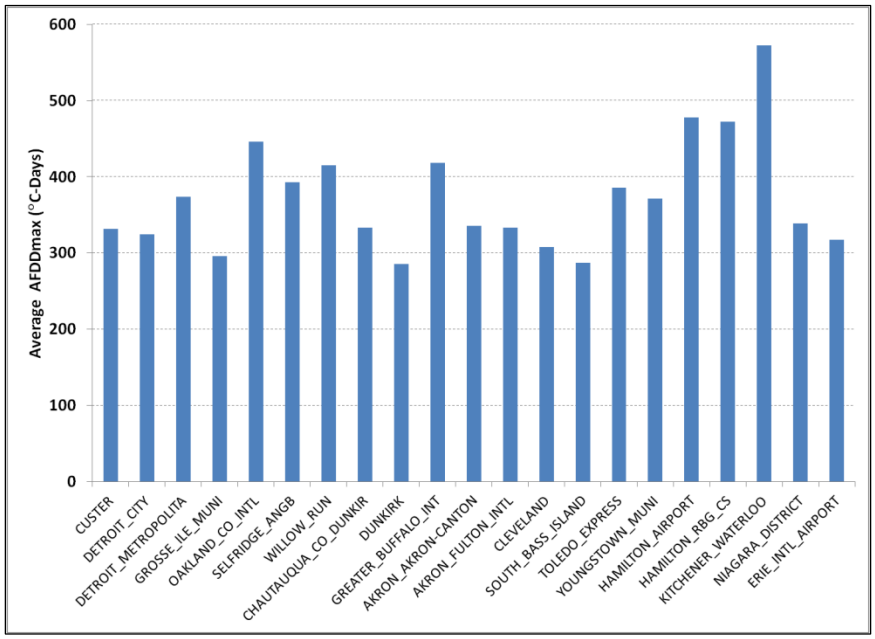

Figure 4. Annual Maximum AFDD for Lake Erie.

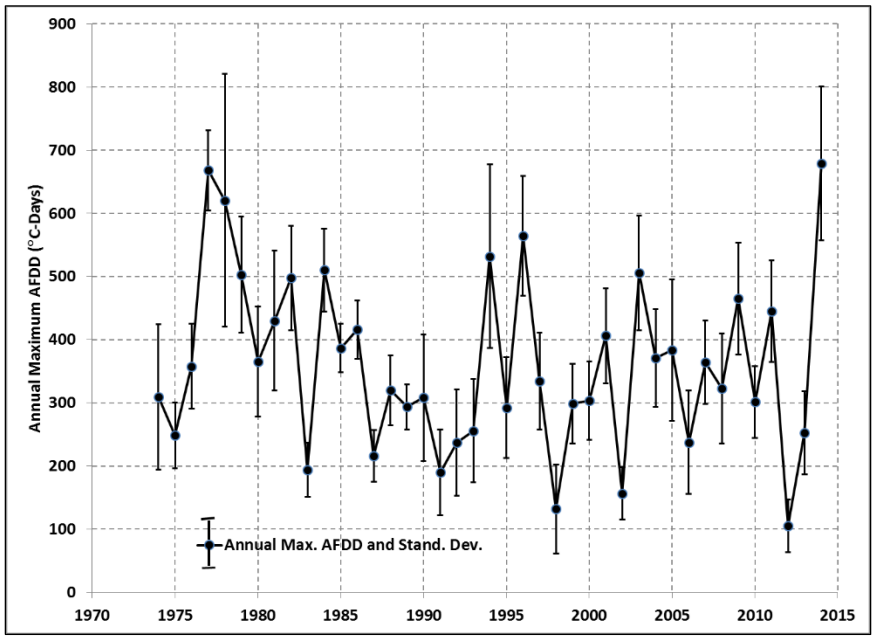

2.3 Ice thickness

2.3.1 Background

The origins of modeling thermal ice growth are generally credited to Josef Stefan (1891) who analyzed ice growth as a moving boundary problem with the growth rate controlled by thermal conduction through the ice.

The Lake Erie analysis starts with the knowledge that surface ice grows on only the bottom of the ice sheet and also assumes that there is no net heat transfer from the ice to the water. The rate of growth of the ice thickness, η, is thus

$$\frac{\partial \eta}{\partial t} = \frac{F_c}{\rho_i \lambda_i} \tag{2}$$

where

t = time;
F_c = the heat flux from the bottom of the ice cover to the surface of the ice cover;
ρ_i = the ice density; and
λ_i = the latent heat of fusion of the ice.

Extensions and modifications to Stefan's original analysis have been applied to a wide variety of phase-change problems (see for example Carslaw and Jaeger 1959 and Crank 1984). Stefan and "sundry authors later" (see Ashton 1986 for an example) used a physical approximation to obtain the solution for the limiting case of very large latent heat compared to the heat capacity of the solid. This approximation, particularly relevant to ice, assumes that behind the slowly moving solidification boundary, the temperature distribution is equivalent to the steady-state distribution that would occur if the boundary were to be fixed in position at that instant (Crank 1984). This approach, variously referred to as the "quasi-steady," "pseudo steady state," "linear temperature profile," or "zero heat capacity" model, is widely used in the field of ice engineering and has seen considerable application for estimating ice thickness through thermal growth. While arrived at through a physical approximation, the quasi-steady approach is a solution to the complete heat conduction equation, albeit a limiting case. Using this approach, the heat flux from the bottom of the ice sheet is

$$F_c = k_i \frac{\left(T_m - T_s\right)}{\eta} \tag{3}$$

where k_i = the thermal conductivity of the ice. Combining Equations (2) and (3),

$$\frac{\partial \eta}{\partial t} = \frac{k_i}{\rho_i \lambda_i} \frac{\left(T_m - T_s\right)}{\eta}. \tag{4}$$

Previous investigators coupled the quasi-steady approach with a variety of boundary conditions. The most direct approach is to assume that the temperature of the upper surface of the ice cover is equal to the air temperature. Making this assumption and integrating Equation (4) leads to the classic result that the ice thickness during growth is proportional to the square root of the AFDD (Ashton 1986; USACE 2006):

$$\eta = \alpha \sqrt{AFDD_n - AFDD_0} \tag{5}$$

where

$AFDD_n$ = the AFDD recorded during the winter up to day n; and
$AFDD_0$ = the number of AFDD recorded before any ice is observed.

The coefficient α, which is theoretically equal to

$$\alpha = \sqrt{\frac{2k_i}{\rho_i \lambda_i}}, \tag{6}$$

is in practice always less than this theoretical value. In fact, α is generally treated as a coefficient that can vary depending on the location, with variations caused by wind conditions, exposure, and the depth and density of any snow cover (Daly 1998). Typical ice-cover conditions that can cause α to vary include “windy lake with no snow,” “average lake with snow,” “average river with snow,” and “sheltered small river” (USACE 2006).

2.3.2 Ice-thickness estimation for Lake Erie

Estimates of the value of α for Lake Erie ice growth used the available contemporaneous observations of ice thickness and AFDD. In general, measurements of ice thickness are very rare in the United States. Fortunately, Sleator (1978) compiled measurements of ice thickness in the Great Lakes for 1965 through 1977. These observations were collected under a program

implemented by the U.S. Lake Survey* starting in winter 1965–66. An archive of these observations is available at the National Snow and Ice Data Center (Sleator 1995). There are a total of 183 measurements of Lake Erie at 6 separate locations (Table 2 and Figure 5). The measurements were made "at least 50 m off shore, preferably in deep water, and free from obstructions that might cause unusual snow drifts. Docks, mouths of rivers and streams, industrial discharge areas, and other areas likely to have unusual ice conditions were to be avoided. Once the site was selected, all of the weekly measurements were made on undisturbed ice as close to the original measurement site as possible" (Sleator 1978). Holes were hand drilled through the ice and a rule was used to measure the ice thickness.

Table 2. Ice-thickness observation locations.

Location Number	Location	Number of Observations	Dates	NCDC meteorological station
403	RONDEAU HARBOR	31	1968–1970	Cleveland Airport
404	LONG POINT BAY	20	1969–1970	Erie Intern. Airport
405	FORT ERIE	8	1969	Greater Buffalo Airport
406	BUFFALO HARBOR	58	1969–1976	Greater Buffalo Airport
407	DELAWARE LAKE-BUFFALO	11	1968–1969	Greater Buffalo Airport
408	MARBLEHEAD-CATAWBA ISLAND	55	1970–1977	Toledo Airport

Figure 5. Locations of ice-thickness measurements (data from Sleator 1978).

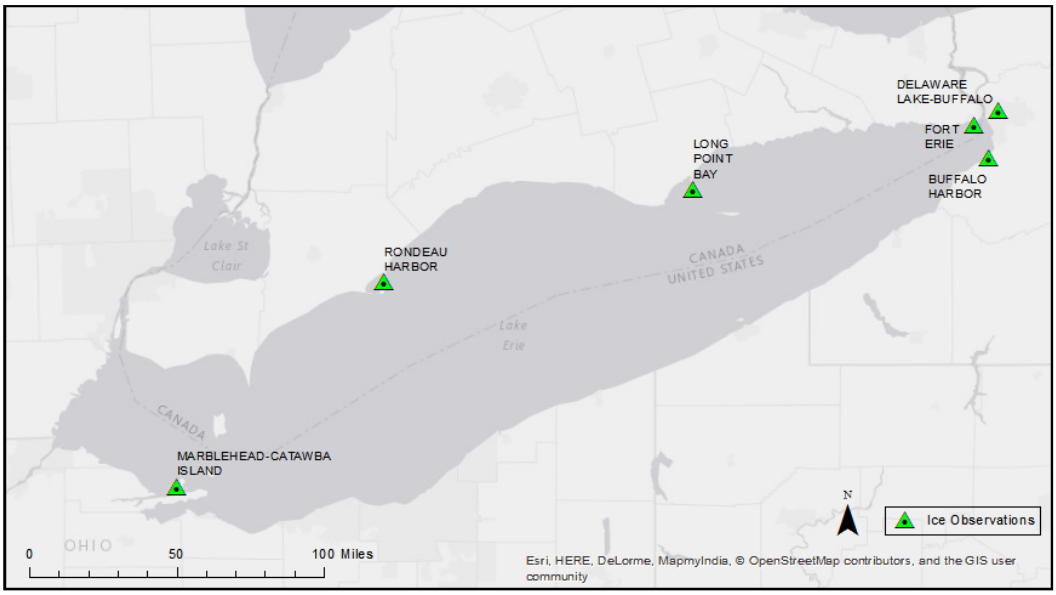

* The U.S. Lake Survey was a part of the U.S. Army Corps of Engineers. It was phased out in 1976 and was split between the Detroit District of the Corps and NOAA.

For each observation, an ice condition code was entered describing the conditions of the ice layers, snow cover, ice, and events for each measurement, along with measurements of the lake ice thickness, snow ice thickness, and total thickness. Most relevant to this study are the ice condition codes listed in Table 3. An ice condition code was included with most of the measurements (Figure 6).

Table 3. Ice condition codes.

Value	Description
1	Thaw Holes
2	Windrowed
3	Puddled
4	Flooded
5	Cracked
6	Dry
7	Solid
8	Melting
9	Candled
10	Piled on Shore
11	Broken

Figure 6. Ice conditions of measurements based on ice condition codes.

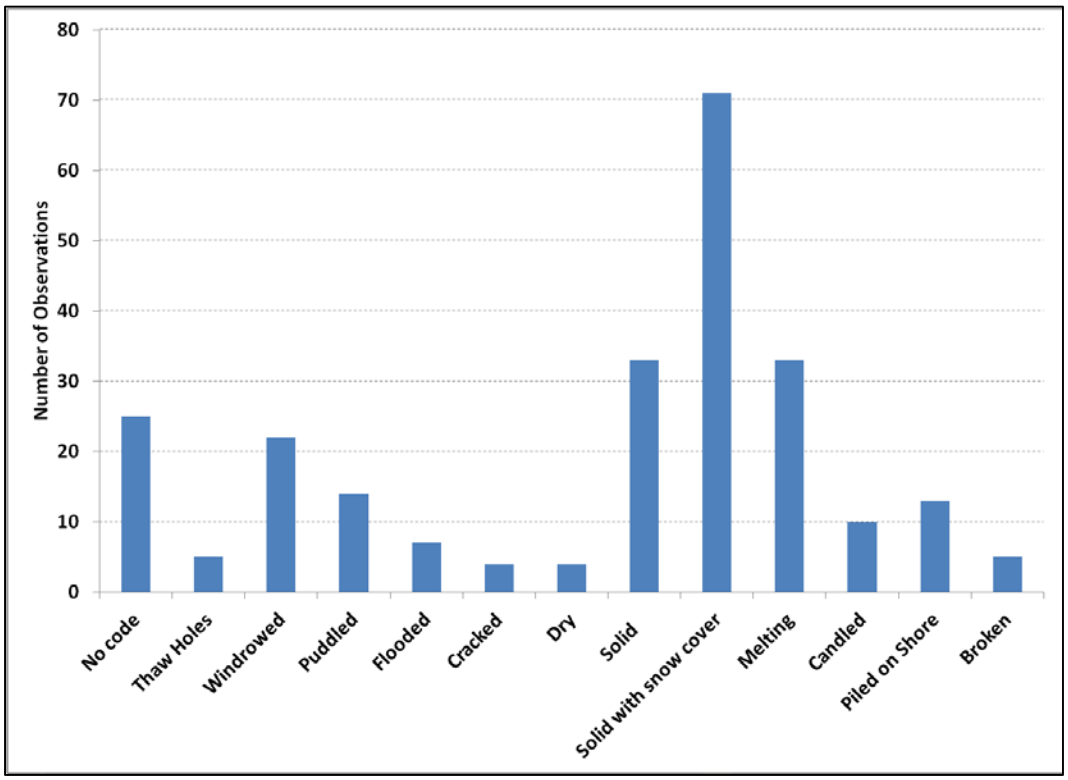

Figure 6 shows the number of measurements with each specific ice code. (Some measurements had more than one code assigned). The current Lake Erie study is most interested in measurements with "Solid" and "Solid with snow cover" codes and assumes that the "Solid" designation reflects conditions with no snow. These codes are most likely to reflect ice thickness that has resulted from thermal growth and has not undergone melting or movement by winds and currents.

Each measurement location, shown in Figure 5, was matched with the closest NCDC meteorological station where AFDD were available on the dates of the measurements (Table 2). Figure 7 shows the measurements coded as "Solid" and "Solid with snow cover" plotted against the AFDD recorded on the measurement date. Also shown in Figure 7 is Equation (5) with the parameter values listed in Table 4. These parameter values were developed by fitting Equation (5) to the data for "Solid" ice-thickness measurements so that the values would provide a reasonable upper bound for ice-thickness measurements. Note that the "Solid with snow cover" measurements generally fall below the limit provided by Equation (5).

Figure 7. Ice thickness and AFDD for all locations. Only measurements with "Solid" and "Solid with snow cover" codes are plotted. The *black line* is Equation (5).

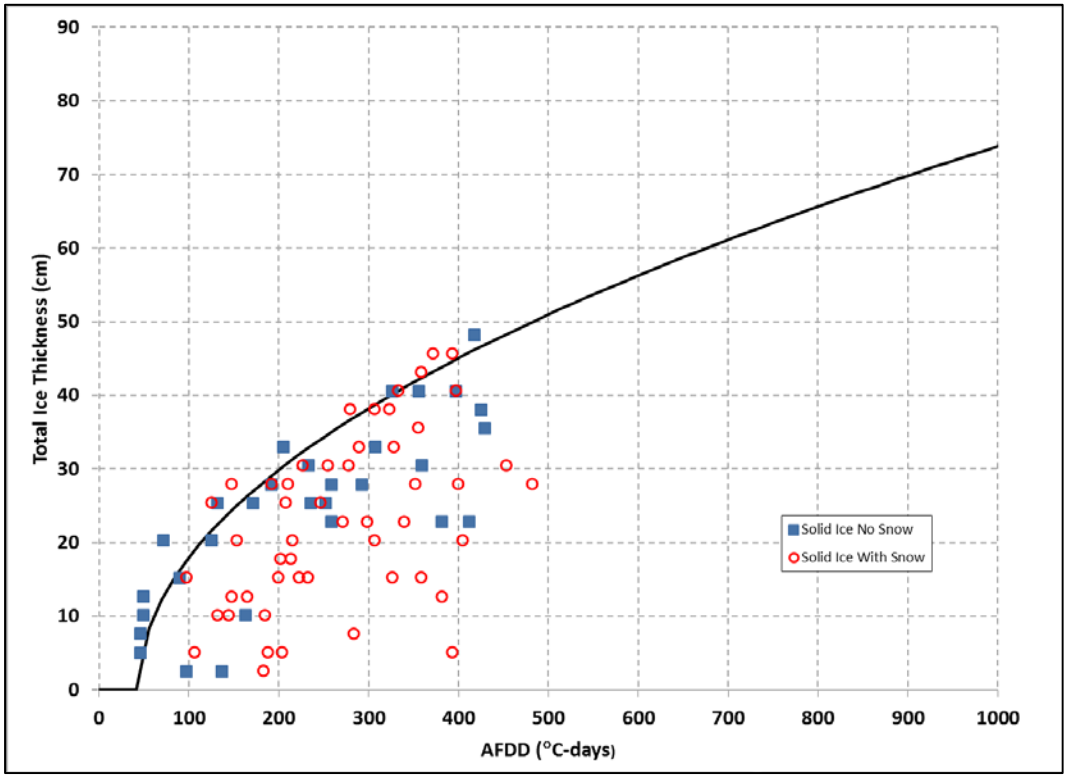

Table 4. Parameter values for the Lake Erie Stefan equation in Equation (5).

Parameter	Value
α	2.39
$AFDD_0$	43.4

In theory, the impact of the snow cover on the ice growth could be taken into account if the date when the snow fell was known; however, it is not. If the snowfall occurred immediately before the ice-thickness measurement was made then the presence of snow may not have had much influence on the ice thickness measured. In fact, a number of the "Solid with snow cover" measurements fall along the thicknesses estimated by Equation (5), suggesting that these measurements were made soon after the snowfall occurred. However, the majority of the "Solid with snow cover" measurements fall far below the thicknesses estimated by Equation (5), suggesting that in these cases the snow had been in place on the ice for some time and had impacted the ice growth.

Figure 8 shows all the measurements coded as "Solid" by location. The ice thickness model of Equation (5) with the parameter values listed in Table 4 is displayed as the black line. Equation (5) provides a reasonable estimate of the measured ice thickness at all the station locations.

Figure 9 shows all of the measurements by location regardless of the code. The ice-thickness model of Equation (5) with the parameter values listed in Table 4 provides an upper bound to all the ice measurements. The two measurements that were considerably above the estimate of Equation (5) are both coded "windrow," which suggests that the ice thickness in these cases was influenced by wind-driven ice pileup and do not reflect thermal ice growth.

Figure 8. Ice thickness and AFDD shown by location. Only measurements with a "Solid" code are plotted. The *black line* is Equation (5).

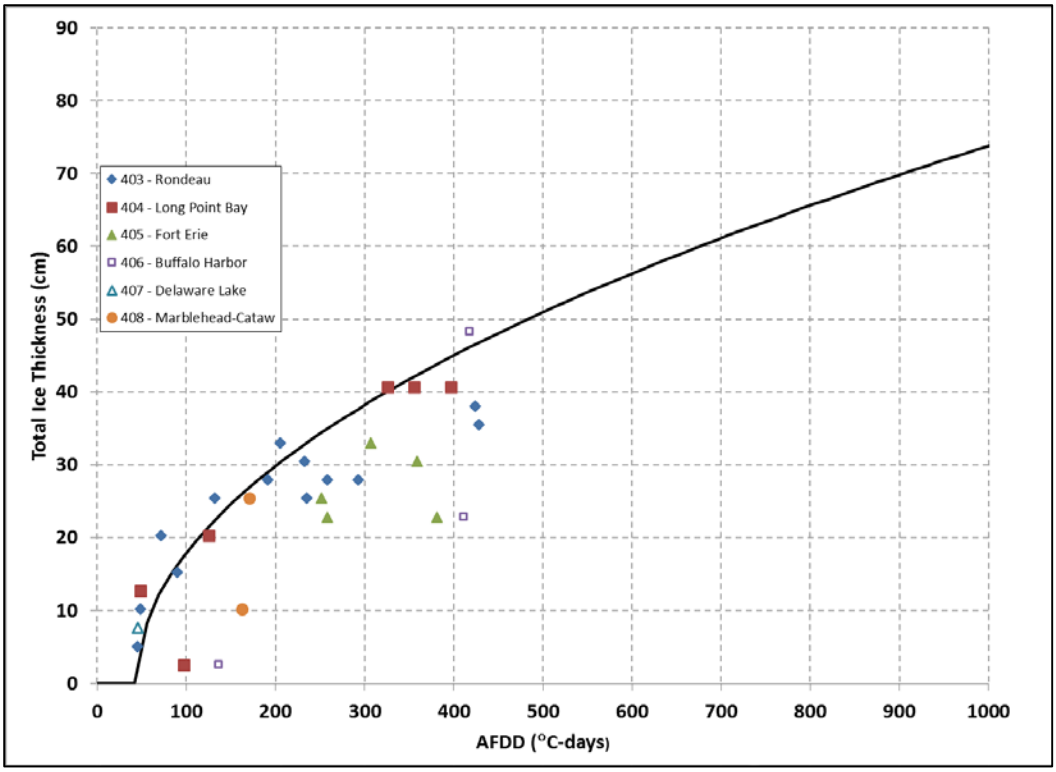

Figure 9. Ice thickness and AFDD shown by location for all measurements regardless of code. The *black line* is Equation (5).

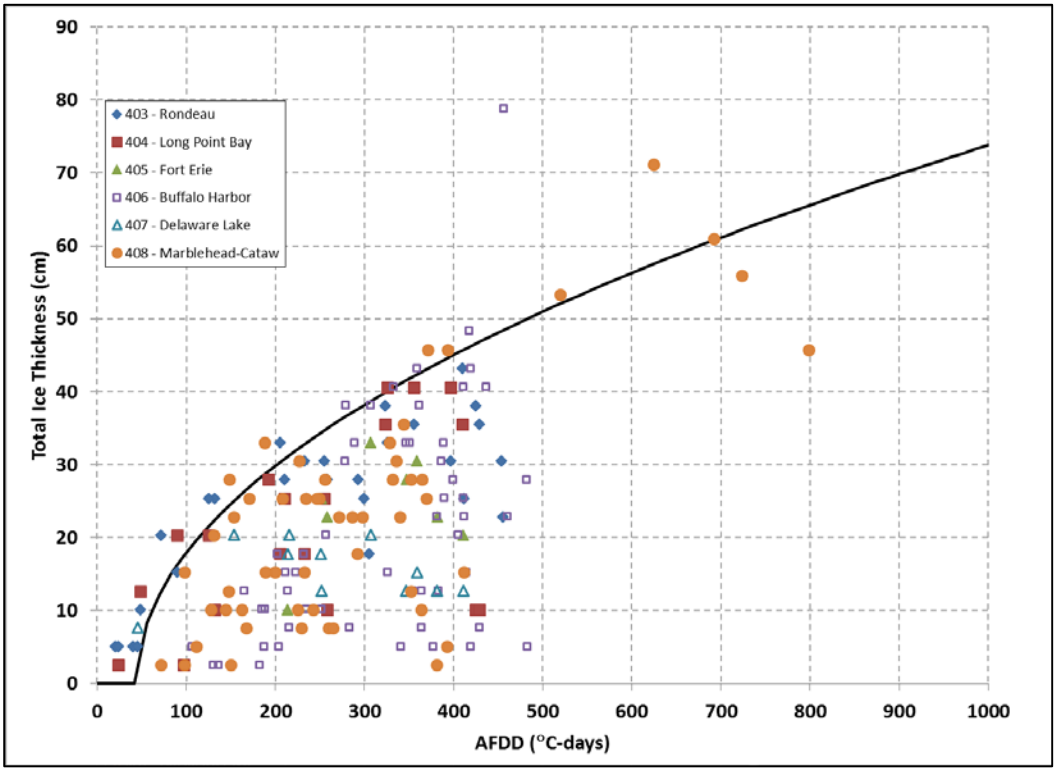

2.4 Extreme-value analysis of annual maximum surface-ice thickness

This section estimates the extreme values of the annual maximum surface ice thickness based on an extreme-value analysis (assuming a lognormal distribution) of the annual maximum series of the AFDD recorded at each station listed in Table 1. The method of moments was used to fit the lognormal distribution to the annual maximum series in the HEC-SSP Program (USACE 2010) by using the procedures described in Bulletin #17B (USGS 1982). The Weibull plotting positions were used and the computed probability found. The threshold procedure described in Bulletin #17B was used to detect outliers, which were all for anomalously warm winters with relatively low values of AFDD. These outliers were not included in the analysis. The overall results are shown in Figure 10 and are listed in Table 5. Appendix A shows the fitted distributions. In general, the results are consistent around Lake Erie with a tendency for higher values of AFDD in the north (Ontario, Canada). There is no one station that stands out particularly.

Figure 10. AFDD with return periods of 10, 20, 50, and 100 years.

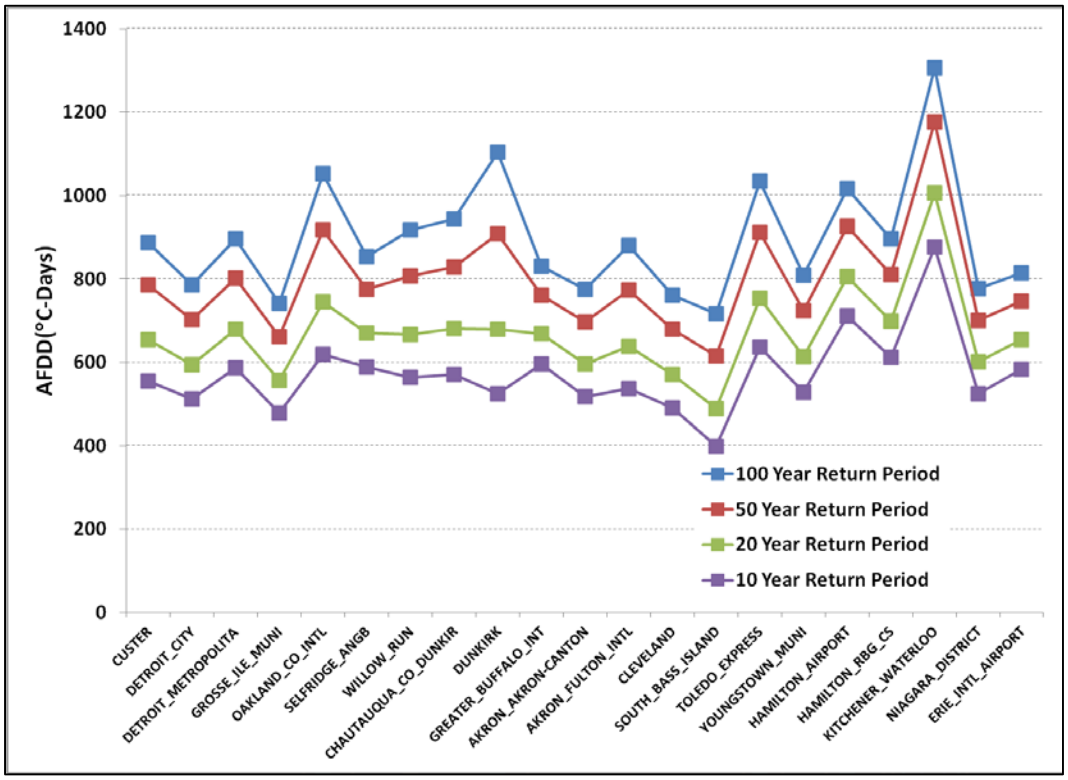

Table 5. Extreme values of AFDD (°C-days).

State/ Province	Station	Return Period (years)			
		100	50	20	10
		Annual Chance Exceedance (%)			
		1	2	5	10
MI	CUSTER	887	785	654	556
MI	DETROIT_CITY	786	703	595	512
MI	DETROIT_METROPOLITA	895	802	680	587
MI	GROSSE_ILE_MUNI	741	661	556	478
MI	OAKLAND_CO_INTL	1053	917	745	619
MI	SELFRIDGE_ANGB	854	775	670	589
MI	WILLOW_RUN	917	808	668	564
NY	CHAUTAUQUA_CO_DUNKIR	944	828	680	571
NY	DUNKIRK	1103	909	679	524
NY	GREATER_BUFFALO_INT	830	761	669	596
OH	AKRON_AKRON-CANTON	775	697	595	517
OH	AKRON_FULTON_INTL	880	774	638	538
OH	CLEVELAND	761	679	572	491
OH	SOUTH_BASS_ISLAND	717	616	489	399
OH	TOLEDO_EXPRESS	1035	912	753	636
OH	YOUNGSTOWN_MUNI	809	724	613	529
ON	HAMILTON_AIRPORT	1017	927	806	712
ON	HAMILTON_RBG_CS	896	811	698	611
ON	KITCHENER_WATERLOO	1306	1177	1007	876
ON	NIAGARA_DISTRICT	777	701	601	524
PA	ERIE_INTL_AIRPORT	814	746	655	583

Equation (5) was used to estimate the extreme values of the thermal ice thickness by using the extreme values of AFDD and the parameters in Table 4. The overall results are listed in Table 6 and shown in Figure 11. As with the AFDD results, the ice-thickness results are consistent around Lake Erie with a tendency for greater thickness in the north (Ontario, Canada). Again, there is no one station that stands out particularly.

The proposed location for offshore wind turbine towers is in the vicinity of Cleveland, OH. The extreme-value analysis of the annual maximum surface-ice thickness for Lake Erie at this location is taken directly from Figure 11 and is listed in Table 7

Table 6. Extreme values of ice thickness (cm).

State/ Province	Station	Return Period (years)			
		100	50	20	10
		Annual Chance Exceedance (%)			
		1	2	5	10
MI	CUSTER	69	65	59	54
MI	DETROIT_CITY	65	61	56	52
MI	DETROIT_METROPOLITA	70	66	60	56
MI	GROSSE_ILE_MUNI	63	59	54	50
MI	OAKLAND_CO_INTL	76	70	63	57
MI	SELFRIDGE_ANGB	68	65	60	56
MI	WILLOW_RUN	70	66	60	54
NY	CHAUTAUQUA_CO_DUNKIR	72	67	60	55
NY	DUNKIRK	78	70	60	52
NY	GREATER_BUFFALO_INT	67	64	60	56
OH	AKRON_AKRON-CANTON	65	61	56	52
OH	AKRON_FULTON_INTL	69	64	58	53
OH	CLEVELAND	64	60	55	50
OH	SOUTH_BASS_ISLAND	62	57	50	45
OH	TOLEDO_EXPRESS	75	70	64	58
OH	YOUNGSTOWN_MUNI	66	62	57	53
ON	HAMILTON_AIRPORT	74	71	66	62
ON	HAMILTON_RBG_CS	70	66	61	57
ON	KITCHENER_WATERLOO	85	80	74	69
ON	NIAGARA_DISTRICT	65	61	56	52
PA	ERIE_INTL_AIRPORT	66	63	59	55

Figure 11. Thermal ice thickness with return periods of 10, 20, 50, and 100 years.

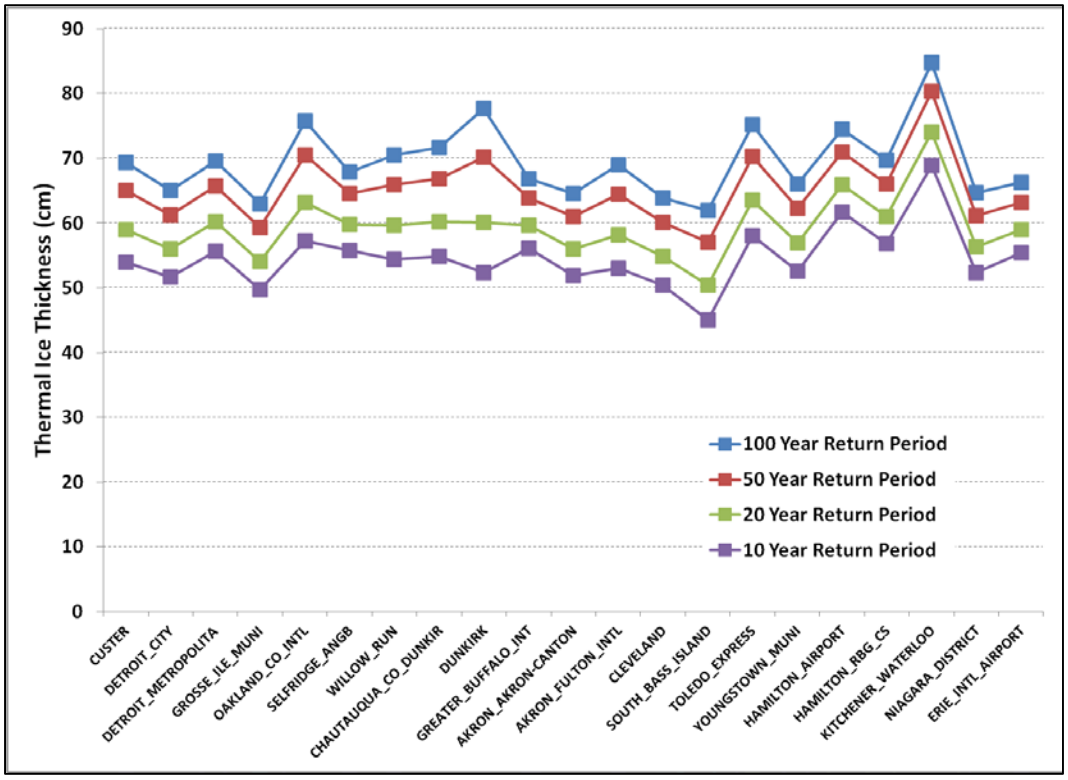

Table 7. Annual maximum surface-ice thickness at Cleveland, OH

Annual Chance Exceedance (%)	Return Period (years)	Thickness (cm)	*AFDD* (°C-Days)
1	100	64	761
2	50	60	679
5	20	55	572
10	10	50	491

2.5 Summary

The floating lake ice that forms in Lake Erie each winter is a very important consideration for the design of the wind turbine towers and foundations. Surface ice forms through heat transfer from the Lake Erie surface to the atmosphere. The ice can caused steady and periodic loads on the wind turbine tower when it is driven by the winds and currents. In this chapter, the extreme values of the thermally grown surface-ice thickness were estimated based on the Lake Erie meteorological conditions.

This analysis used 21 meteorological stations that are still producing information and that provide at least ten years of data. These stations are located in all the states surrounding Lake Erie (Michigan, Ohio, PA, and New York) and in the Canadian Province of Ontario. The AFDD were calculated for each station over its period of record.

The study then developed a model (Stefan equation) of the thermally grown ice thickness of Lake Erie as a function of the AFDD based on the available ice-thickness measurements. The extreme values of the annual maximum thermal ice-growth thickness were estimated based on an extreme-value analysis of the annual maximum series of the AFDD recorded at each station.

As the proposed location for offshore wind turbine towers is in the vicinity of Cleveland, OH, this study determined the extreme-value analysis of the annual maximum surface-ice thickness for Lake Erie at this location.

3 Ice-Cover Statistics

3.1 Introduction

This chapter describes the extent and distribution of the Lake Erie ice cover based on a 41-winter digital ice-cover data set (1973–2013). This data set was available in in three groups that covered 1973–2002, 2003–2006, and 2007–2013*. All the data were extracted from ice charts developed by CIS and NIC (NIC 2015). The current study processed this data so that the information was all in a common projection and grid cell size. The grid cells were interpolated in time to arrive at a daily estimate of the fraction of each grid cell that was covered by ice for each winter season.

The first part of this chapter describes the digital ice-cover data sets and the processing done to put the data sets into a consistent resolution and geographic projection. It next reviews the Lake Erie bathymetry and the wintertime meteorological conditions, describing in detail the two major meteorological influences on the lake ice cover, the AFDD recorded each winter and the wind speed and direction. Additionally, the chapter explores the overall relationship between the maximum ice cover extent and the maximum AFDD each winter; and the final section shows a series of charts of the spatial statistics of the Lake Erie ice cover. These charts show the variability of the ice cover throughout the winter season and from year-to-year; and they also address questions of when does the first ice form throughout the lake, how long does the ice cover last, and when is the last day that ice can be expected.

3.2 Digital ice-cover data sets

The NOAA Great Lakes Environmental Research Laboratory (GLERL) provided a 41-winter digital ice cover data set (1973–2013) that was available in three groups: 1973–2002, 2003–2006, and 2007–2013. All the data were based on ice charts developed by CIS and NIC (NIC 2015) and are available from the NIC. Figure 12 provides the dates of the ice charts.

* Note that the year convention is equivalent to that of the U.S. Geologic Survey “water year.” For example, the data for the winter of 1973 starts in the fall of 1972.

Figure 12. Dates of the ice charts.

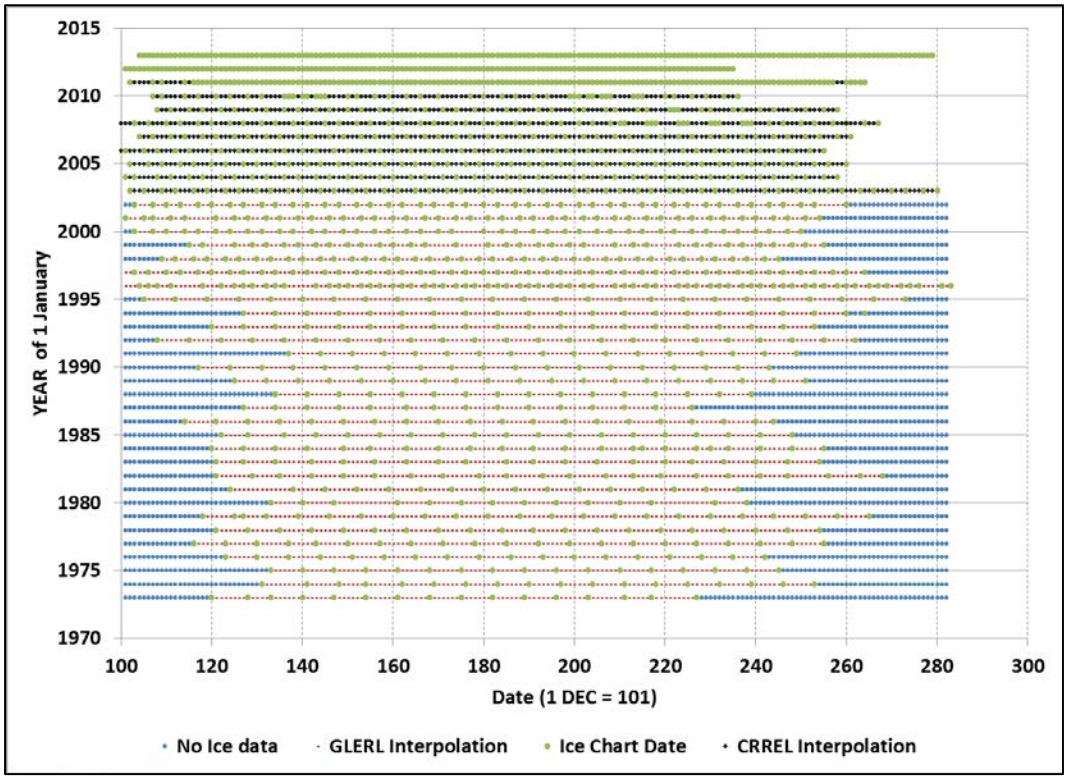

1973–2002: The first group (Assel et al. 2002) was developed from digitized paper copies of ice charts developed by the CIS and NIC up to 1995 and then GIS data from the NIC after 1995. The original paper ice charts were available approximately every 7 days. The paper copies were digitized into grid cells approximately 2.5 km on a side. The fraction of the grid cell covered by ice was expressed as a percent (100% ice cover was coded as 99 to save room). GLERL produced daily grids by using linear interpolation between consecutive ice charts. The daily grids started on 1 December each year and ended on 31 May and were assigned the year in which 1 January occurred during that winter. All cells in the daily grids prior to the date of the first ice chart and after the date of the last ice chart each winter were recorded as zero ice coverage.

2003–2006: The second group of data (Assel 2005; Wang et al. 2012) was based on GIS data that the NIC produced directly from the ice charts. The size of the grid cells were approximately 2.5 km on a side, the same as the first data set. The fraction of the grid cell covered by ice was expressed as a percent from 0% to 100%. The ice chart data was available every 2 to 5 days. Daily grids were produced for this report starting on the date of the

first ice chart and ending on the date of the last ice chart for each winter season.

2007–2013: The third group of data (Assel 2005; Wang et al. 2012) was based on GIS data the NIC produced directly from the ice charts. However, the map projection of the GIS data was not the same as the previous groups. The grid cell size was also reduced to approximately 1.8 km. These changes caused the effective lake area to change slightly from the previous data sets. The fraction of the grid cell covered by ice was expressed as a percent from 0% to 100%. The ice chart data was available about every 4 days for 2007–2010 and was available every day after that time.

To analyze the digital ice-cover data sets, it was necessary to produce daily grids with consistent geographic attributes for all the years of record. The first step was to develop daily grids for missing days. Daily grids were available from GLERL before 2003; and after 2010, the NIC produced daily ice charts. As a result, it was necessary to produce daily grids for only 2003–2010. The daily grids were produced for missing days by using linear interpolation between consecutive ice charts.

Next, the daily gridded ice cover data files for the 1973–2006 winters were processed so that their projection, cell size, and the lake surface area extent would match those used in the 2007–2013 group. This process used the following steps:

1. Each plain-text daily gridded ice-cover data file for the 1973–2006 winters was converted to a raster data file.
2. The raster cells outside of the boundary of Lake Erie were assigned to No Data.
3. To match the lake surface area extent of the 2007–2013 group, the ice cover values on the lake boundary were first expanded outwards using a rectangular 3 × 3 cell neighborhood to calculate the mean value in the No Data cells around the lake. This step effectively caused the ice cover values to expand outwards.
4. The ice-cover raster was projected to match the projection parameters of the 2007–2013 group shown in Table 8 by using nearest neighbor resampling. The cell size was set to match the cell size of the 2007–2013 group.
5. The ice-cover cells along the lake boundary were clipped back to match the boundary of the lake surface area extent of the 2007–2013 group.

6. The final raster was then converted back to a plain-text data file.

Table 8. GIS metadata and data file header information.

Parameter	1973–2002	2003–2006	2007–2013
GIS Metadata Information			
Projection	Mercator	Mercator	Mercator
False_Easting	0.0	0.0	0.0
False_Northing	0.0	0.0	0.0
Central_Meridian	−84.14	−84.14	0.0
Standard_Parallel_1	45.04	45.04	0.0
Linear Unit	Meter	Meter	Meter
Geographic Coordinate System	GCS_Clarke_1866	GCS_Clarke_1866	WGS 1984
Data File Header Information			
ncols	516	516	1024
nrows	510	510	1024
xllcorner	−649446.25	−649446.25	−10288021.9553
yllcorner	3306260	3306260	4675974.1583
cellsize	2550	2550	1800
NODATA_value	−9999	−9999	−9999

3.3 Lake Erie bathymetry

Figure 13 shows the bathymetry of Lake Erie. The lake can effectively be divided into three parts based on its bathymetry. The western portion of the lake is relatively shallow with depths generally less than 10 m. This part is bounded on the east by islands and the Point Pelee peninsula on the north. The shallow water of the western portion of the lake allows this area to cool quickly in the fall, and ice is consistently observed first in the western portion. The large middle portion of the lake is the widest part of the lake with depths up to about 24 m. The middle portion is the largest of the three sections and is roughly bounded on the east by the Long Point Peninsula on its north shore. The third and eastern portion of the lake is the deepest part of the lake with a maximum depth of 64 m off of the end of the Long Point Peninsula.

Figure 13. Lake Erie bathymetry.

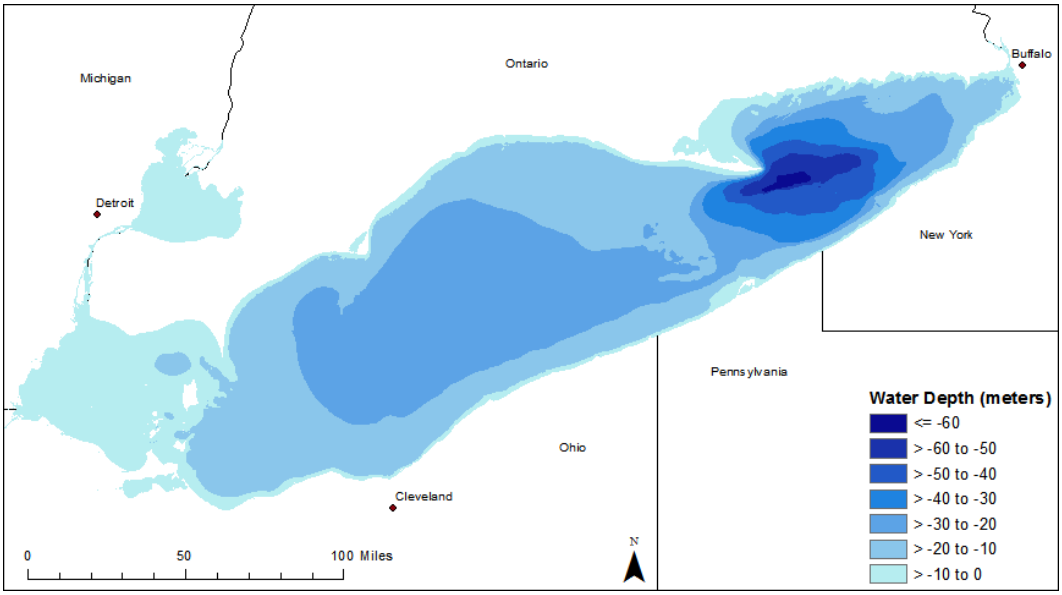

3.4 Winter meteorological conditions

The two important meteorological conditions that significantly influence the ice conditions on Lake Erie are the air temperature and the wind speed and direction. Figure 14 shows the average daily air temperatures for the winter months (December through April) for four major cities around Lake Erie. The average daily air temperatures at all four sites track each other closely, falling below 0°C at the beginning of December and staying below freezing until early March. This time frame roughly defines the period when ice exists on the lake. The ice-covered area of the lake generally increases throughout the winter and reaches a maximum in mid-February. After this time, the ice-cover area generally declines and melts away completely by the middle of April. There can be large variations in the air temperature and the resulting ice-covered area of the lake from year to year.

Figure 14. Average daily air temperatures throughout the winter around Lake Erie.

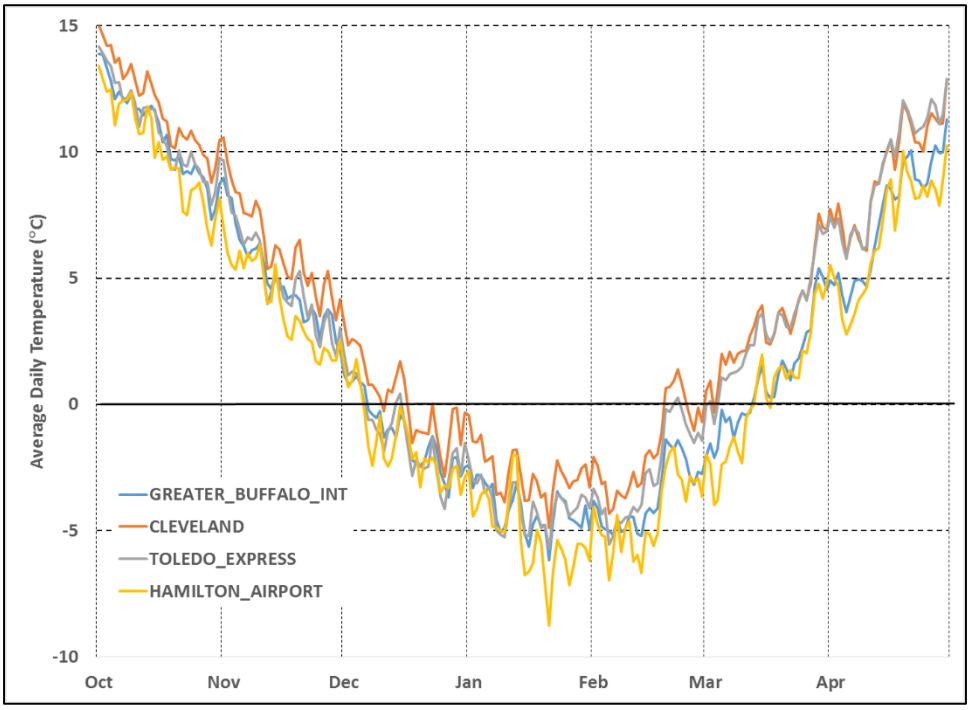

The AFDD were found for the entire lake by averaging the AFDD for each of the 21 meteorological stations that were analyzed earlier. The number of AFDD serves as a good indicator of the severity of the winter with respect to surface-ice growth. The AFDD is a monotonically increasing function calculated as the sum of the positive difference between freezing and the average daily temperature for each day of the winter season. (If the average daily temperature is greater than freezing, the difference is ignored). Figure 15 shows the maximum of AFDD recorded each winter over the period of record. Figure 16 shows the maximum AFDD and the maximum ice-cover extent on Lake Erie for each winter, clearly showing the influence of the maximum AFDD on the ice extent. The relationship between AFDDs and ice extent is clearly shown in Figure 17 where the maximum ice extent is plotted against the maximum AFDD. It can be seen that the when the maximum AFDD is greater than about 200°C-Days, the ice cover will cover the entire lake. There is a roughly linear relationship between the AFDD and ice extent for maximum AFDD less than that.

Figure 15. AFDD recorded each winter.

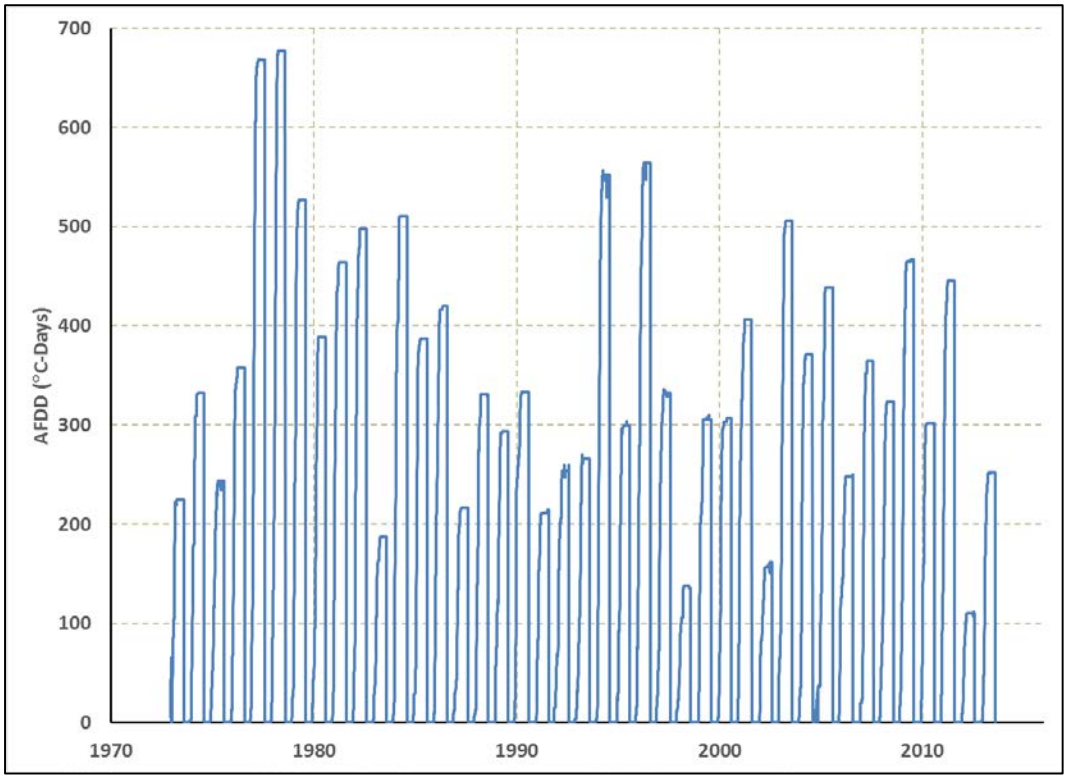

Figure 16. Maximum AFDD (average for lake) and maximum ice coverage (%) for each winter season.

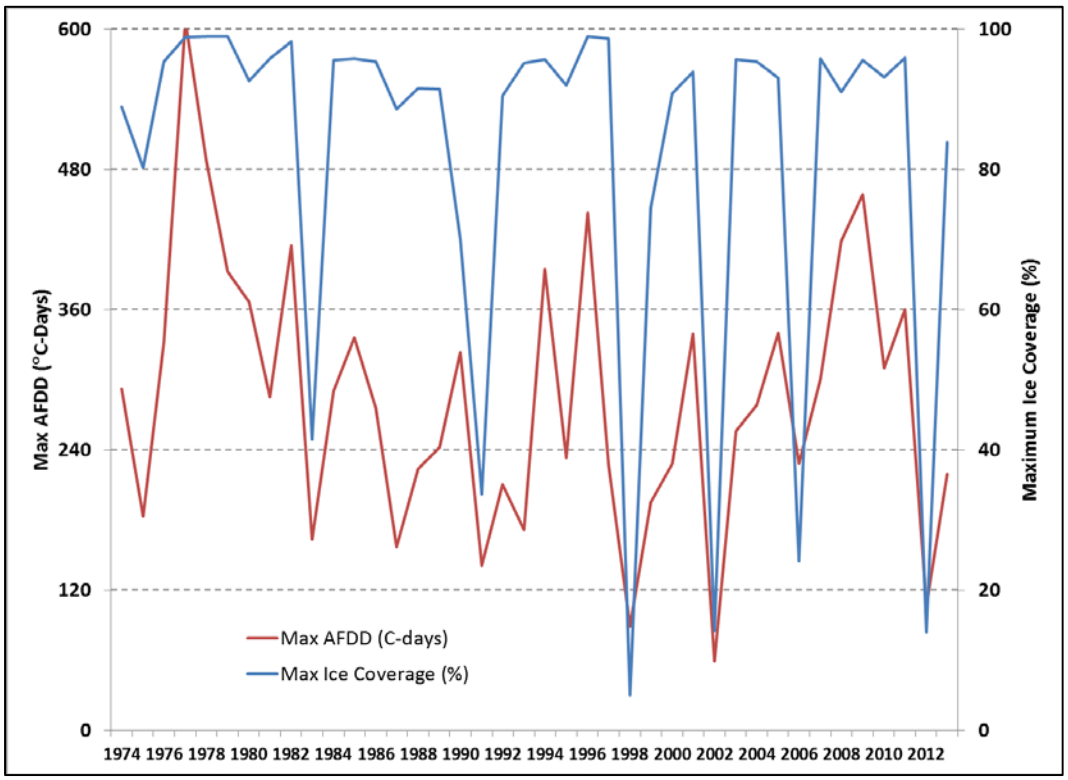

Figure 17. The annual maximum ice coverage (%) plotted against the maximum AFDD (average for the lake).

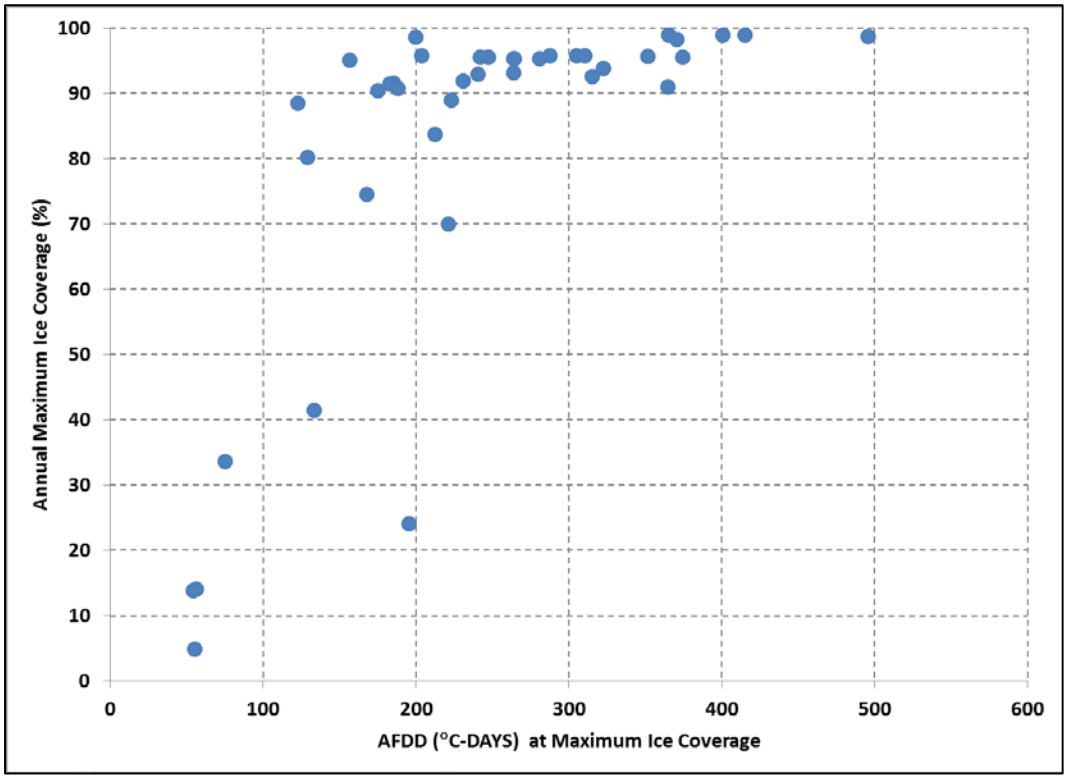

The wind-direction and wind-speed information is shown for Toledo, OH, in Figure 18; Cleveland, OH, in Figure 19; and Buffalo, NY, in Figure 20 (NRCS 2015). Toledo is on the western end of the lake, Cleveland towards the middle of the lake, and Buffalo at its western end. In December, the winds are generally from the southwest at Toledo and Cleveland and directly from the west at Buffalo. The winds generally remain from the southwest throughout the winter at Toledo and Cleveland, although they display more variability in March and April. The wind direction is consistently from the west at Buffalo. This dominance of a west wind has a tendency to push the ice cover of the lake towards its eastern end. In general, the last ice of the season is observed in the eastern end of the lake near Buffalo.

Figure 18. Monthly wind directions throughout the winter at Toledo, OH.

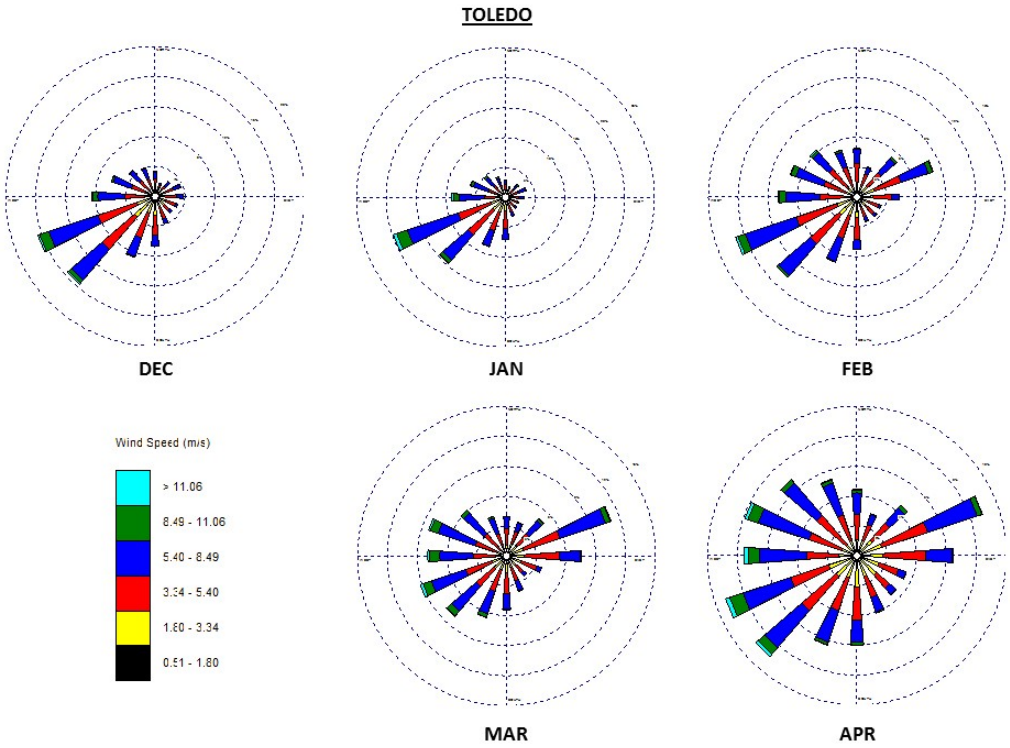

Figure 19. Monthly wind directions throughout the winter at Cleveland, OH.

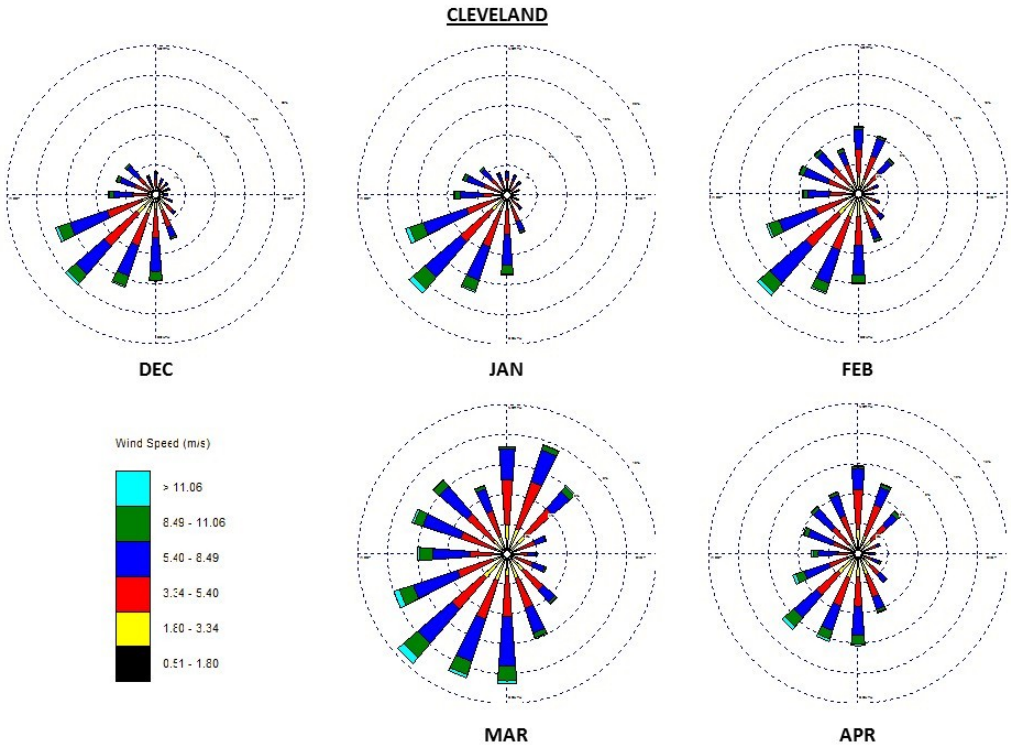

Figure 20. Monthly wind directions throughout the winter at Buffalo, NY.

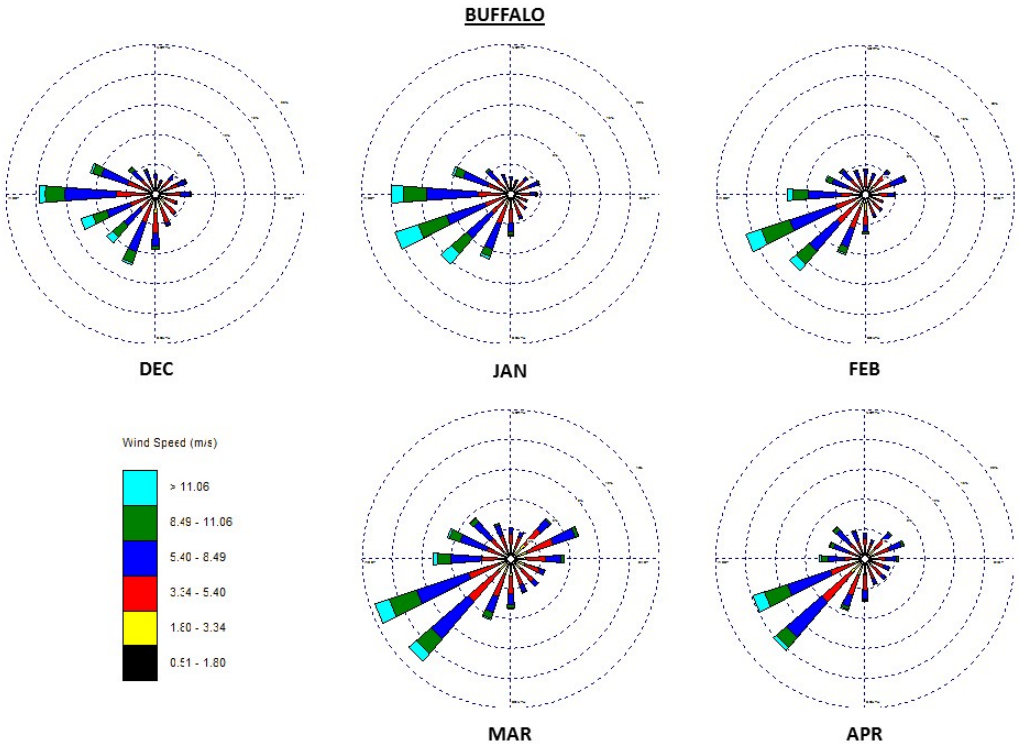

3.5 Ice-cover spatial statistics

Once the daily grids with consistent geographic attributes were created over the entire period of record, this study processed the grids to determine the daily statistics of the Lake Erie ice cover and determined the following information:

Overall lake ice coverage

- Daily ice-cover extent as a fraction of the total Lake Erie surface area
- Fraction of Lake Erie covered by ice, on average, for each day of the winter season
- Statistics of ice-cover extent, on average, for each day of the winter season
- Percent of years that each grid cell had some ice

Days with ice

- The average number of days each winter that each grid cell had some ice
- The minimum number of days each winter that each grid cell had some ice

- The maximum number of days each winter that each grid cell had some ice

Ice start date

- The earliest day of the winter that ice was first observed in each grid cell
- The average day of the winter that ice was first observed in each grid cell
- The latest day of the winter that ice was first observed in each grid cell

Ice end date

- The earliest day of the winter that ice was last observed in each grid cell
- The average day of the winter that ice was last observed in each grid cell
- The latest day of the winter that ice was last observed in each grid cell

3.5.1 Overall lake-ice coverage

Figure 21 shows the daily ice-cover extent as a fraction of the total Lake Erie surface area. There was ice observed every winter over the period of record, but the maximum ice-cover extent can be highly variable from year to year. In many years, the ice-cover extent covers almost the entire lake surface. In Figure 22 is the fraction of Lake Erie covered by ice for each day of winter (horizontal axis) for each year (vertical axis). The ice fraction is displayed in four categories, 0–0.25, 0.26–0.50, 0.51–0.75, and 0.76–1.00. This plot shows quite clearly the year-to-year variability in the Lake Erie ice cover. Figure 23 shows the statistics for each day of the winter and includes the maximum, 75th percentile, 50th percentile, and 25th percentile ice extents. Figure 24 shows the percent of years with at least some ice for each grid cell; western Lake Erie has at least some ice every year. The percent of years with ice varies throughout the rest of the lake surface area, but every part of the lake has at least some ice 85% of years or more.

Figure 21. Daily ice-cover extent as a fraction of the total Lake Erie surface area.

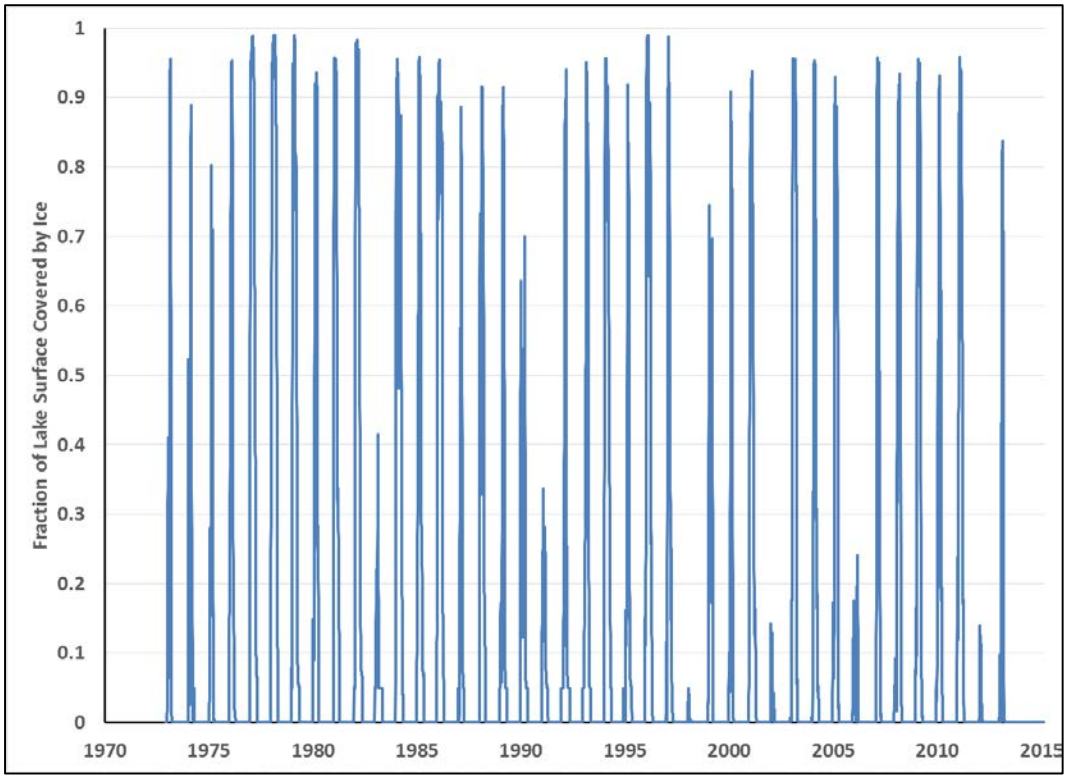

Figure 22. The fraction of Lake Erie covered by ice each day of each winter.

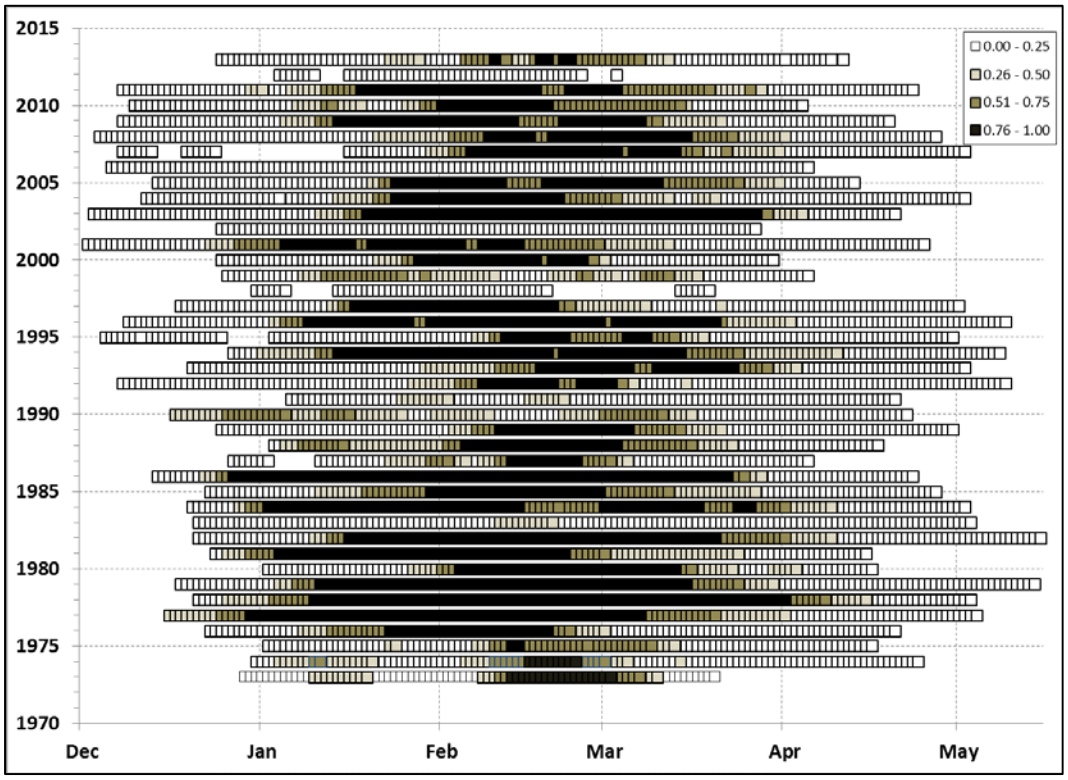

Figure 23. Statistics of ice-cover extent for each day of the winter.

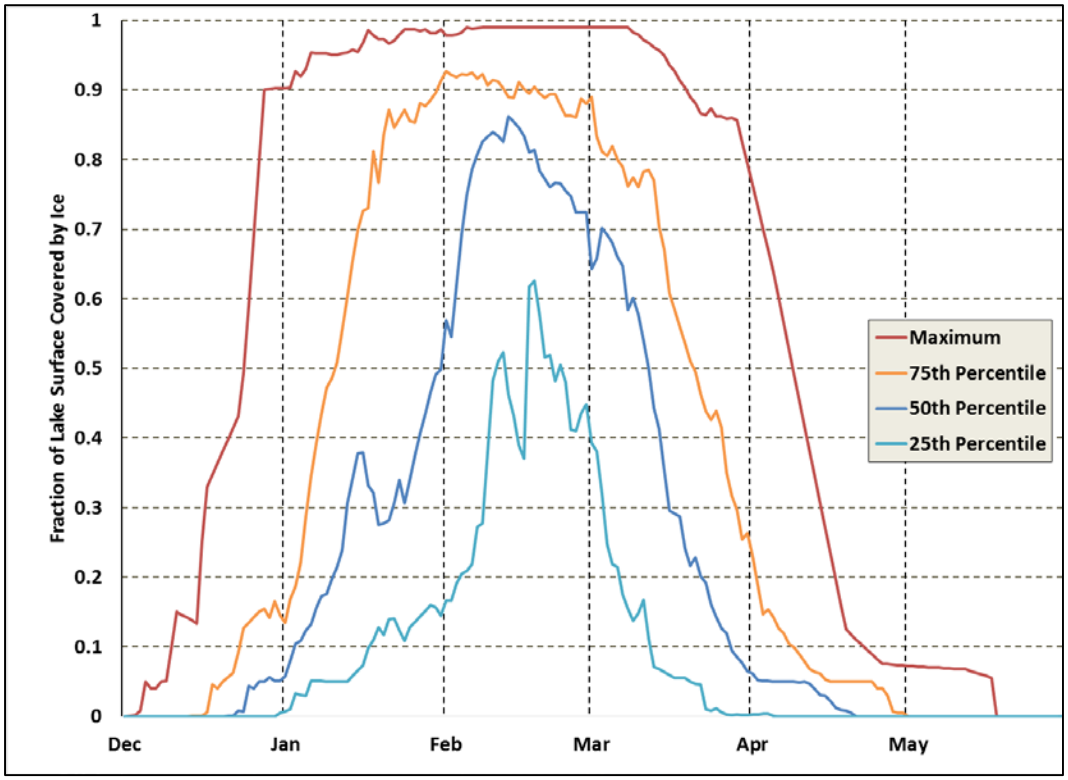

Figure 24. Percent of years with ice.

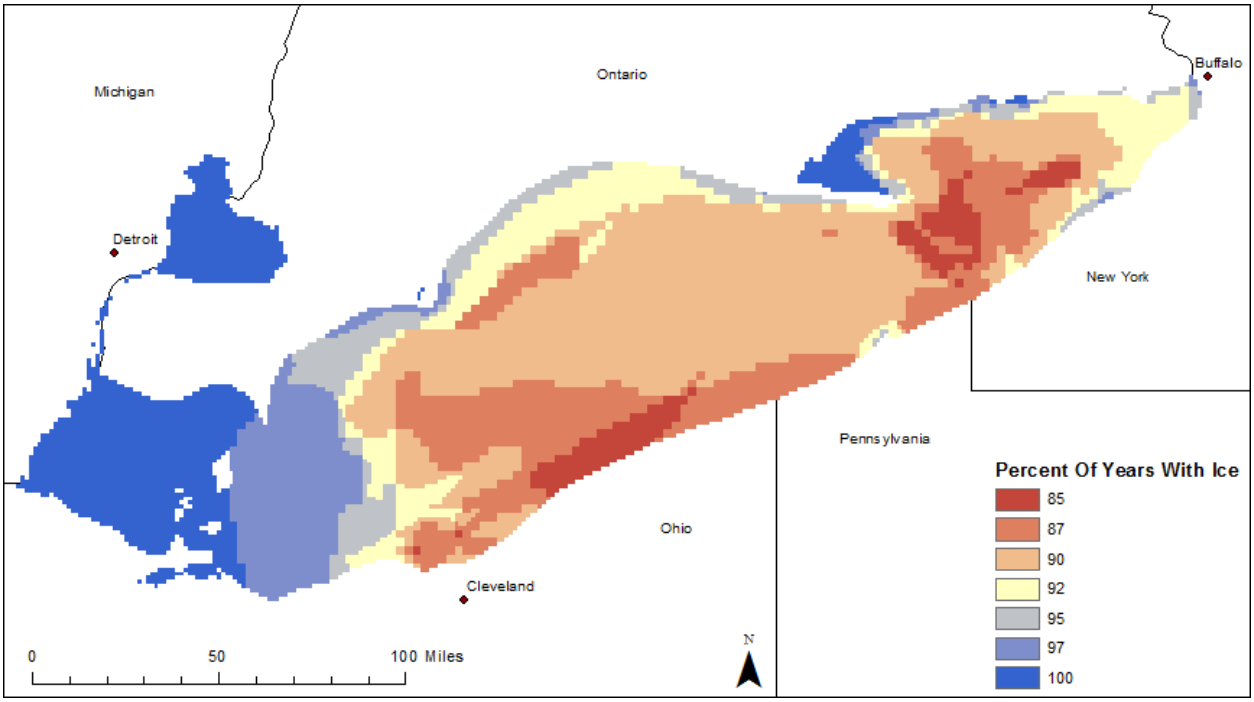

3.5.2 Days with ice

Figure 25 shows the average number of days with at least some ice over the period of record. One can see that on average Lake Erie is covered with ice between 49 and 90 days with the longest average coverage at the eastern end of the lake. The middle portion of the lake generally has the fewest number of ice-covered days. Figure 26 shows the minimum number of days with at least some ice over the period of record. Much of the lake surface has been ice free at least one winter with only the western, relatively shallow end of the lake ice covered every year. Figure 27 shows the maximum number of days with at least some ice over the period of record.

Figure 25. Average days with ice.

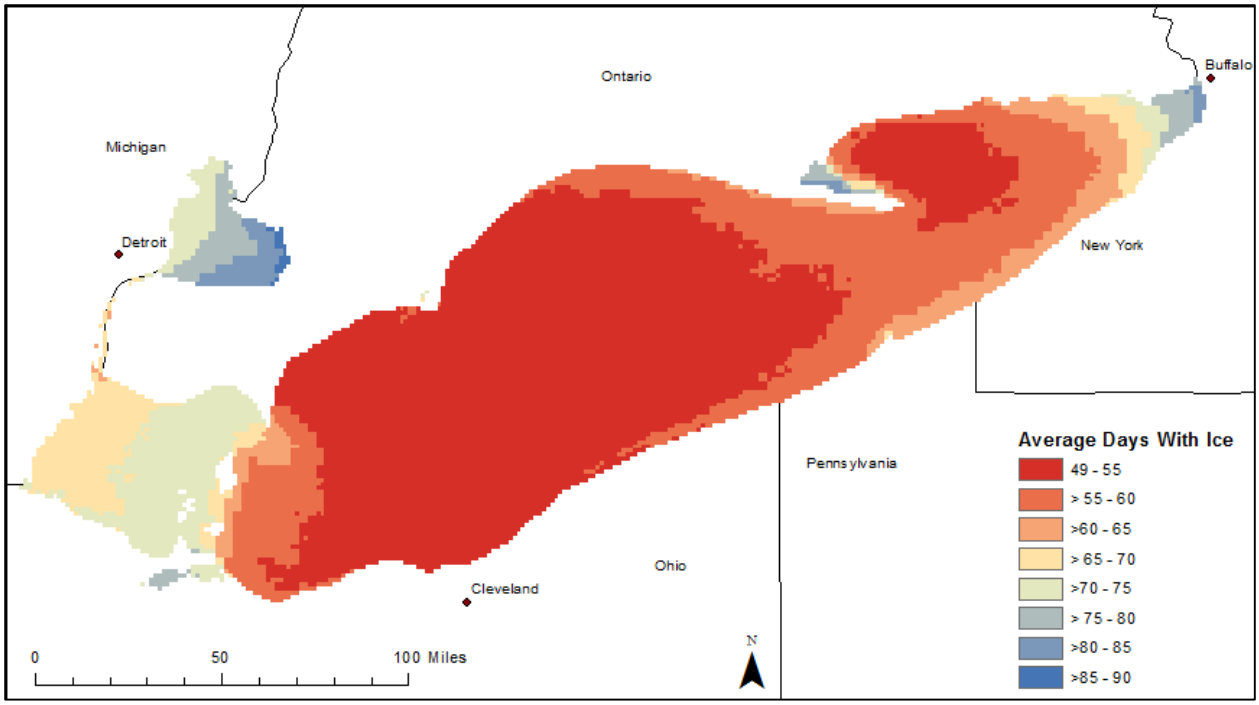

Figure 26. Minimum days with ice.

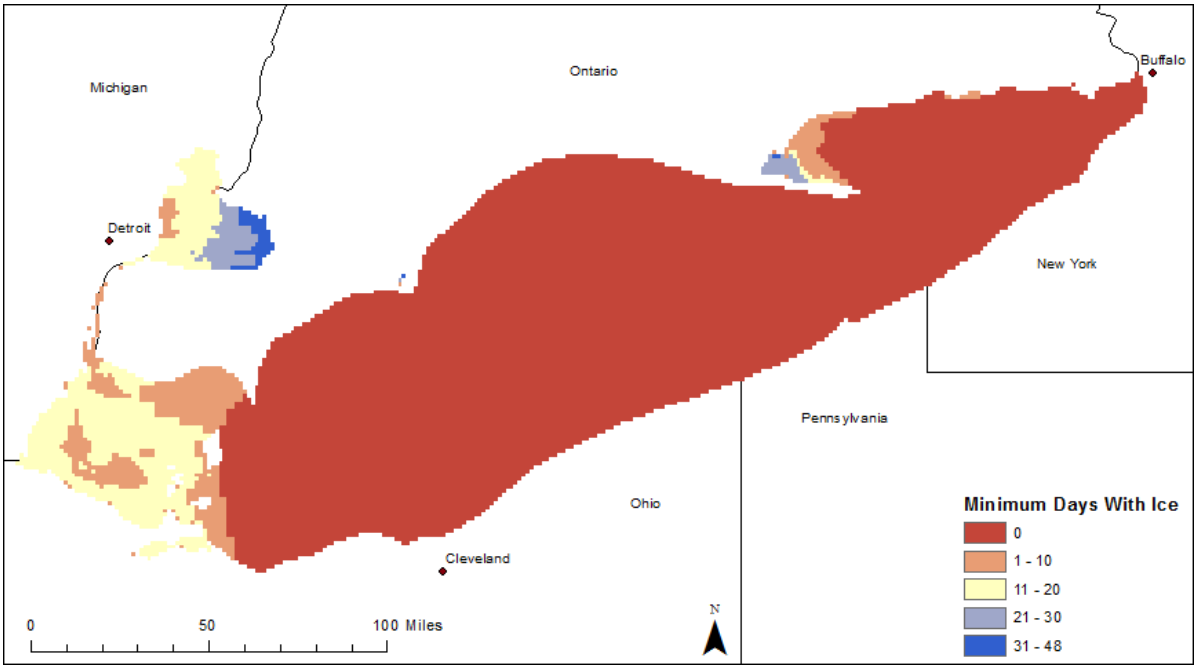

Figure 27. Maximum days with ice.

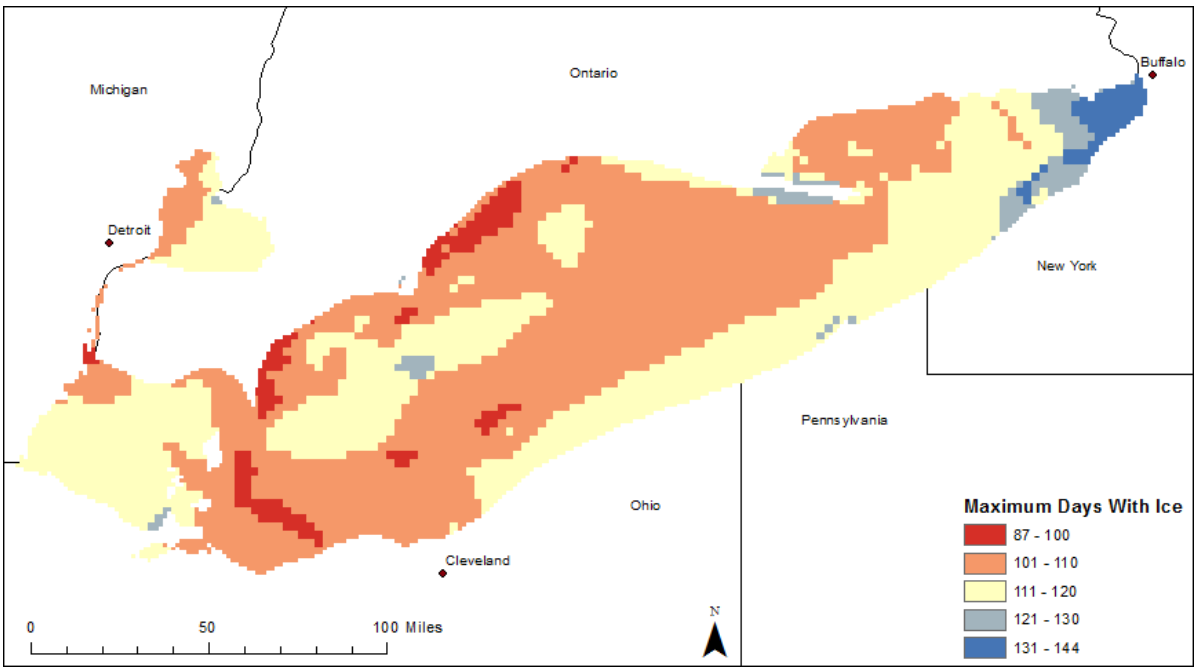

3.5.3 Ice start date

Figure 28 shows the average first day of winter with at least some ice cover over the period of record. The ice cover starts in the western, relatively shallow end of the lake first. The remaining portions of the lake then freeze with the portions of the lake closest to the shore freezing first. The ice

cover extends in concentric rings with the center of the lake covering last. Figure 29 shows the earliest day of winter with at least some ice over the period of record. The pattern of the earliest day ice cover formation follows the average day ice cover formation in form. Figure 30 shows the latest day of winter with at least some ice over the period of record.

Figure 28. Average ice start date.

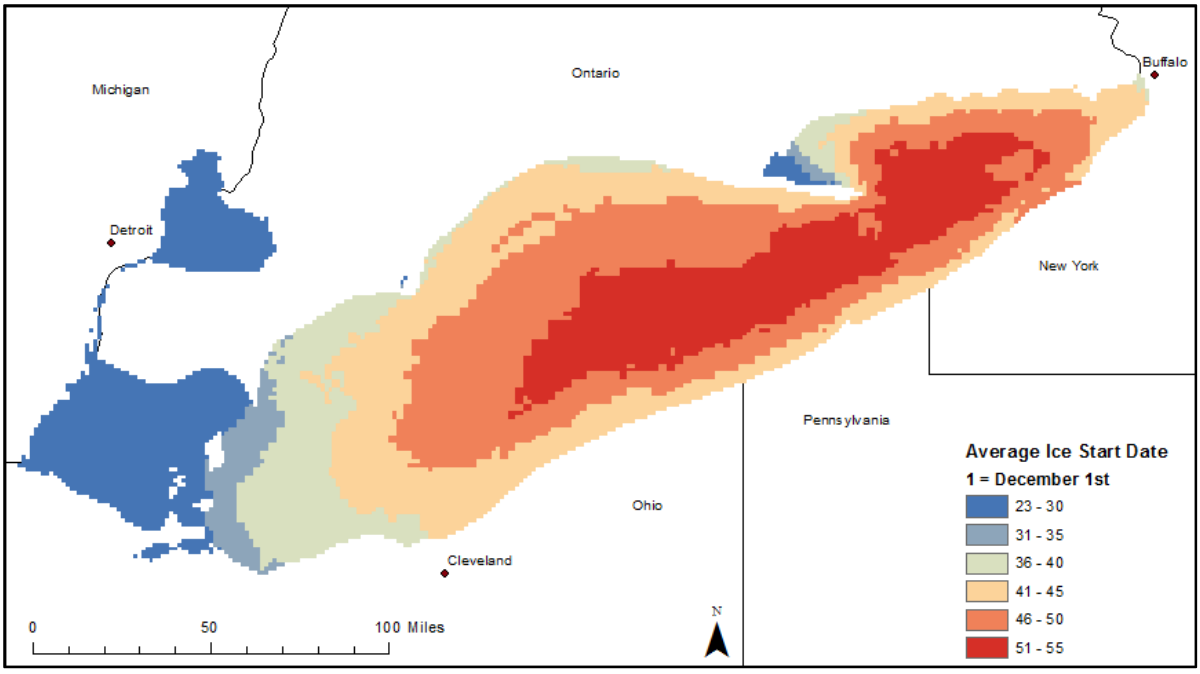

Figure 29. Earliest ice start date.

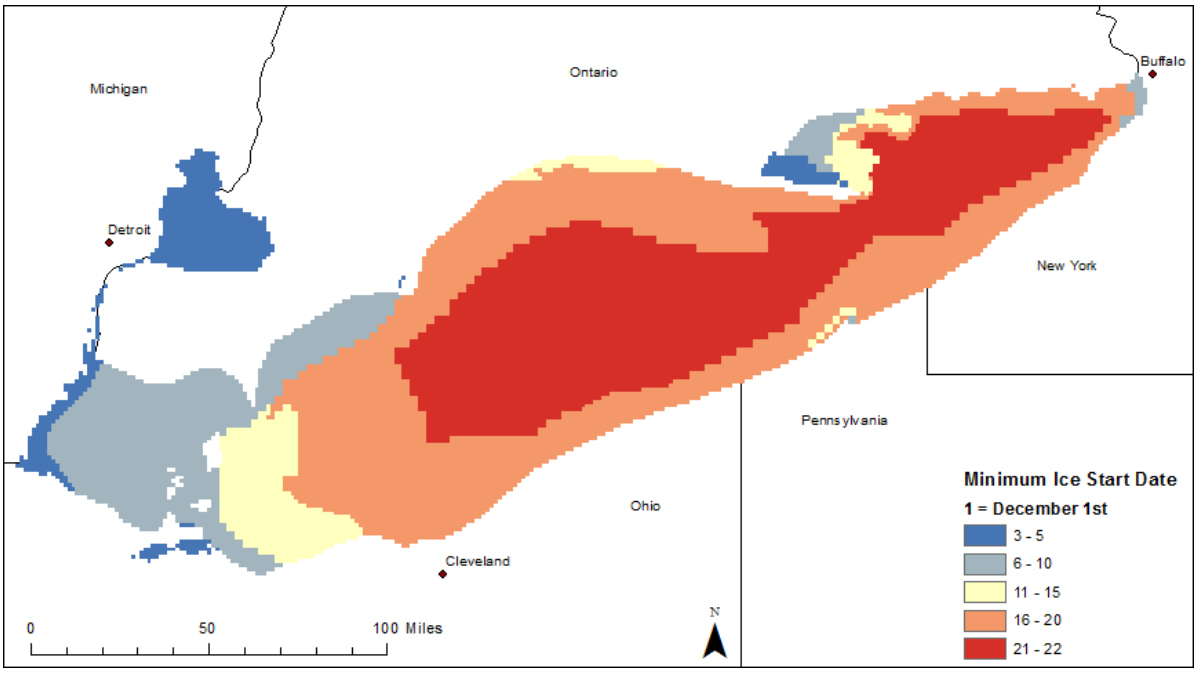

Figure 30. Latest ice start date.

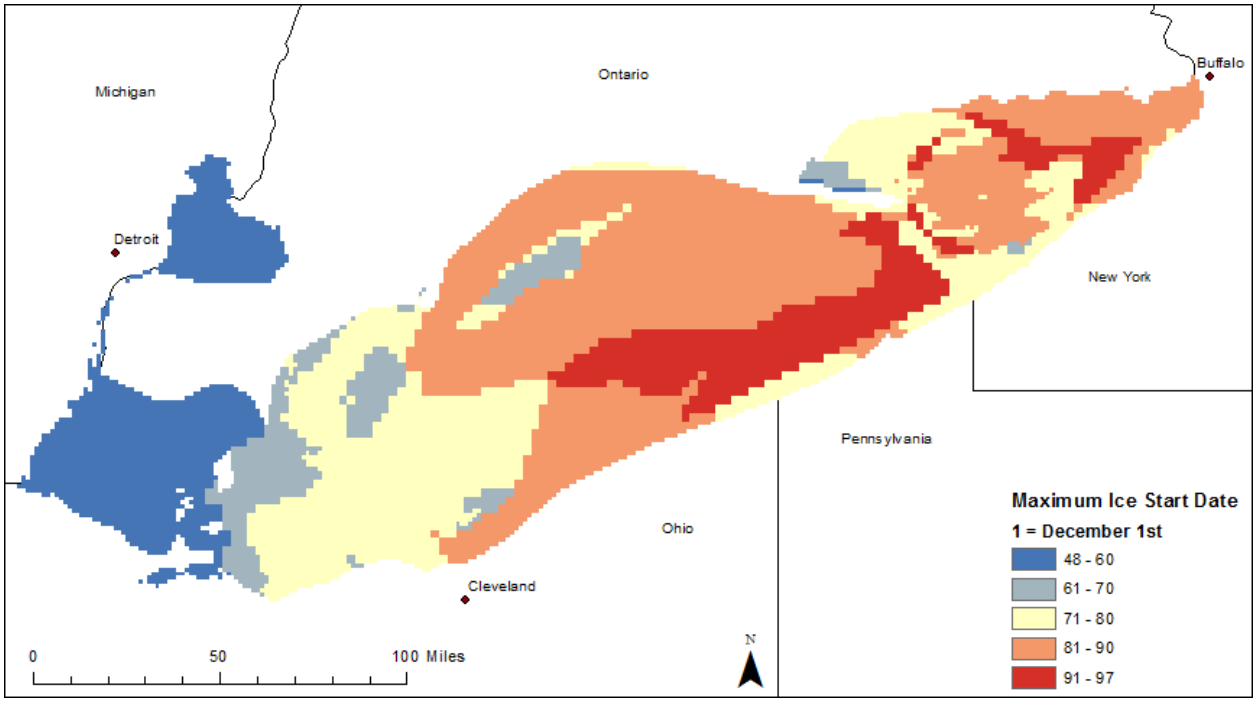

3.5.4 Ice end date

Figure 31 shows the average last day of winter with at least some ice cover over the period of record. The ice cover melts out in the western, relatively shallow end of the lake first. The remaining portions of the lake then melt out steadily eastward with the final ice melting out at the eastern end of the lake. Generally, the western end of the lake opens up about 24 days before the eastern end. Figure 32 shows the earliest day of winter when the last ice was observed, and Figure 33 shows the latest day of winter when the ice was observed.

Figure 31. Average ice end date.

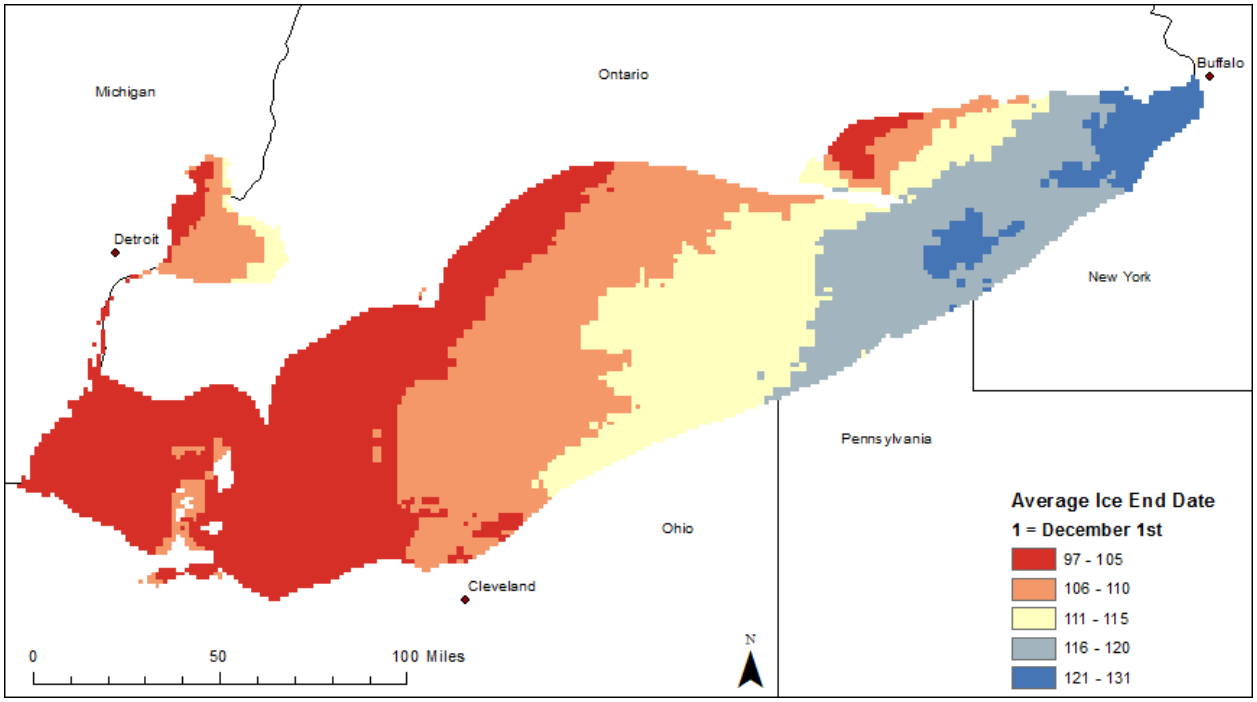

Figure 32. Earliest ice end date.

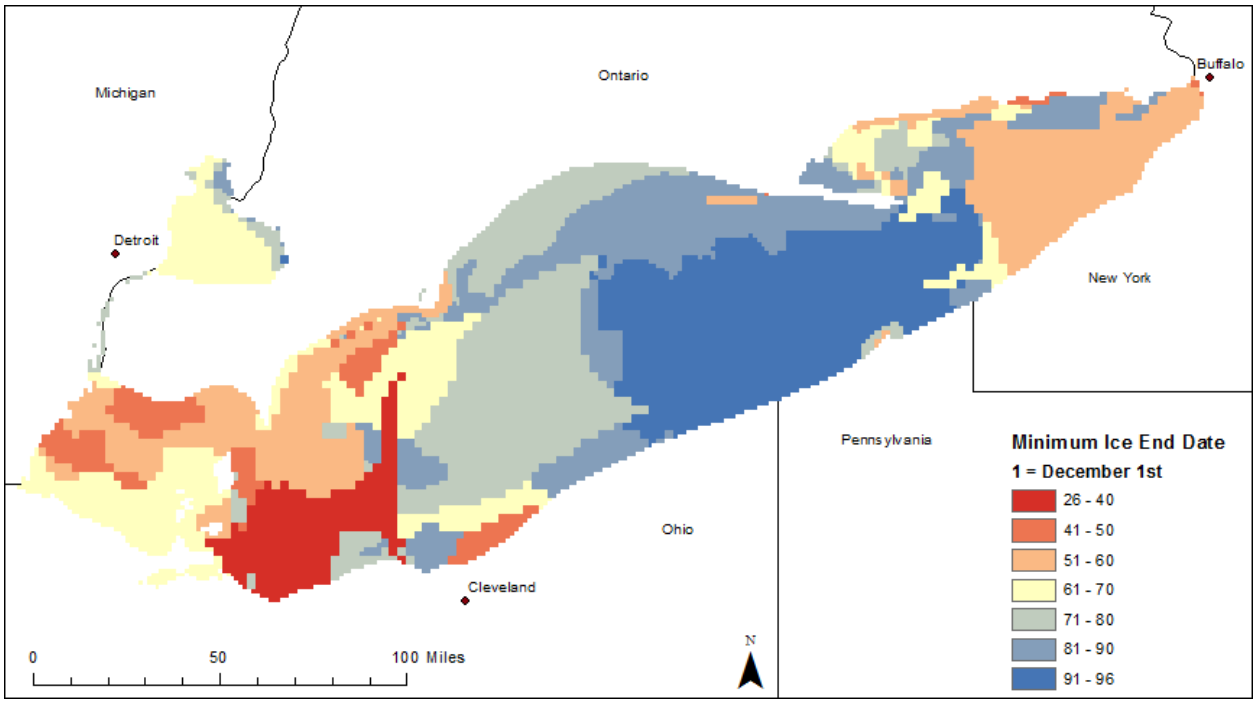

Figure 33. Latest ice end date.

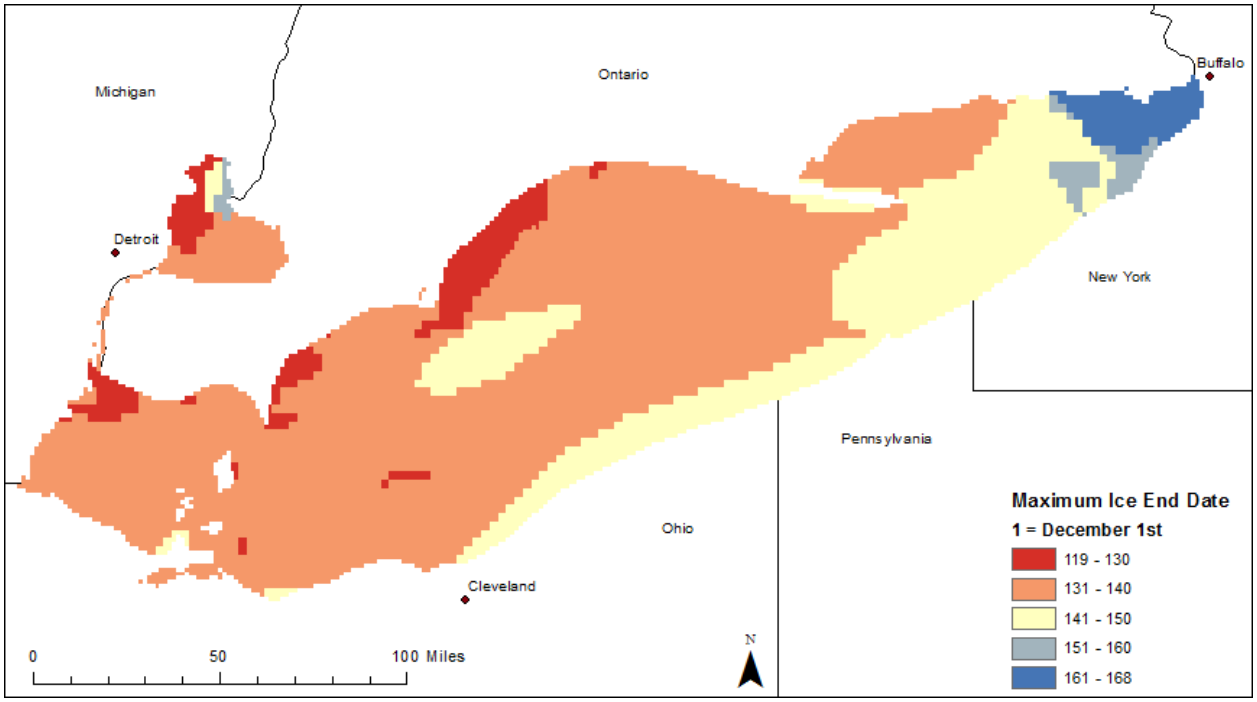

3.6 Summary

The spatial and temporal extent of the Lake Erie surface ice each winter was estimated based on 41 years of ice charts prepared by CIS and NIC (NIC 2015) of the Lake Erie ice cover. The GIS analysis based on these records resulted in 41 years of gridded daily ice-cover information with a roughly 2 km grid cell size. The ice cover distribution of Lake Erie is strongly influenced by the lake bathymetry and the wintertime meteorological conditions, particularly the duration and magnitude of the subfreezing air temperatures and the overall wind direction and speed. The gridded daily ice cover information was used to explore the overall relationship between the maximum ice-cover extent and the maximum AFDD each winter. The variability of the ice cover of the entire lake throughout the winter season and from year to year was described. The earliest, average, and latest dates of the first and last ice each winter for each grid cell and the minimum, average, and maximum duration of ice for each grid cell was found based on the period of record.

4 Satellite Detection of Ice Ridges

4.1 Introduction

The presence of ice ridges in Lake Erie is an important consideration in the design of offshore wind turbine towers and their foundations. The evidence for the presence of ice ridges in Lake Erie is conclusive but indirect, as will be discussed in Chapter 5. Very few ridges in Lake Erie have actually been observed and described in the literature. Winter expeditions to detect and monitor the formation of ice ridges in Lake Erie would involve aircrafts or ice-breaking ships and would be expensive and time consuming. A possible alternative to this effort is remote sensing using satellite-synthetic aperture radar (SAR). Today, SAR is commercially available from several vendors and offers significant advantages for the detection of ice ridges. In general, radar supplies its own illumination and does not require sunlight to produce images. It operates at wavelengths long enough to penetrate cloud cover, smoke, and precipitation, which is particularly important when imaging regions that experience significant cloud cover and lower sun angles during winter months. At centimeter wavelengths, radar also provides information about surface roughness and dielectric material properties of objects with which it interacts. Radar has been used to detect and classify the surface-ice cover of the Arctic regions for many years (see Melling 1998 for a review). Studies have also described the ability of satellite-based SAR to detect ice ridges and other “deformed ice” (Melling 1998; Dierking et al. 2006; and Dierking and Dall 2007). SAR has also been applied to the Great Lakes: Leshkevich and Nghiem (2013) classified ice types in Lake Superior by using SAR although they did not specifically look for ice ridges.

This chapter describes detecting ice ridges by using satellite-based SAR. A commercial radar satellite (TerraSAR-X) was tasked by CRREL to acquire imagery over Lake Erie during February and March 2015. The TerraSAR-X satellite operates an X-Band (approximately 1 cm wavelength) radar, and collected imagery over two locations in the lake (Figure 34). These locations encompass regions of known ice-ridge surveys (three images acquired offshore of Erie, PA) and proposed wind turbine deployment (one image acquired near Cleveland, OH). The acquisition dates were as follows: 10 February 2015 (Figure 35), 21 February 2015 (Figure 36), 4 March 2015 (Figure 37), and 14 March 2015 (Figure 38). The first three images were acquired over the exact same area of Lake Erie near Erie, PA. Based

on previous work, the study chose this area for image acquisition because gouges made by ice ridges, as described in Chapter 5, had been detected in this region of the lake. The fourth image was acquired on 14 March 2015 offshore of Cleveland, OH.

Figure 34. Four TerraSAR-X 2015 images were collected during 2015. Three images were near Erie, PA, *right* (10 February, 21 February, and 4 March), and one outside of Cleveland, OH, *left* (14 March). (Image ©DLR e.V. 2015, Distribution Airbus DS/Infoterra GmbH.)

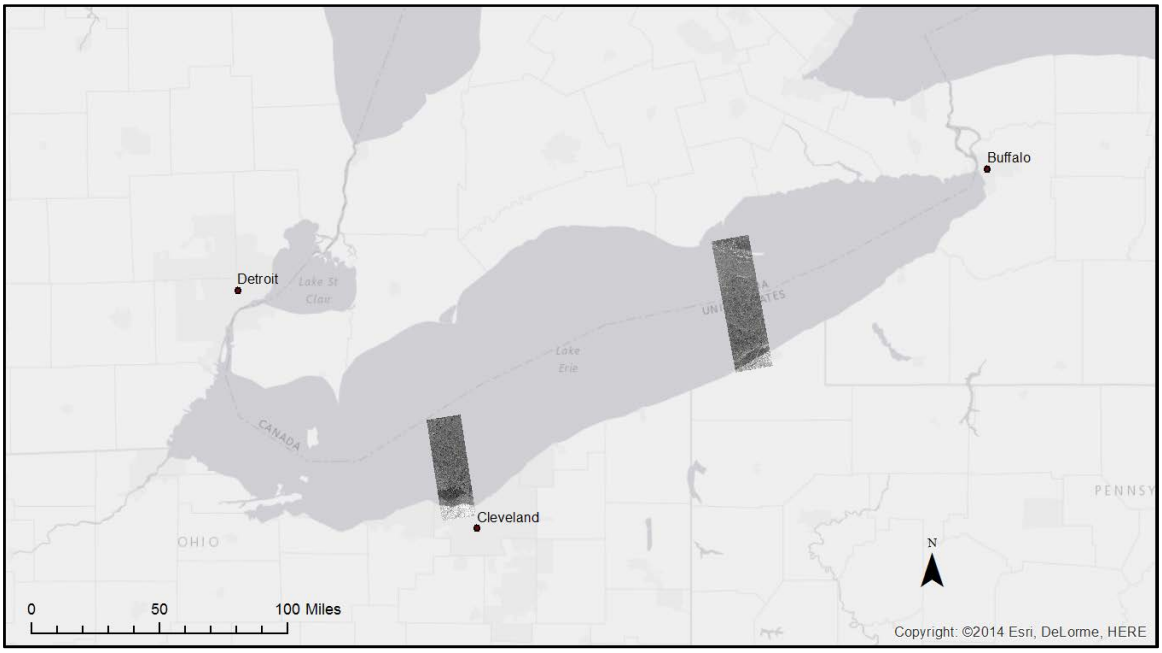

Figure 35. SAR image near Erie, PA, on 10 February 2015. The *arrow* indicates the position of a potential ice ridge. (Image ©DLR e.V. 2015, Distribution Airbus DS/Infoterra GmbH.)

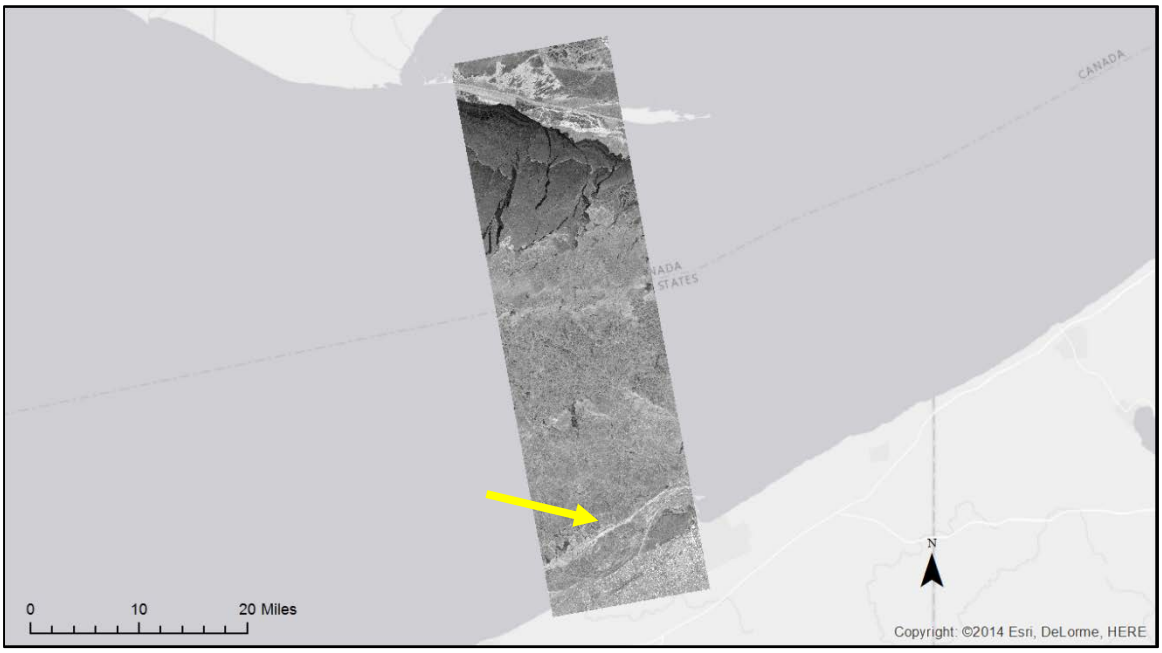

Figure 36. SAR image near Erie, PA, on 21 February 2015. The *arrow* indicates the position of a potential ice ridge. (Image ©DLR e.V. 2015, Distribution Airbus DS/Infoterra GmbH.)

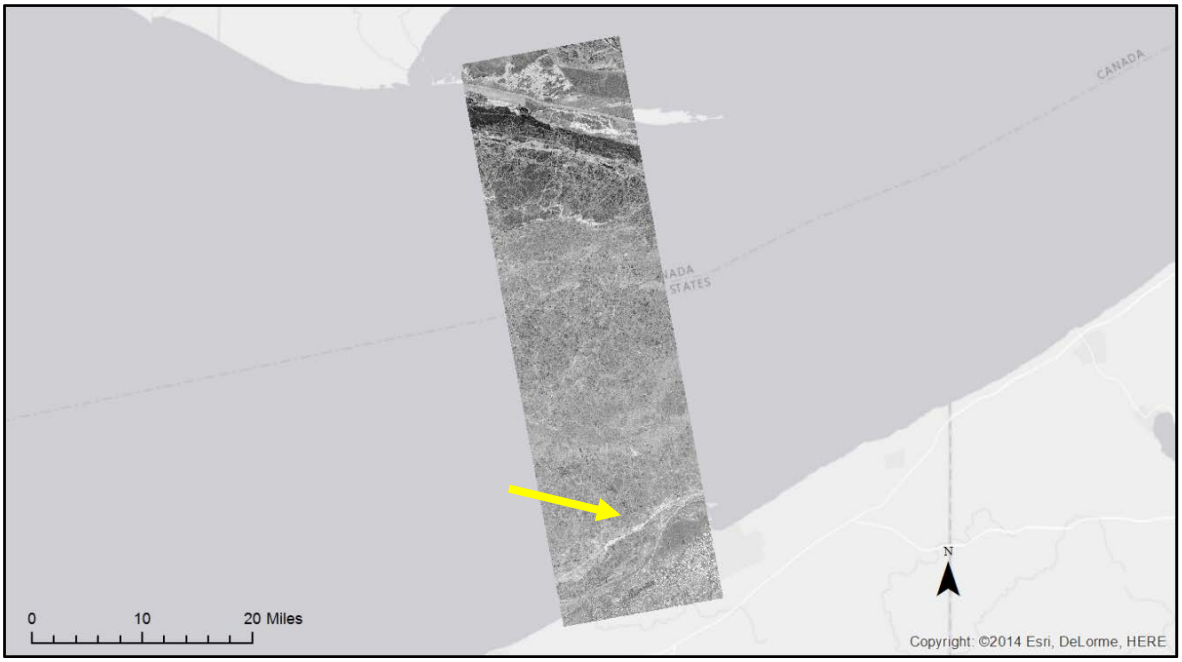

Figure 37. SAR image near Erie, PA, on 4 March 2015. The *arrow* indicates the position of a potential ice ridge. (Image ©DLR e.V. 2015, Distribution Airbus DS/Infoterra GmbH.)

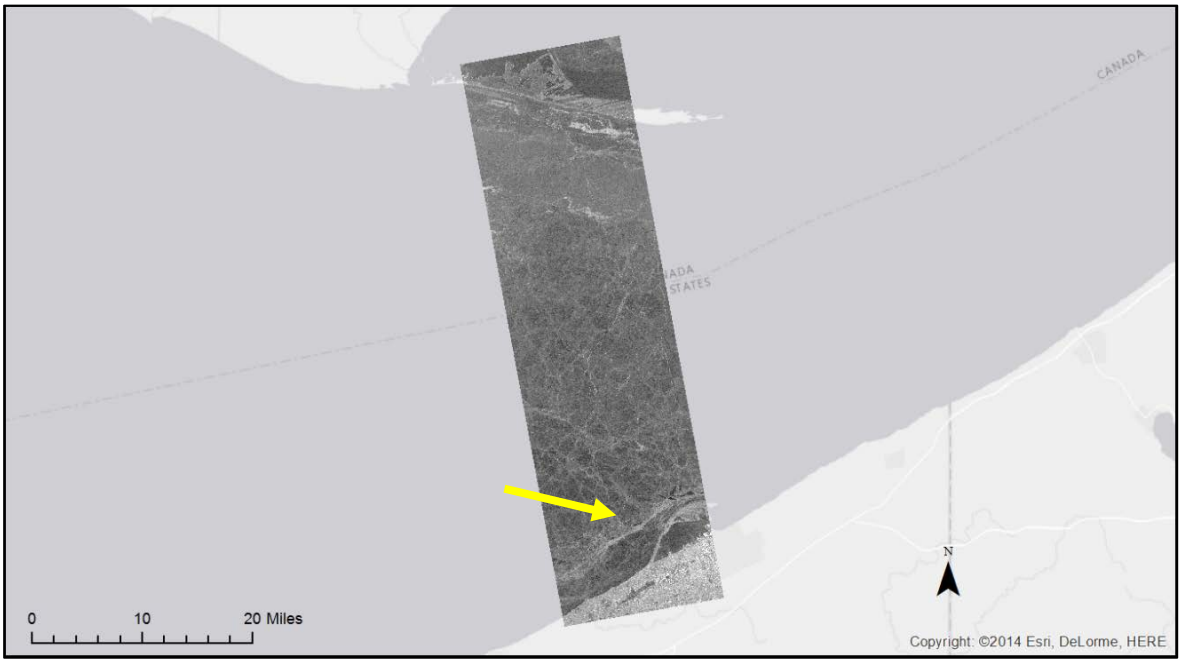

Figure 38. SAR image near Cleveland, OH, on 14 March 2015. (Image ©DLR e.V. 2015, Distribution Airbus DS/Infoterra GmbH.)

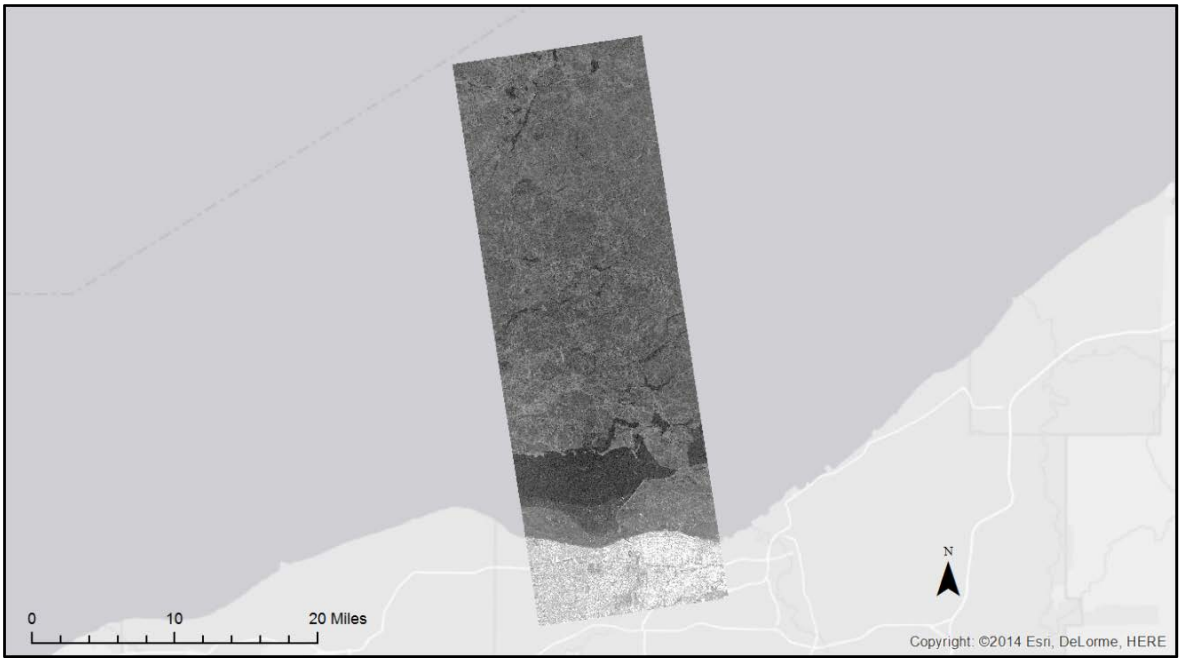

4.2 Analysis of Lake Erie ice-ridge formation from satellite imagery

A linear feature potentially representing an ice ridge was immediately apparent in each of the images offshore of Erie, PA (Figures 35–37) and was located in exactly the same location of each image. These images were acquired as interferometric pairs. This means that each image has the same viewing geometry (34° incidence angle, ascending orbit, right-looking) and an exact 11-day repeat orbit (Table 9). Unfortunately, it was not possible to use the insights that interferometry could potentially provide because of low coherence, or a measure of how the scattering characteristics have changed, between each pair. The most likely reason for low coherence between interferometric pairs was that the fine scale physical or dielectric properties of the ice ridge had changed sufficiently between each 11-day acquisition to cause significant differences in the surface scattering properties. Regardless, tracking between images confirmed that the linear feature remained in the same location and that ice located away from the ridge did not remain the same between images. Figure 39 shows the proposed ice ridge formation digitized from the three SAR images. The estimated length of this feature is approximately 12 km.

Table 9. SAR image parameters.

Parameter	Mode
Product	StripMap
Polarization	HH/VV
Incidence Angle	33.10° – 34.41°
Pass/look direction	Ascending/right
Resolution	4 m

Figure 39. The approximate centerline of the ice ridge and nearby lake bathymetry. (The *arrow* indicates the position of a potential ice ridge.)

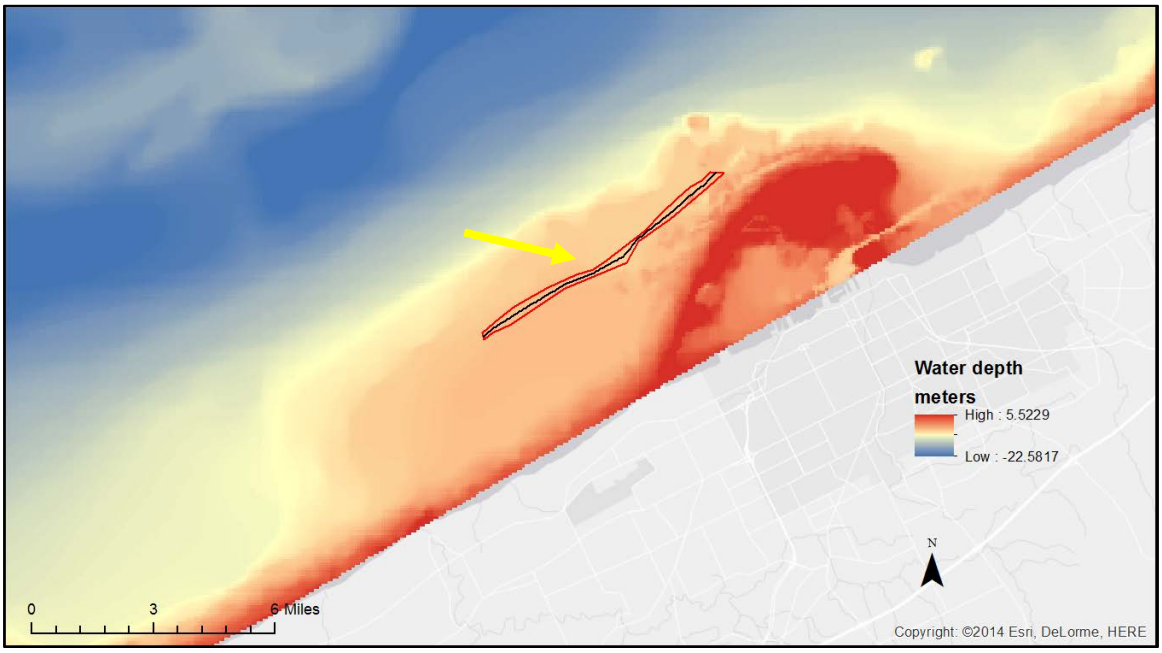

Figure 39 shows the bathymetry of Lake Erie in the vicinity of the potential ice ridge, and Figure 40 shows the water depth of the lake along the centerline of the ridge. The depths range from 5 to 9 m. Next, the cross-sectional width of the ice ridge was estimated at 500 m intervals, and Figure 41 that the width varied between 150 and about 550 m.

Figure 40. Elevation profile across the transect depicted in Fig. 39.

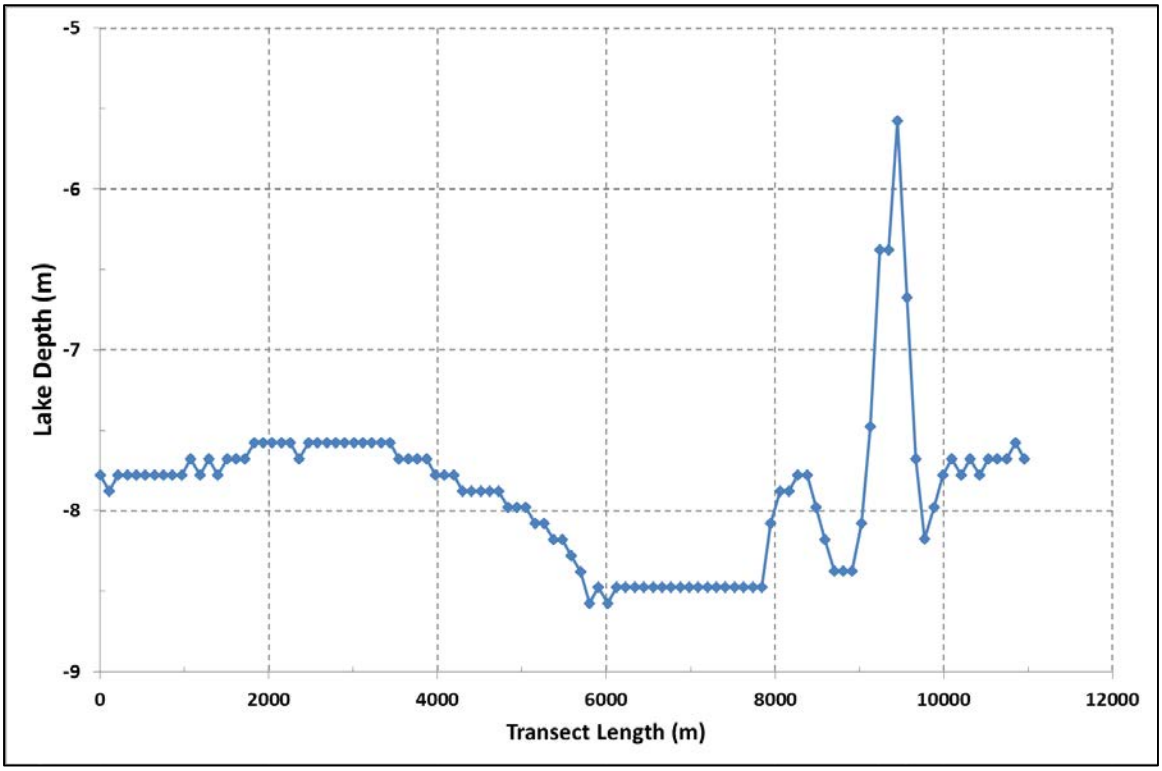

Figure 41. Cross-sectional widths across the ice-ridge feature estimated every 500 m.

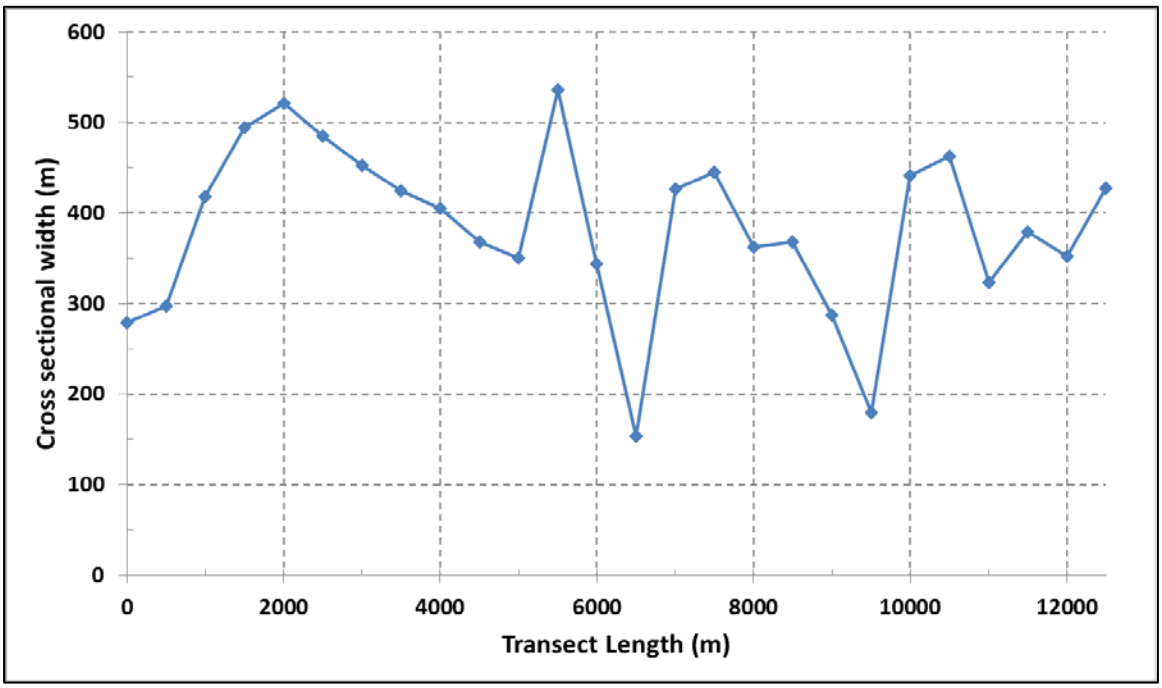

4.3 Summary

Commercially available, satellite-based SAR imagery (TerraSAR-X) was acquired over Lake Erie during February and March 2015. Based on the time series of satellite images acquired offshore Erie, PA, a linear feature potentially representing an ice ridge was immediately apparent in each of the images. Over the 33-day period that spanned the three satellite acquisitions, the location of this feature did not move though ice surrounding this linear feature had moved. The estimated length of this feature was approximately 12 km. Determined using existing bathymetry of Lake Erie, the lake depths across the 12 km range from 5 to 9 m. The cross-sectional width of the ice ridge estimated at 500 m intervals varied between 150 and about 550 m. At that time of this publication, this is the first satellite based evidence of ice ridges in Lake Erie.

5 Estimated Properties of Lake Erie Ice Ridges

5.1 Introduction

Ice ridges are a common feature in ice-covered oceans and seas. They are found in the Arctic Ocean, where they have been well documented in the Beaufort Sea, and in more temperate regions, including the Labrador Sea, Baltic Sea, Northumberland Strait, and the south Bering Sea (Timco and Burden 1997). The ridges form when the ice cover moving under the action of winds and currents encounters stationary ice. The moving ice fractures and piles on and up against the stationary ice cover. The volume of piled ice above the waterline is termed the *sail*; the volume of ice below the waterline is the *keel*. Typical ratios of keel depth to sail height are 4.5 for first-year ridges (Timco and Burden 1997). Once the ridge has formed, further exposure to frigid air causes the interstitial water between the broken ice pieces to freeze, forming a *consolidated layer*.

Ridges can be large, formidable presences in ice-covered waters. Once ice ridges form, they can move under the influence of wind and currents; and when they collide with structures, they can generate large loads on the structures. The type of ridge; the dimensions and properties of the ridge sail, keel, and consolidated layer; and the dimensions and design of the structure will determine the load. In the Arctic, there are two general types of ridges determined by their age: *first-year* and *multi-year* ridges. In Lake Erie, all the ice melts out every summer; so only first-year ridges are possible. The interaction of first-year ice ridges and structures has been described by Timco et al. (2000). They divided structures into two broad classes: *wide* and *narrow*. Wide structures have waterline widths on the order of 100 m and are primarily offshore structures used for oil production. Narrow structures have waterline widths of 10 m or less and include some lighthouses, bridge piers, some oil production platforms, and wind turbine towers. The various failure modes of first-year ice ridges interacting with narrow structures have been observed for the piers of the Confederation Bridge, located in the St Lawrence River in Canada; Cook Inlet platforms in Alaska; and against lighthouses located in the Baltic Sea.

There is conclusive evidence that ice ridges form in Lake Erie and that their keels can be 25 m deep or more. Most of the evidence is indirect and consists of ice scours in the lake bed that were created by the keels of ice

ridges in contact with the bed. Most of the scours were detected during lake-bed surveys made using sidescan sonars or sub-bottom profilers to document the size and depth of the scours along proposed pipeline or cable crossings of the lake. The water depth in which the scours were detected was provided for 210 scours in the C-CORE (1999) summary. These observed water depths *do* provide some information on the possible range of the maximum keel depths of ice ridges formed in Lake Erie. As will be shown below, this information can be useful for evaluating the applicability of different approaches for estimating the ice-ridge keel depths.

The large loads that ice ridges pose to wind turbine towers in Lake Erie result from the collision of a moving ice ridge and a tower. There is currently not sufficient information on the ice conditions in Lake Erie to define the likelihood of a collision. However, it is possible to estimate the risk of given ridge properties if a collision should occur. The important ridge properties are the consolidated-layer thickness and the keel depth as they both strongly influence the magnitude of the load. This report estimates the annual probability of occurrence of a given consolidated-layer thickness and given keel depth based on the time series of their annual maximums. The time series are calculated for each year from 1973 to 2013 based on the available information on the ice cover of the lake and the meteorological conditions. Each property is calculated separately.

5.2 Evidence of Lake Erie ice ridges

The many ice scours detected in the bed of Lake Erie compose the majority of evidence for ice ridges in Lake Erie. Ice scours have been found in the sea floor in many areas of the globe, such as in the Beaufort Sea in the Arctic Ocean (Weeks et al. 1983) and off of Antarctica (Barnes and Lien 1988). Ice scours have been dated to the pre-Pleistocene and Pleistocene Epochs (Eden and Eyles 2001) and are formed in bodies of water where the keels of ice ridges or ice bergs contact the bed. In general, it is assumed that the gouge is created by the motion of the ice-ridge keel, which is imparted through the influence of wind and water currents on the ridge. The design and protection of petroleum pipelines buried in the seabed has been the primary driver of research into ice scours, particularly in the Beaufort Sea.

Two proposed lake crossing projects, never constructed, collected data on ice scours in the bed of Lake Erie. The first was Ontario Hydro's 1980 proposal for construction of a high-voltage transmission cable system across the eastern basin of Lake Erie (Grass 1983). Surveys of the lake bed were

conducted in 1981 and 1982, and helicopter surveys of the ice conditions supported this project. The second investigation was for the Millennium Pipeline Project, a natural-gas pipeline proposed to cross Lake Erie in an excavated trench. In 1997, Racal-Pelagos conducted surveys of the pipeline route as did Canadian Seabed Research (CSR) in 1998 (described in C-CORE 1999). C-CORE (1999) collected most of the available survey data, including the data from the Ontario Hydro study. The C-CORE report lists a total of 210 scours. Lever (2000) reviewed the Millennium Pipeline Project to determine the potential for pipeline damage by ice scours. They also included data from an unpublished survey of the lake bed that had been conducted by the U.S. Geological Survey (USGS). The USGS survey, while mentioned, was not described in detail in the C-CORE (1999) study. To develop a probability of exceedance for the ice scour depth into the lakebed, Lever (2000) analyzed only ice scours in or near the proposed Millennium Pipeline route that were deemed "recent." That assessment also excluded ice scours with no discernible scour depths into the lake bed, which eliminated a number of the detected scours. This discrimination by Lever (2000) resulted in 112 scours. Of those, 16 scours were included in both studies; and a total of 306 separate scours were enumerated between both studies (Table 10).

Table 10. Ice-scour surveys.

Survey		Number of Ice Scours	
		C-CORE (1999)	Lever (2000)
Racal-Pelagos Survey 1997		19	0
Ontario Hydro Surveys	Ice Island 1982	1	0
	Coho 1981–82	32	8
	Nanticoke 1981–82	51	0
USGS Survey 1995		Not listed	96
CSR Survey 1988		107	8
Total		210	112

The most detailed, currently available data is from the Coho and Nanticoke surveys conducted by Ontario Hydro in 1981 and 1982. The C-CORE (1999) report detailed these surveys' data collected on scour location, scour widths, the depth of water in which the scour occurred, and the depth of the scour into the lake bed. These surveys used side-scan sonar and echo sounding equipment. The Coho Survey was near the southern end of the proposed crossing near the Pennsylvania shoreline, and the

Nanticoke Survey was near the northern end of the proposed crossing. Figure 42 shows the locations of the ice scours detected in the surveys. The ice scours were discovered in 13 to 25 m of water, were approximately 4.5 to 6 km long, were 60 to 100 m wide, and were gouged up to 2 m deep into the lakebed. Information on scour widths, the depth of water, and the depth of the scour in the lake bed was also available for the Racal-Pelagos and CSR Surveys (C-CORE 1999) Water depth information was not available for the USGS Survey.

Figure 42. The location of ice scours detected in the Ontario Hydro Surveys (data from C-CORE 1999).

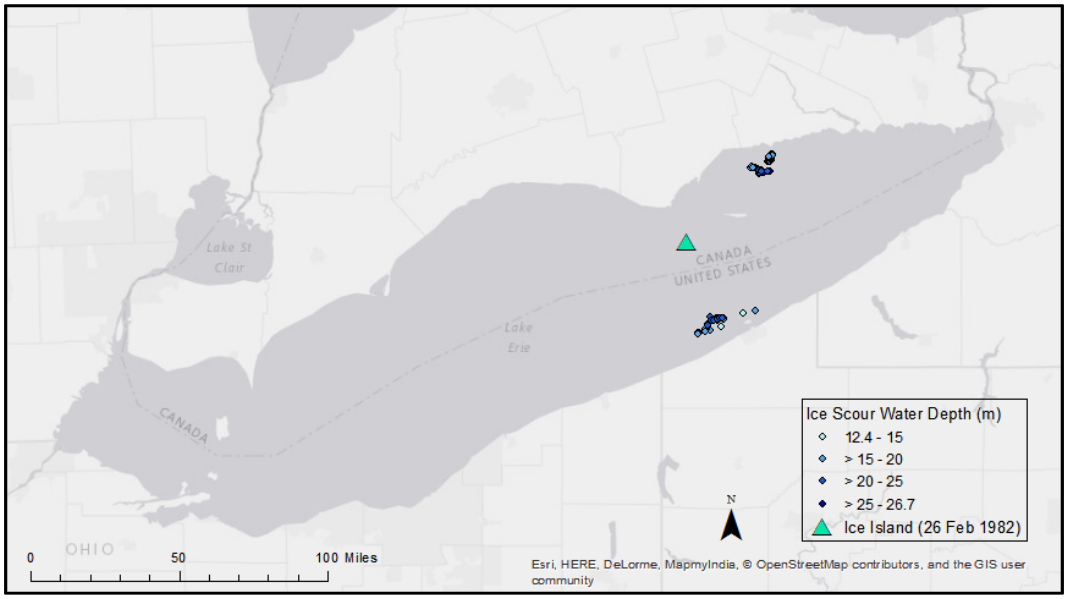

Figure 43 shows the water depths in which the scours were detected for the Ontario Hydro, Racal-Pelagos, and CSR Surveys. Most of the scours were detected between 17 and 21 m of water depth, with a minimum of 6.75 m and a maximum of 26.7 m; and all were detected within about 16.5 km (10 miles) of shore. These observed water depths provide little insight into the rate of ridge formation or the spatial distribution of ice-ridge occurrence. The rate of ridge formation could not be estimated because the age of the scours was difficult to determine beyond categorizing them as “old” or “new” based on qualitative estimates of sediment deposition in the scour trenches. The spatial distribution throughout the lake cannot be estimated because the surveys concentrated on the proposed routes of the lake crossings and were not designed to provide insight into the general lake conditions. However, this information does provide some information on the approximate depth of the bottom of the ice-ridge keels that created the scours. The actual keel depths were probably a little deeper than the water

depths in order to create the scours in the sediments of the bed. Given that the scour depths were usually much less than 1 m, the error in using the recorded water depths to approximate the keel depths is small. These observed water depths *do* provide some information on the possible range of the maximum keel depths of ice ridges formed in Lake Erie. As will be shown in the following sections, this information can be useful for evaluating the applicability of different approaches for estimating the ice-ridge keel depths.

Figure 43. Water depths of detected ice scours (data from C-CORE 1999).

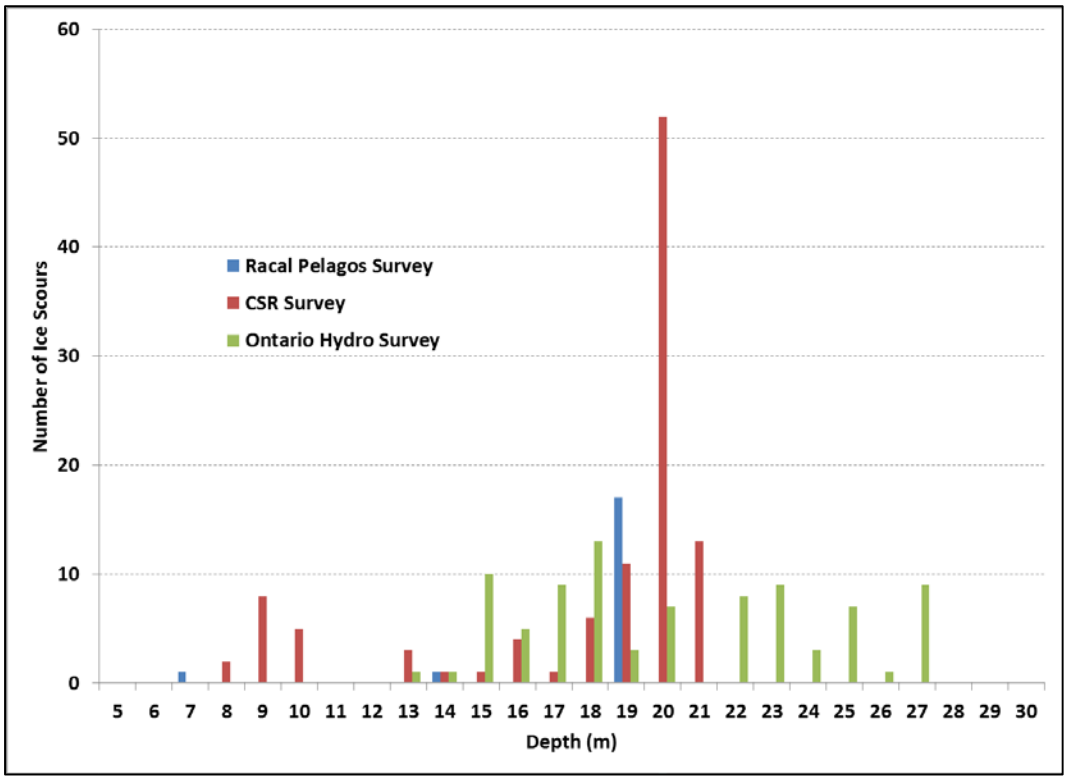

In addition to the surveys of the lake bottom, Ontario Hydro also conducted a helicopter-supported ice observation program in the eastern part of the lake during the winters of 1980–81 and 1981–82 (Grass 1983). On 26 February 1982, a helicopter survey observed an ice ridge (referred to as an ice island) estimated to be 100 m wide and 250 m long. Figure 42 shows the location of the ice island. This ice ridge was observed during its formation as the surface ice to the west of the ridge was moving "quite rapidly" eastwards under strong westerly winds. As described by Grasse (1983),

> The ice island was acting as a barrier to the moving ice mass with the result that a lee side slot was being cut out of the lake ice forming a large tear drop shaped open water area at the east end of the island. The island was oriented with its long axis in an eastwest direction. On the windward side of the island the flat ice sheet was moving and colliding with the island causing the ice to break and pile up into a 2–3 m high ridge. . . . The moving ice sheet was also being driven down beneath the ice ridge to help form the deep ice keel. . . . Bottom mud was observed being churned up into the water column by the action of the descending ice blocks.

Later that same year, during the open-water season, a bottom survey was conducted in the area of the ice island. The ice scour found was 2.5 km long, 30 m wide, up to 1.5 m deep, and located in 16 m to 20 m of water. In this case, the ice scour had been created during the ridge formation and not due to ridge motion.

It is interesting to review the lake ice-cover information immediately before and after the ice island formed. Figure 44 shows the Lake Erie ice conditions on 23 February 1982. This is the nearest date with ice information available prior to the formation of the ice-island ridge. The entire lake was covered by an ice-cover concentration of 90% or higher at that time. The next date when ice information was available was 03 March 1982 (Figure 45). A long, narrow area near the northern shore of the lake had significantly reduced ice concentration at this time. It is likely that the strong winds and moving ice observed during the formation of the ice-island ridge led to the areas of lower ice concentration.

Figure 44. Lake Erie ice cover conditions for 23 February 1982 before the formation of the ice island on 26 February 1982.

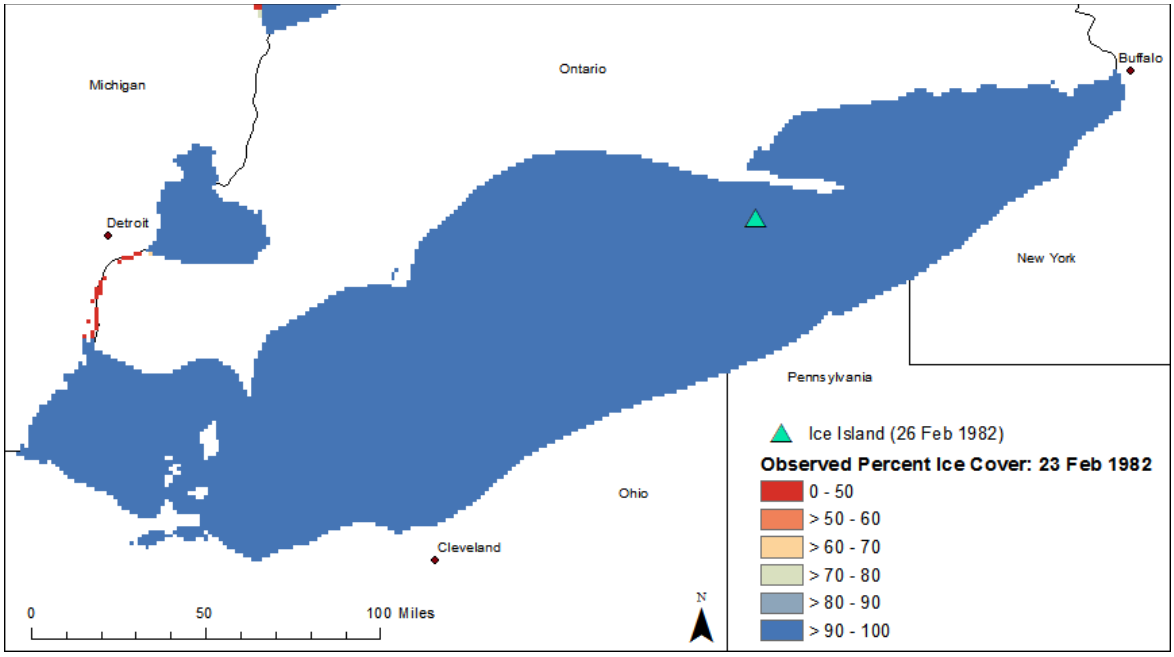

Figure 45. Lake Erie ice cover conditions for 3 March 1982 after the formation of the ice island on 26 February 1982.

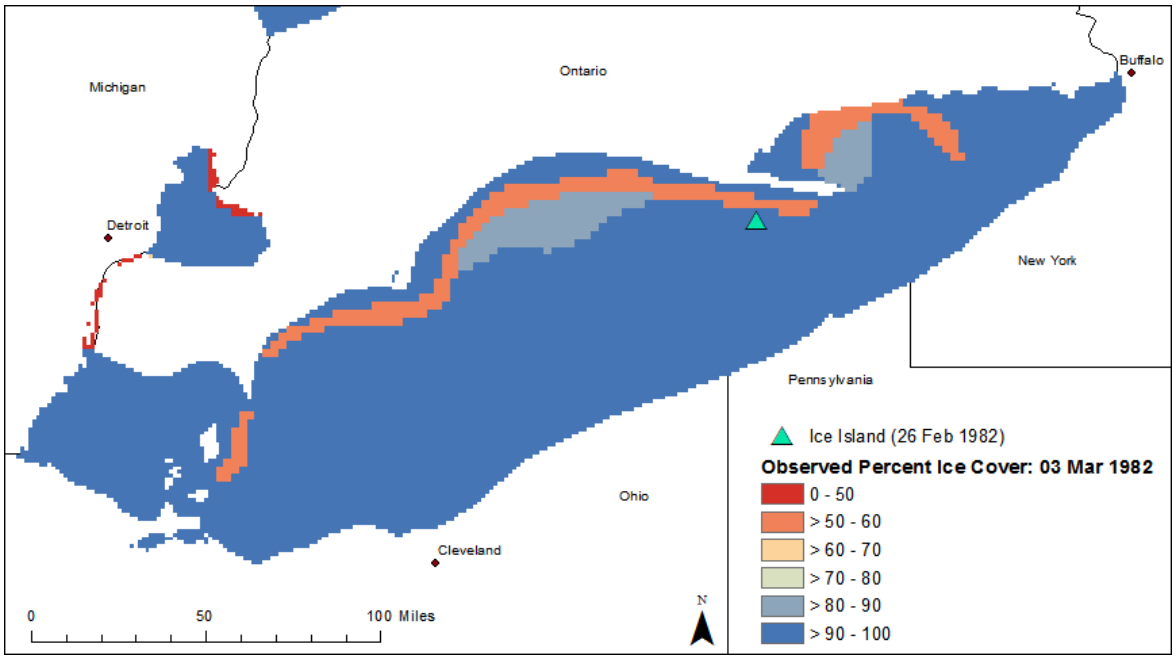

5.3 Ridge formation in oceans and seas

There are two broad classes of ridges determined by their age: *first-year* and *multi-year* ridges. Only the first-year ridges are of interest to this

study as no ice ridge in Lake Erie lasts longer than one winter season. Burden and Timco (1995) created a detailed catalogue of the geometries of 112 first-year ridges described in 22 different studies. All of these ridges were formed in salt water as there has been no systematic study of ridge formation in fresh-water to date.

The process of ice-ridge formation has also been the focus of study, either based on field observations (Palmer and Croasdale 2013; Melling and Riedel 1996; Tucker et al. 1984) or through numerical modeling (Hibler 1980; Hopkins 1998). Hopkins (1998) used a highly detailed discrete element model to numerically simulate the formation of ice ridges in the Arctic. He described four stages of ridge formation. In the first stage, an intact sheet of surface ice is pushed against stationary ice. In Lake Erie as in the oceans, it is the wind drag on the surface-ice cover that provides the impetus to push the intact surface ice into the ridge. Hopkins' results indicated that the thickness of the immovable ice did not affect the final ridge geometry. As the intact sheet of surface ice collides with the stationary ice, it fails, either in flexure or by buckling, creating rubble blocks that accumulate to form the ridge structure. The first stage ends when the sail reaches its maximum height. The second stage, in which the ridge keel grows wider and deeper, ends when the maximum keel draft is reached. In the third stage, the continual addition of surface ice causes the keel to widen, creating a rubble field of more or less uniform thickness. The third stage ends when the supply of surface ice is exhausted. In the fourth stage, the rubble field is compressed by converging floes. In Lake Erie, the study is concerned with only the first two stages, which determine the maximum depth of the ice-ridge keel. It is not clear that the fourth stage ever occurs in the Great Lakes.

How much of the current understanding of ice ridge formation in the oceans can be applied to ice-ridge formation in Lake Erie given the differences between the material properties of sea ice and freshwater ice? To approach this question, it is best to view ridge formation as a mechanical process and to determine how the difference in material properties would affect each component of the process. Overall, ridge formation is a process in which the work done by the force transmitted through the moving surface-ice cover is dissipated through friction, inelastic contacts, and the change in potential energy of the surface ice (Hopkins 1998). Surprisingly, the differences in the material properties of sea ice and freshwater ice probably do not significantly impact the dissipative processes. Frictional

dissipation through ice-on-ice contact is the largest sink of energy, accounting for roughly 80% or more of the total energy dissipated (Hopkins 1998). There is unlikely to be significant differences for frictional dissipation given that the ice-on-ice friction coefficients of sea ice and freshwater ice are quite similar (Kennedy et al. 2000; Fortt and Schulson 2011) and that snow often covers the surface-ice in both cases. The changes in potential energy and inelastic contacts each account for less than 10% of the work done in creating the ridge (Hopkins 1998). The change in potential energy results from gravity acting on the ice pushed into the ridge sail and from buoyancy acting on the submerged ice pushed into the ice-ridge keel. Field measurements of the density of first-year sea ice range from 840 to 910 kg m^{-3} for ice above the waterline (Timco and Frederking 1996), which is within 10% of the density of freshwater ice, 920 kg m^{-3}. The buoyancy of the submerged ice results from the density difference between the ice and liquid. The density of sea ice below the water line ranges from 900 to 940 kg m^{-3} (Timco and Frederking 1996), and the density of seawater is roughly 1029 kg m^{-3}, which results in a ratio (specific gravity) of 0.89 to 0.91 compared to the specific gravity of freshwater ice of 0.92. It is difficult to determine how the third dissipative process, that resulting from inelastic contacts, would vary between freshwater and sea ice given the "lack of knowledge of the rheological behavior of sea ice" (Timco and Weeks 2010). However, differences are not likely to be significant given the relatively small contribution of inelastic dissipation to the overall dissipation during ridge formation.

While the differences in the material properties of sea ice and freshwater ice probably do not significantly affect the dissipative processes, they can impact the work that the moving surface-ice cover can accomplish. The flexural strength of freshwater ice is about three times greater than the flexural strength of sea ice as will be discussed below. This greater flexural strength would allow larger forces to be transmitted through the freshwater surface-ice cover driven into the ice ridge as compared to a sea ice cover of the same thickness. This suggests that the current understanding of ice-ridge formation in the oceans can be applied to the freshwater ice conditions of Lake Erie if the difference in flexural strength of the surface-ice cover is accounted for.

5.4 Ice-ridge formation in Lake Erie

This section applies to Lake Erie the understanding gained from ice-ridge formation in the oceans. This section will concentrate on the two aspects

of ice ridges that control the influence of the ridge on structures: the thickness of the consolidated layer and the maximum keel depth. This section will determine the annual likelihood of a given consolidated-layer thickness and a maximum keel depth based on the available historical data, which consists of two parts. The first part is the ice charts that indicate the period of time each winter for 1973–2013 when at least a portion of the lake surface was covered by ice (NIC 2015). These are also the periods when ice ridges are possible, as ice ridges form only when surface ice is present. The second part is the recorded meteorological conditions during these time periods, especially the AFDD (NOAA 2015). The recorded AFDD during these periods allow both the surface-ice thickness and the consolidated-layer thickness of the ice ridges to be estimated. The maximum keel depth of the ice ridges is estimated based on the estimated surface-ice thickness by using a modified form of Equation (5), as described below.

Figure 46 shows the period of each of the recorded winters when there was ice. This data was described earlier and is based in the ice charts developed by NIC. On average, there were 122 days with ice. The minimum number of days was 49, recorded in the winter of 1997–98; the maximum number of days was 153, recorded in the winter of 1991–92. The first ice generally appears in December, and the last melts out in April. In some years, the ice can completely melt away and then reform.

The areas where ice ridges form in Lake Erie is not known with any certainty, nor is the likelihood of the ice ridge moving under the influence of wind and water currents. The AFDD for each winter season are therefore estimated for the entire lake area based on an average of the meteorological stations available on each day. Figure 47 shows the recorded AFDD for each winter season.

Figure 46. Periods of ice on Lake Erie for each winter.

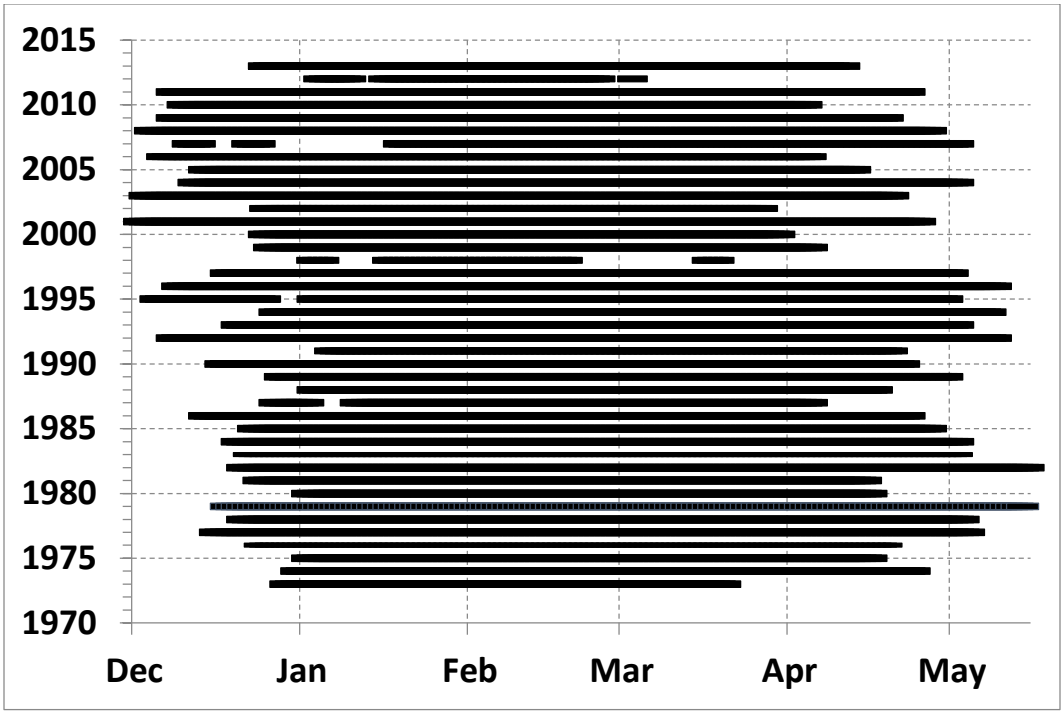

Figure 47. The AFDD recorded during each ice-covered period.

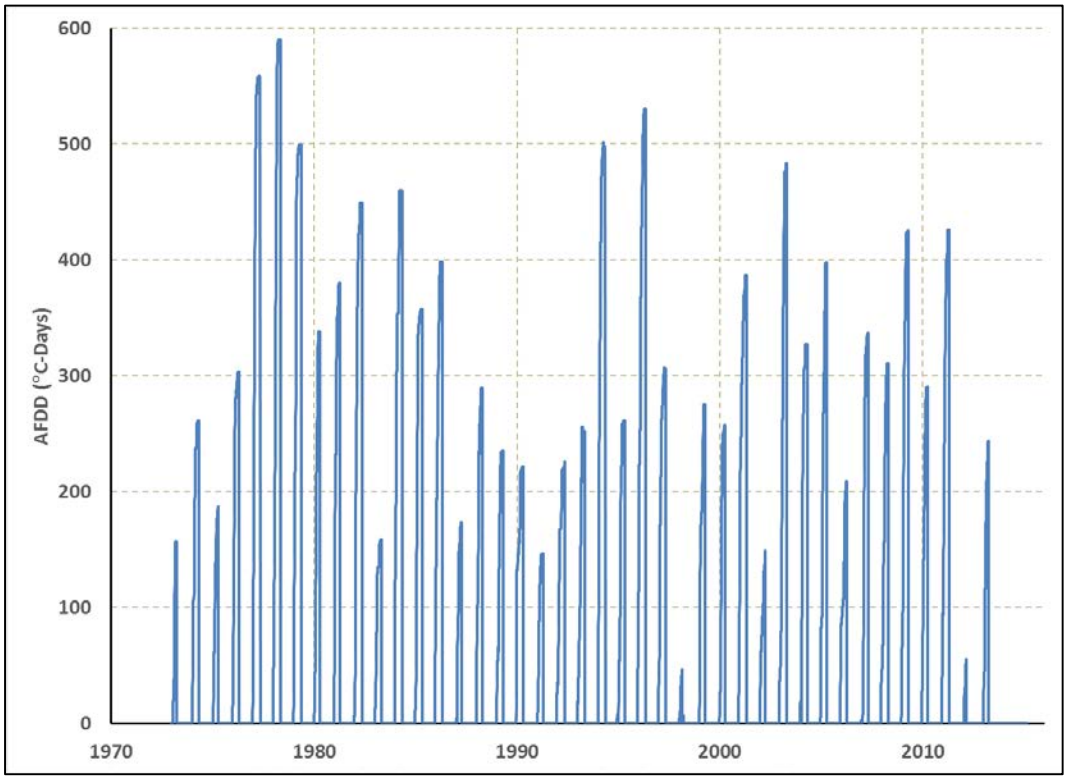

5.4.1 Consolidated-layer thickness

Immediately after the ice ridge forms, the keel of the ridge consists of broken ice pieces and liquid water. The water that fills the interstitial spaces between the broken ice pieces in the keel loses heat to the frigid air, which leads to the creation of a *consolidated layer* of solid ice. Hoyland (2002a) presents a good description of the process of ice-ridge consolidation in the ocean. There are two basic approaches that previous studies have used to estimate the growth of the consolidated layer. The first is analytical and represented best by Lepparanta and Hakala's (1992) modifications of the Stefan equation to account for the porosity of the keel. The second approach is numerical and involves estimating the heat transfer from the keel to the atmosphere by using a multi-dimensional heat conduction model. The numerical solutions require detailed descriptions of the keel geometry, either based on field surveys (Hoyland 2002b) or conceptual models of ridges (Marchenko 2008). Numerical approaches have also proven useful to address the impacts of salinity on the growth of the consolidated layer (Shestov and Marchenko 2014; Marchenko 2008). Given that the salinity is not an issue in Lake Erie and that there is only indirect evidence of the ice-ridge geometry, the Lake Erie study will use the analytical approach of Lepparanta and Hakala (1992) to estimate the consolidated-layer thickness of ice ridges.

The consolidated layer initially forms at the water surface and proceeds downwards. The growth rate of the consolidated layer can be faster than the growth of surface ice because the keel contains ice and only the interstitial water must freeze. The growth rate of the consolidated layer can be estimated by accounting for the porosity of the keel:

$$\frac{\partial \eta_c}{\partial t} = \frac{k_i}{\rho_i \lambda_i p_0} \frac{\left(T_m - T_s\right)}{\eta_c} \tag{7}$$

where

η_c = the thickness of the consolidated layer;
t = time;
k_i = the thermal conductivity of the ice;
ρ_i = the ice density;
λ_i = the latent heat of fusion of the ice;

p_0 = the porosity of the keel (expressed as a fraction between 0 and 1);
T_m = the ice/water interface temperature (0°C); and
T_s = the surface temperature.

Solving Equation (7) arrives at a modified form of the Stefan equation:

$$\eta_c = \frac{\alpha}{\sqrt{p_0}}\sqrt{AFDD_2} \tag{8}$$

where $AFDD_2$ = the AFDD recorded after the ridge formed; α, which is theoretically equal to

$$\alpha = \sqrt{\frac{2k_i}{\rho_i \lambda_i}} \tag{9}$$

is, in practice, usually less than this theoretical value.

There are a number of observations of the porosity of first-year ice ridges in the Baltic Sea (Lepparanta and Hakala 1992; Kankaanpaa 1988, 1989). Table 11 summarizes these observations. These studies sampled a total of 15 ridges. Note that the measurements of Kankaanpaa (1988) were six cross sections of a single ridge. A reasonable value to use for the porosity of ice ridges in Lake Erie, based on these three studies, would be 29.4%.

Table 11. Ice-ridge keel porosity field measurement.

Lepparanta and Hakala (1992)							
	Ridge Number						
	1	2	3	4	5	6	Average
Keel porosity (%)	30	23	28	32	33	28	29
Kankaanpaa (1988)							
	Cross Sections in a Single Ridge						
	A	B	C	D	E	F	Average
Keel porosity (%)	21.2	32.3	31.6		29.6	22.1	27.4
Kankaanpaa (1989)							
	Ridge Number						
	RI	R2	RJ	T	A	SI	S2	SJ	Average
Keel porosity (%)	22	37	34	29	24	28	32	33	30
Overall Average Porosity (%)									29.4

The period each winter when surface ice existed on the lake, which is known from the NIC Ice Charts and is shown in Figure 46, determines when ice ridges could potentially form. While this period defines the maximum time each winter when ridges might have occurred, it is only when the required combination of wind drag, ice-cover fetch length, competent ice, and ice-cover strength coincided that ice ridges do, in fact, occur. It is not possible at this time to make a reasonable determination of the specific time or times when the required combination of factors did occur in any winter. Rather, our study assumes that an ice ridge formed on the first day that the ice cover was in place as indicated by the NIC ice charts. This approach leads to an estimate of the maximum possible consolidated-layer thickness that could form during each winter.

Estimating the consolidated-layer thickness that formed each winter used Equation (8) above with a value for α, estimated previously for thermal growth on Lake Erie of 2.39 cm (°C-Day)$^{-1/2}$, a keel density of 29.4% (Table 11) taken from measurements of first-year ice ridges in the Baltic Sea (Lepparanta and Hakala 1992; Kankaanpaa 1988, 1989), and the value of $AFDD_2$ equal to the AFDD recorded during the entire period each winter the ice cover was in place (Figure 47). For winters in which the ice cover melted out more than once, the AFDD recorded for each ice cover period were estimated, and then the consolidated-layer thickness was calculated by using the period with the maximum recorded AFDD. Table 12 lists the maximum value of $AFDD_2$ recorded each winter season. Table 13 lists the maximum consolidated-layer thicknesses for each winter season for each year of the period of recorded.

Table 12. Extreme values of the consolidated-layer thickness.

Annual Chance Exceedance (%)	Return Period (years)	Consolidated-Layer Thickness (m)
1	100	1.17
2	50	1.11
5	20	1.03
10	10	0.96

Table 13. Estimation of annual maximum ice-ridge consolidated-layer thickness.

Winter	Earliest Date of Ridge Formation	$AFDD_2$ (°C-Days)	Consolidated thickness (m)
1973	29-Dec-72	243.1	0.68
1974	1-Jan-74	257.6	0.70
1975	4-Jan-75	188.5	0.60
1976	23-Dec-75	303.0	0.76
1977	16-Dec-76	558.6	1.03
1978	18-Dec-77	589.9	1.06
1979	24-Dec-78	475.4	0.95
1980	2-Jan-80	337.9	0.80
1981	24-Dec-80	375.7	0.85
1982	21-Dec-81	448.8	0.92
1983	21-Dec-82	158.6	0.55
1984	20-Dec-83	459.9	0.94
1985	23-Dec-84	357.1	0.82
1986	14-Dec-85	400.5	0.87
1987	11-Jan-87	173.2	0.57
1988	3-Jan-88	278.3	0.73
1989	25-Dec-89	235.5	0.67
1990	17-Dec-89	221.1	0.65
1991	6-Jan-91	146.5	0.53
1992	8-Dec-91	220.3	0.65
1993	20-Dec-92	241.4	0.68
1994	27-Dec-93	477.0	0.95
1995	3-Jan-95	261.2	0.71
1996	9-Dec-95	530.5	1.01
1997	18-Dec-96	305.7	0.76
1998	14-Jan-98	46.0	0.30
1999	26-Dec-98	268.3	0.71
2000	25-Dec-99	257.3	0.70
2001	2-Dec-00	386.9	0.86
2002	25-Dec-01	149.8	0.53
2003	3-Dec-02	483.3	0.96
2004	6-Jan-04	327.3	0.79
2005	14-Dec-04	397.6	0.87
2006	6-Dec-05	208.7	0.63
2007	16-Jan-07	336.3	0.80
2008	4-Dec-07	310.3	0.77
2009	8-Dec-08	425.2	0.90
2010	10-Dec-09	290.6	0.74
2011	8-Dec-10	425.8	0.90
2012	16-Jan-12	56.5	0.33
2013	25-Dec-12	244.7	0.68

Next, the extreme values of the annual maximum consolidated-layer thickness were estimated based on the values listed in Table 13. The extreme-value analysis of the annual maximum series of the consolidated-layer thicknesses assumed a lognormal distribution. The method of moments was used to fit the lognormal distribution to the annual maximum series in the HEC-SSP Program (USACE 2010) by using the procedures described in Bulletin #17B (USGS 1982). Weibull plotting positions were used and the computed probability found. The threshold procedure described in Bulletin #17B was used to detect outliers, all of which were for anomalously warm winters with relatively low values of consolidated-layer thicknesses. Outliers were not included in the analysis. The extreme value results for the consolidated layer are listed in Table 12 and are shown in Figure 48.

Figure 48. Extreme values of the consolidated-layer thickness.

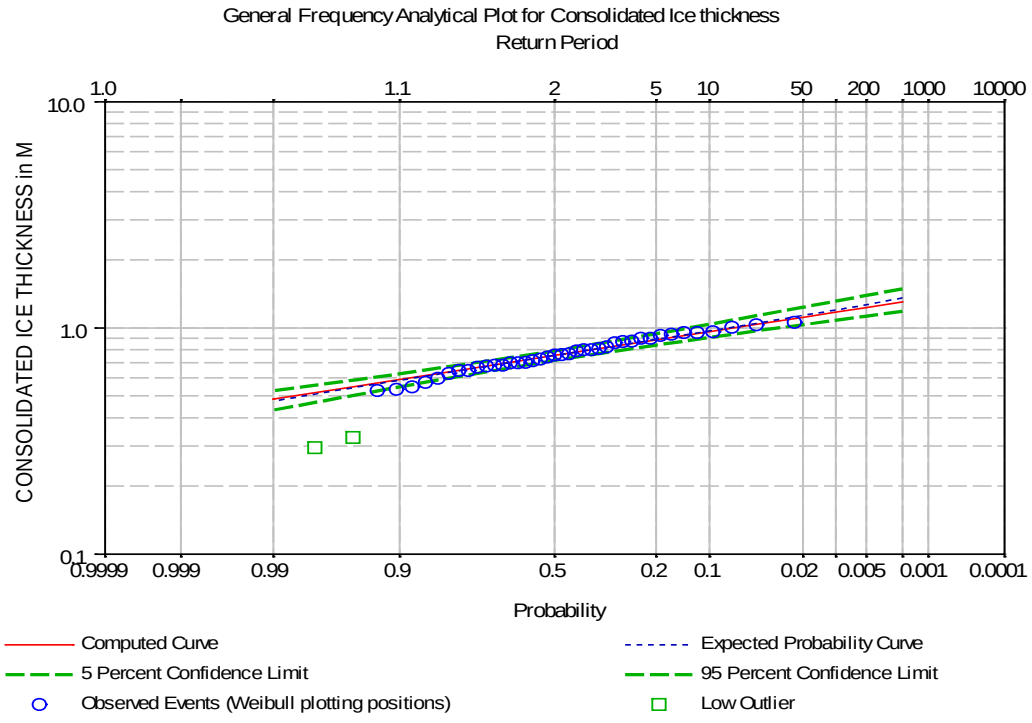

5.4.2 Bounds on maximum keel depth

Observations of ridge keel depths in the ocean have shown that the maximum keel depth is bounded (Amundrud et al. 2004, Melling and Riedel 1996; and Kankaanpaa 1989) and that the magnitude of the bound is proportional to the square root of the surface-ice thickness. This relationship was described by Hopkins (1998), who suggested that the maximum height of a ridge sail is reached when the force needed to push another ice

block beyond the top of the ridge exceeds the force that will buckle the level ice next to it. If the force exceeds the buckling limit, the surface-ice cover will fracture away from the ice ridge, forming rubble ice but not a ridge. In a similar fashion, the maximum ridge keel depth is also limited by the buckling limit of the floating ice. The stress required to buckle an ice sheet is proportional to the square root of the ice thickness (Kovacs and Sodhi 1980; Tucker et al. 1984; Amundrud et al. 2004).

Field observations of ice-ridge keel depths and ice-cover thickness (Amundrud et al. 2004; Melling and Riedel 1996; and Kankaanpaa 1989) display a relationship between the bound on the maximum keel depth and the surface-ice thickness of the form:

$$H_{Ksimax} = c_{si}\sqrt{\eta_{si}} \tag{10}$$

where

$_{max}$ = the maximum keel depth for sea ice;
c_{si} = an empirical coefficient; and
η_{si} = the surface sea-ice thickness.

Previous studies used field observations and numerical simulations to estimate the value of the coefficient of proportionality, c_{si}. Melling and Riedel (1996) estimated its value at 16 $m^{1/2}$ and Amundrud et al. (2004) at 20 $m^{1/2}$ based on field observations in the Arctic, while the data of Kankaanpaa (1989) collected in the Baltic Sea provided an estimate of 12.2 $m^{1/2}$. The numerical simulations of Hopkins (1998), conducted over a range of surface-ice thicknesses, in general tended to support Melling and Riedel's (1996) estimation of c_{si}. It must be noted that Equation (10) is a bound for the maximum keel depth and that field measurements most often found keel depths less than this value. Amundrud et al. (2004) described the condition required for the ridge to reach the bound value: there must be sufficient contiguous surface ice to provide the raw material for the ridge; the stress developed by the wind and/or current drag must cause failure of the ice; and finally, the critical stress must last long enough to complete building the ridge.

A relationship of the form of Equation (10) with the values of c_{si} suitably modified could likely be applied to estimate the bounds on maximum keel depths of ice ridges formed of freshwater ice. This modification could be

done in several ways; probably the most direct approach is to use a freshwater ice thickness in Equation (10) that provides the same flexural strength as a given sea-ice thickness. Unfortunately, it is difficult to simply characterize the flexural strength of ice, either freshwater ice or sea ice, as it depends on a number of factors, including temperature; the loading direction on the ice; the ice grain structure; the grain size; the test type (cantilever or simple beam); the loading rate; the beam size; and, for sea ice, the ice salinity and brine volume. (See Timco and Weeks [2010] for a review of sea ice properties and Timco and Frederking [1982] for a review of freshwater ice properties). A representative flexural strength for sea ice is 0.6 MPa with the understanding that the actual flexural strength may vary. This value falls in the middle of the extensive collection of sea-ice data collected by Timco and O'Brien (1994), which is also presented in Timco and Weeks (2010). The average flexural strength for tests of freshwater ice with the bottom in tension is 1.77 MPa (Timco and Frederking 1982), and this is also the limiting strength of sea ice as the salinity of the ice goes to zero (Timco and O'Brien 1994). As with the value selected for the sea ice flexural strength, this value should be considered representative or typical, with the understanding that the actual flexural strength may vary. Let β equal the ratio of the flexural strength of freshwater ice, σ_f, to sea ice, σ_{fsi}. The value of β is estimated as

$$\beta = \frac{\sigma_f}{\sigma_{fsi}} \approx \frac{1.77\text{MPa}}{0.60\text{MPa}} = 2.95. \tag{11}$$

Equation (10) can now be rewritten as

$$H_{K\,max} = c_{si}\sqrt{\beta\eta} \tag{12}$$

where

$H_{K\,max}$ = the maximum keel depth for ice ridges formed in Lake Erie;
c_{si} = an empirical coefficient taken from observations of ice ridges in the ocean;
η = the surface-ice thickness of Lake Erie.

Equation (12) is restated as

$$H_{K\,max} = c_{fw}\sqrt{\eta} \tag{13}$$

where the factor for seawater, c_{si}, has been modified for freshwater, c_{fw}, and found as

$$c_{fw} = c_{si}\sqrt{\beta}\,. \tag{14}$$

The value of c_{fw} depends on the estimated value of c_{si} that is used. As discussed above, several values for c_{si} have been put forward based on different sets of observations and are listed in Table 14. It is not immediately clear which value would be most applicable to Lake Erie.

Table 14. Values for the empirical coefficient.

Source	c_{si}	c_{fw}
Kankaanpaa (1989)	12.2	21.0
Melling and Riedel (1996)	16	27.5
Amundrud et al. (2004)	20	34.4

This Lake Erie study used the following procedure to estimate the maximum keel depth that formed each winter. First, the maximum surface-ice thickness was estimated for each winter by using the AFDD listed in Table 13 and Equation (8) with α set equal to 2.39 cm (°C-Day)$^{-1/2}$ (this value was estimated previously for thermal growth on Lake Erie) and the porosity set equal to 1. The bound on the maximum keel depth was then calculated using Equation (7) for each of the c_{fw} values listed in Table 14. The maximum keel depths found in this manner for each winter are shown in Figure 49 and listed in Table 15. These results were then compared to the water depths in which the scours were detected (Figure 43) to determine which of the three sets of calculated maximum keel depths were most representative of the conditions in Lake Erie. Figure 50 shows the combined data from the three available surveys and compares them to the range of results of each set of results. It can be seen in Figure 50 that the results based on the data of Kankaanpaa (1989) and Melling and Riedel (1996) tend to be less than the range of keel depths observed in Lake Erie while the results of Amundrud et al. (2004) cover the range of observed keel depths. Given this, the extreme values of the annual maximum consolidated-layer thickness were estimated using the coefficient of Amundrud et al. (2004). As before, the extreme-value analysis was done assuming a lognormal distribution. The method of moments was used to fit the lognormal distribution to the annual maximum series in the HEC-SSP Program (USACE 2010) by using the procedures described in Bulletin

#17B (USGS 1982). Weibull plotting positions were used and the computed probability found. The threshold procedure described in Bulletin #17B was used to detect outliers. All outliers detected were for anomalously warm winters with relatively low values of the maximum keel depths. Outliers were not included in the analysis. The extreme value results for the maximum keel depth are listed in Table 16 and are shown in Figure 51.

Figure 49. Maximum keel depth calculated each winter.

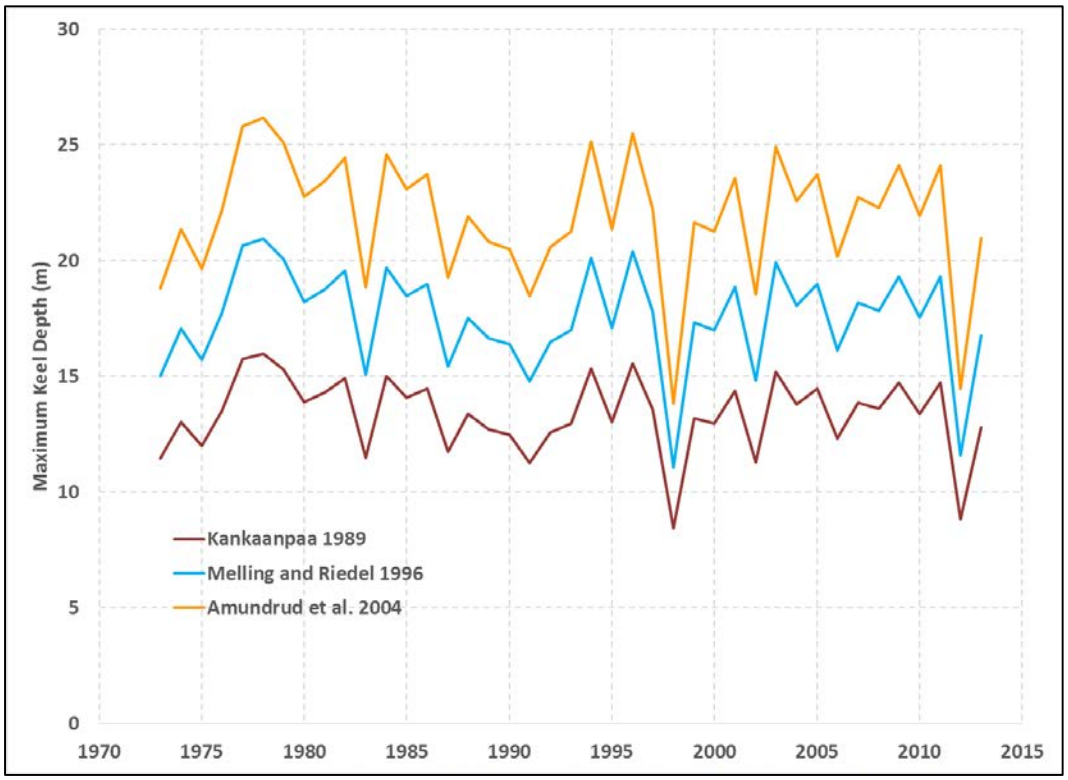

Table 15. Estimates of annual maximum ice-ridge keel depth.

Winter	Maximum Thermal Ice Growth (m)	Maximum Keel Depth (m)		
		Kankaanpaa (1989)	Melling and Riedel (1996)	Amundrud et al. (2004)
1973	0.37	11.5	15.0	18.8
1974	0.39	13.0	17.1	21.3
1975	0.33	12.0	15.7	19.6
1976	0.42	13.5	17.7	22.2
1977	0.57	15.8	20.7	25.8
1978	0.58	16.0	20.9	26.2
1979	0.53	15.3	20.1	25.1
1980	0.44	13.9	18.2	22.8
1981	0.47	14.3	18.8	23.4
1982	0.51	14.9	19.6	24.4
1983	0.30	11.5	15.1	18.8
1984	0.51	15.0	19.7	24.6
1985	0.45	14.1	18.5	23.1
1986	0.48	14.5	19.0	23.7
1987	0.32	11.8	15.4	19.3
1988	0.41	13.4	17.5	21.9
1989	0.37	12.7	16.6	20.8
1990	0.36	12.5	16.4	20.5
1991	0.29	11.3	14.8	18.5
1992	0.36	12.6	16.5	20.6
1993	0.38	13.0	17.0	21.2
1994	0.54	15.3	20.1	25.1
1995	0.39	13.0	17.1	21.3
1996	0.55	15.5	20.4	25.5
1997	0.42	13.6	17.8	22.2
1998	0.16	8.4	11.1	13.8
1999	0.40	13.2	17.3	21.6
2000	0.38	13.0	17.0	21.3
2001	0.47	14.4	18.8	23.6
2002	0.29	11.3	14.8	18.5
2003	0.53	15.2	19.9	24.9
2004	0.43	13.8	18.1	22.6
2005	0.48	14.5	19.0	23.7
2006	0.35	12.3	16.1	20.2
2007	0.44	13.9	18.2	22.7
2008	0.42	13.6	17.8	22.3
2009	0.49	14.7	19.3	24.1
2010	0.41	13.4	17.5	21.9
2011	0.49	14.7	19.3	24.1
2012	0.18	8.8	11.6	14.5
2013	0.37	12.8	16.8	21.0

Figure 50. Observed keel depths and the range of calculated maximum keel depths.

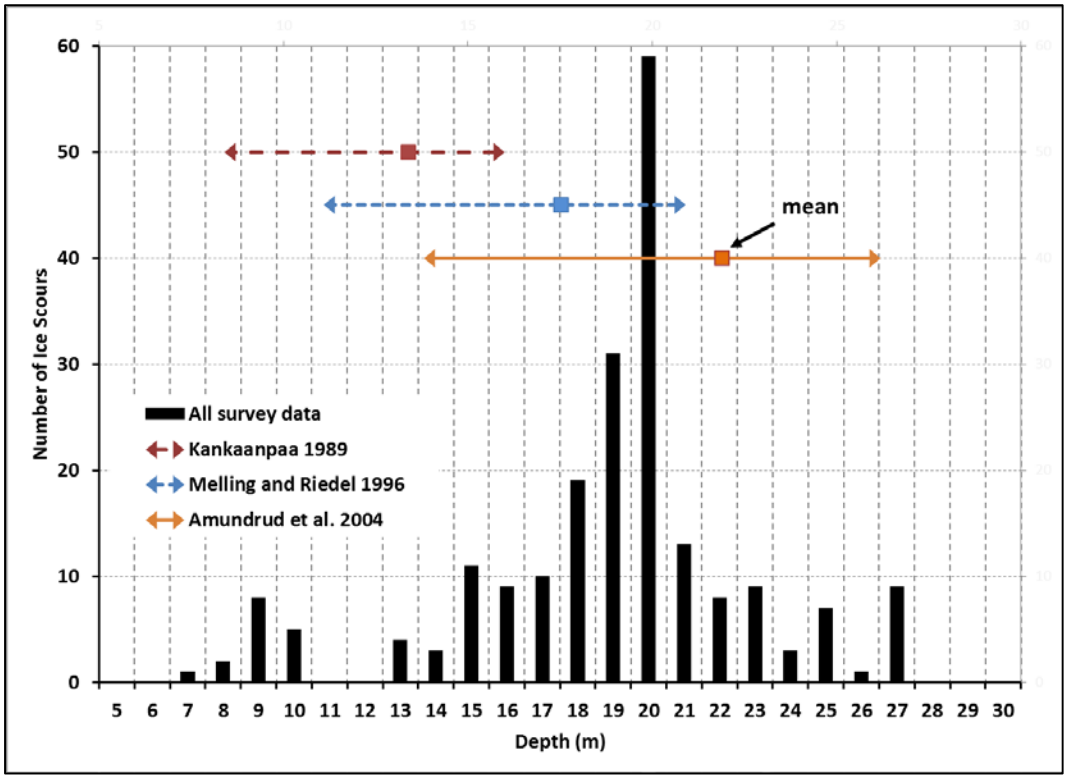

Table 16. Extreme values of maximum keel depth.

Annual Chance Exceedance (%)	Return Period (years)	Maximum Keel Depth (m)
1	100	27.8
2	50	27.0
5	20	26.0
10	10	25.0

Figure 51. Extreme values of maximum keel depth.

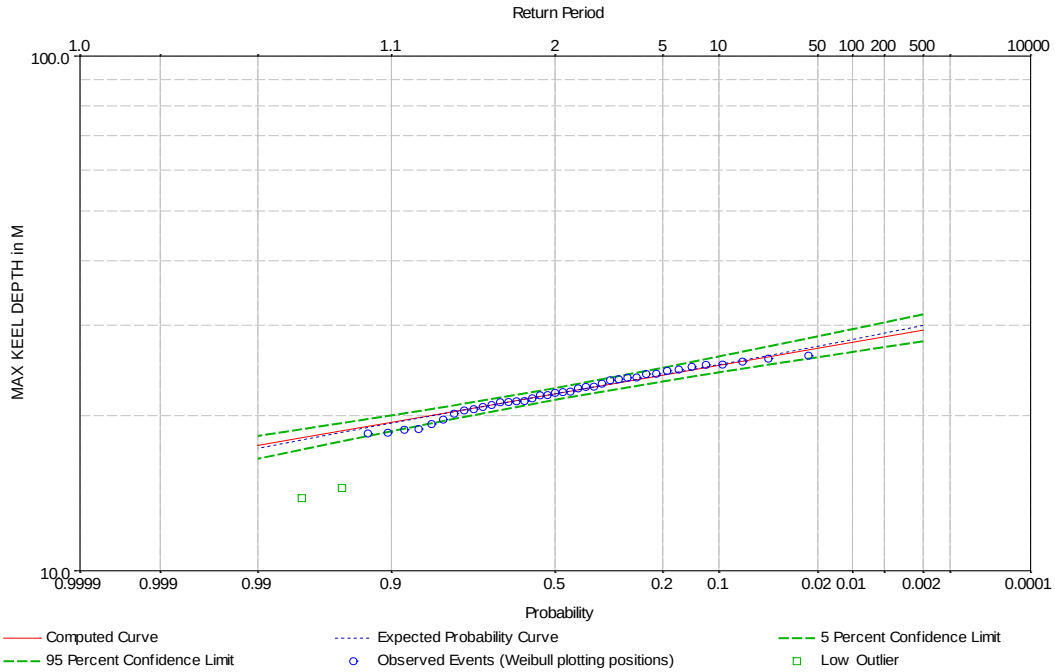

5.5 Summary

There is conclusive evidence that ice ridges form in Lake Erie and that their keels can be 25 m deep or more. Most of the evidence is indirect and consists of ice scours created by the keels of ice ridges in contact with the lake bed.

The water depth in which the scours were detected was available for 210 scours. These observed water depths provide little insight into the rate of ridge formation or the spatial distribution of ice-ridge occurrence, but they *do* provide some information on the possible range of the maximum keel depths of ice ridges formed in Lake Erie. This information was used to evaluate the applicability of different approaches for estimating the ice-ridge keel depths.

The large loads that ice ridges pose to wind turbine towers in Lake Erie results from the collision of a moving ice ridge and a tower. The important ridge properties are the consolidated-layer thickness and the keel depth as they both strongly influence the magnitude of the load.

To estimate the time series of annual maximum consolidated-layer thicknesses, the study first assumed that ice ridges form each winter as soon as the initial ice cover has formed on the lake. Ice ridges that form at this

early point in time experience more frigid air temperatures than ridges that form later in the winter. As a result, these ridges develop the maximum consolidated-layer thicknesses for that winter. The porosity of the ice ridges was based on observations of first-year ridges made in the ocean. The AFDD recorded during the ice-cover period each winter were used to estimate the maximum consolidated-layer thickness for each winter from 1973 to 2013.

Observations made in the ocean show that the surface-ice thickness can be used to estimate a bound for the maximum ice-ridge keel depth. The coefficients of proportionality found for each of the three sets of field observations was modified for Lake Erie to account for the difference between the flexural strength of freshwater ice and sea ice. The AFDD recorded during the ice cover period each winter were used to estimate the maximum surface-ice thickness for each winter from 1973 to 2013, and the bound for the maximum keel depth was determined for each winter by using each of the three estimated coefficients. These results were compared to the water depths in which the ice scours were detected in Lake Erie. The range of estimated keel depths that most closely matched the range of detected scour depths was then used to estimate the extreme values of the bounds of the ice-ridge keel depths.

6 Conclusion

The development of an offshore wind energy industry in Northern Ohio looks to place wind turbines in Lake Erie. The floating lake ice that forms in Lake Erie each winter is a very important consideration for the design of the wind turbine towers and foundations sited in the lake. In this report historical meteorological and surface ice thickness observations, 41 years of ice chart information, and lake-bed surveys of ice scours were used to estimate the characteristics of the Lake Erie ice cover important to the design of offshore wind turbine towers. These characteristics include the expected thickness of the ice cover due to thermal growth, the historical spatial and temporal distribution of the ice cover throughout the winter season; and estimated consolidated-layer thickness and maximum keel depths of ice ridges formed in the lake.

The expected thickness of the ice cover due to thermal growth was estimated using the Stefan equation, calibrated using historical observations of AFDD and ice thickness, which were all made in the 1960s and 1970s. It is very fortunate that these observations exist as apparently none have been made since that time. New ice-thickness observations would be extremely welcomed.

The spatial and temporal extent of the Lake Erie surface ice each winter was estimated based on 41 years of ice charts of the Lake Erie ice cover prepared by CIS and NIC (NIC 2015). The GIS analysis based on these records resulted in 41 years of gridded daily ice-cover information with a roughly 2 km grid cell size. The ice cover distribution of Lake Erie is strongly influenced by the lake bathymetry and the wintertime meteorological conditions, particularly the duration and magnitude of the subfreezing air temperatures and the overall wind direction and speed. The gridded daily ice cover information was used to explore the overall relationship between the maximum ice-cover extent and the maximum AFDD each winter. The variability of the ice cover of the entire lake throughout the winter season and from year to year was described. Finally, maps were presented displaying the earliest, average, and latest dates of the first and last ice each winter for each grid cell and the minimum, average, and maximum duration of ice for each grid cell.

A satellite-based SAR survey of the lake ice cover during the winter of 2014–15 showed a stationary linear feature potentially representing an ice

ridge; it was apparent in each of three overlapping images, suggesting a grounded ice ridge. Satellite-based SAR provides an economical alternative to winter expeditions involving aircraft or ice-breaking ships. However, actually traveling to an ice ridge in Lake Erie opens the possibility for extensive and valuable field measurements. Combined with satellite-based SAR, a field campaign of this nature would rapidly advance our understanding of Lake Erie ice ridges.

There is conclusive evidence that ice ridges form in Lake Erie and that their keels can be 25 m deep or more. Almost all of the evidence is indirect and consists of ice scours in the lake bed created by the keels of ice ridges in contact with the bed. The available lake bed survey information was analyzed to provide water depth information on 210 ice scours. The thickness of the consolidated layers of ice ridges was characterized based on the historical ice cover duration and meteorological conditions. An estimation of the maximum keel depths of the ice ridges in Lake Erie was developed based a relationship between the surface-ice thickness and maximum possible keel depths that have been observed for ocean ice ridges. The relationship was modified to account for the differences in strength between sea ice and the freshwater ice of Lake Erie. The relationship was further tuned by comparing the results to the water depths in which the ice scour depths were observed. The water depths provide information on the approximate depth of the bottom of the ice-ridge keels that created the scours, given that the actual scour indentation into the bed were usually much less than 1 m. Further surveys of the Lake Erie bed could provide information on the distribution of scours throughout the lake and the rate of scour formation.

References

Amundrud, T. L., H. Melling, and R. G. Ingram. 2004. Geometrical Constraints on the Evolution of Ridged Sea Ice. *Journal of Geophysical Research* 109:C06005. doi:10.1029/2003JC002251.

Ashton, G. D., ed. 1986. *River and Lake Ice Engineering*. Highlands Ranch, CO: Water Resources Publications, LLC.

Assel, R. A. 2005.*Great Lakes Ice Cover Climatology Update: Winters 2003, 2004, and 2005*. NOAA Technical Memorandum GLERL-135. Ann Arbor, MI: National Oceanic and Atmospheric Administration, Great Lakes Environmental Research Laboratory. http://www.glerl.noaa.gov/ftp/publications/tech_reports/glerl-135/.

Assel, R. A., D. C. Norton, and K. C. Cronk. 2002. *A Great Lakes Digital Ice Cover Data Base for Winters 1973–2000*. NOAA Technical Memorandum GLERL-121. Ann Arbor, MI: National Oceanic and Atmospheric Administration, Great Lakes Environmental Research Laboratory. http://www.glerl.noaa.gov/ftp/publications/tech_reports/glerl-121/tm-121.pdf.

Barnes, P. W., and R. Lien. 1988. Icebergs Rework Shelf Sediments to 500 m off Antarctica. *Geology* 16 (12): 1130–1133.

Burden, R. P., and G. W. Timco. 1995. *A Catalogue of Ice Ridges*. Technical Report TR-1995-27. Ontario, Canada: National Research Council Canada.

Carslaw, H. S., and J. C. Jaeger. 1959. *Conduction of Heat in Solids*. 2nd ed. New York, NY: Oxford University Press.

C-CORE. 1999. *Lake Erie Ice Scour/Pipeline Design, Final Report*. C-CORE Publication 98-C34-Final. Newfoundland, Canada: C-CORE.

Crank, J. 1984. *Free and Moving Boundary Problems*. Oxford, UK: Clarendon Press.

Daly, S. F. 1998. Thermal Ice Growth: Real-Time Estimation. *Journal of Cold Regions Engineering* 12 (1): 11–28.

Dierking, W., and J. Dall. 2007. Sea-Ice Deformation State from Synthetic Aperture Radar Imagery—Part I: Comparison of C- and L-Band and Different Polarization. *IEEE Transactions on Geoscience and Remote Sensing* 45 (11): 3610–3623.

Dierking, W., T. Busche, C. V. Saldern, J. Hartmann, C. Haas, C. Lüpkes, I. Hajnsek, R. Scheiber, R. Horn, J. Fischer, J. Dall. 2006. Sea Ice Deformation Mapping by Means of SAR. In *EUSAR 2006, 6th European Conference on Synthetic Aperture Radar, 16–18 May, Dresden, Germany*.

Eden, D. J., and N. Eyles. 2001. Description and Numerical Model of Pleistocene Iceberg Scours and Ice-Keel Turbated Facies at Toronto, Canada. *Sedimentology* 48:1079–1102.

Fortt, A. L., and E. M. Schulson. 2011. Frictional Sliding Across Coulombic Faults in First-Year Sea Ice: A Comparison with Freshwater Ice. *Journal of Geophysical Research* 116:C11012. doi:10.1029/2011JC006969.

Grass, J. D. 1983. Ice Scour and Ice Ridging Studies in Lake Erie. In *Proceedings of the International Association for Hydrological Research, Ice Symposium, Hamburg, Germany*, 33–43.

Hibler, W. D., III. 1980. Modelling a Variable Thickness Sea Ice Cover. *Monthly Weather Review* 108:1943–1973.

Hopkins, M. A. 1998. Four Stages of Pressure Ridging. *Journal of Geophysical Research* 103 (C10): 21,883–21,891.

Hoyland, K. V. 2002a. Consolidation of First-Year Sea Ice Ridges. *Journal of Geophysical Research* 107 (C6): 3062. doi:10.1029/2000JC000526.

———. 2002b. Simulations of the Consolidation Process in First-Year Sea Ice Ridges. *Cold Regions Science and Technology* 34 (2002): 143–158.

Kankaanpaa. P. 1988. Morphology of a Baltic Sea Ice Pressure Ridge. *Geophysica* 24 (1–2): 15–33.

———. P. 1989. Structure of First Year Pressure Ridges in the Baltic Sea. In *POAC '89: The 10th Port and Ocean Engineering under Arctic Conditions, 12–16 June, Lulea, Sweden*, vol. 1. Lulea, Sweden: Lulea University of Technology.

Kennedy, F. E., E. M. Schulson, and D. E. Jones. 2000. The Friction of Ice on Ice at Low Sliding Velocities. *Philosophical Magazine A* 80 (5): 1093–1110.

Kovacs, A., and D. S. Sodhi. 1980. Shore Ice Pile-Up and Ride Up: Field Observations, Models, Theoretical Analyses. *Cold Regions Science and Technology* 2:209–288.

Lepparanta, M., and R. Hakala. 1992. The Structure and Strength of First-Year Ice Ridges in the Baltic Sea. *Cold Regions Science and Technology* 20 (3): 295–311.

Leshkevich, A., and S. V. Nghiem. 2013. Great Lakes Ice Classification Using Satellite C-Band SAR Multi-Polarization Data. *Journal of Great Lakes Research Supplement* 39 (2013): 55–64.

Lever, J. H., ed. 2000. *Assessment of Millennium Pipeline Project Lake Erie Crossing: Ice Scour, Sediment Sampling, and Turbidity Modeling*. ERDC/CRREL TR-00-13. Hanover, NH: U.S Army Engineering Research and Development Center.

Marchenko, A. V. 2008. Thermodynamic Consolidation and Melting of Sea Ice Ridges. *Cold Regions Science and Technology* 52 (3): 278–301.

Melling, H. 1998. Detection of Features in First-Year Pack Ice by Synthetic Aperture Radar (SAR). *International Journal of Remote Sensing* 19 (6): 1223–1249.

Melling, H., and D. A. Riedel. 1996. Development of Seasonal Pack Ice in the Beaufort Sea During the Winter of 1991–1992: A View From Below. *Journal of Geophysical Research* 101:11975–11992.

NIC (U.S. National Ice Center). 2015. NIC Products. U.S. National Ice Center, Naval Ice Center. http://www.natice.noaa.gov/Main_Products.htm.

NOAA. 2015. *Global Summary of the Day Data*. Data from 1950 to 2015. Asheville, North Carolina: National Climatic Data Center. http://www.ncdc.noaa.gov/oa/climate/climatedata.html

NRCS (National Resources Conservation Service). 2015. Wind Rose Data. National Resources Conservation Service, National Water and Climate Center. http://www.wcc.nrcs.usda.gov/climate/windrose.html.

Palmer, A., and K. Croasdale. 2013. *Arctic Offshore Engineering*. Hackensack, NJ: World Scientific Publishing Co.

Shestov, A. S., A. V. Marchenko. 2014. Thermodynamic Consolidation of Ice Ridge Keels in Water at Varying Freezing Points. *Cold Regions Science and Technology* 121:1–10. doi:10.1016/j.coldregions.2015.09.015.

Sleator, F. E. 1978. *Ice Thickness and Stratigraphy at Nearshore Locations on the Great Lakes (English Units)*. NOAA Data Report ERL GLERL-1-1. Ann Arbor, MI: National Oceanic and Atmospheric Administration, Great Lakes Environmental Research Laboratory. http://www.glerl.noaa.gov/ftp/publications/tech_reports/glerl-001/.

———. 1995. *GLERL Great Lakes Ice Thickness Data Base, 1966–1979, Version 1. Lake Erie*. Boulder, CO: National Snow and Ice Data Center. http://dx.doi.org/10.7265/N5KW5CXG.

Stefan, J. 1891. Über die Theorie der Eisbildung, insbesondere Über die Eisbildung im Polarmeere. Annalen der Physik 278:269–286. doi:10.1002/andp.18912780206.

Timco, G. W., and R. P. Burden. 1997. An Analysis of the Shapes of Sea Ice Ridges. *Cold Regions Science and Technology* 25:65–77.

Timco, G. W., and R. M. W. Frederking. 1982. Comparative Strengths of Freshwater Ice. *Cold Regions Science and Technology* 6:21–27

———. 1996. A Review of Sea Ice Density. *Cold Regions Science and Technology* 24:1-6.

Timco, G. W., and S. O'Brien. 1994. Flexural Strength Equation for Sea Ice. *Cold Regions Science and Technology* 22:285–298.

Timco, G. W., and W. F. Weeks. 2010. A Review of the Engineering Properties of Sea Ice. *Cold Regions Science and Technology* 60:107–129.

Timco, G. W., K. Croasdale, and B. Wright. 2000. *An Overview of First-Year Sea Ice Ridges*. Technical Report HYD-TR-047. Ontario, Canada: National Research Council Canada.

Tucker, W. B., III, D. S. Sodhi, and J. W. Govoni. 1984. Structure of First Year Pressure Ridge Sails in the Prudhoe Bay Region. *The Alaskan Beaufort Sea: Ecosystems and Environment*, ed. P. W. Barnes, D. M. Shell, and E. Reimnitz, 115–135. San Diego, CA: Academic Press.

USACE (U.S. Army Corps of Engineers). 2006. *Ice Engineering*. EM 1110-2-1612. http://www.usace.army.mil/publications/eng-manuals/em1110-2-1612/toc.htm.

———. 2010. *HEC-SSP Statistical Software Package, User's Manual, Version 2.0*. CPD-86. Davis, CA: Hydrologic Engineering Center.

USGS (U.S. Geological Survey). *Guidelines for Determining Flood Flow Frequency*. Bulletin #17B of the Hydrology Subcommittee. Reston, VA: Office of Water Data Coordination, Interagency Advisory Committee on Water Data.

Wang, J., R. A. Assel, S. Walterscheid, A. H. Clites, and X. Bai. 2012. *Great Lakes Ice Climatology Update: Winter 2006–2011: Description of the Digital Ice Cover Dataset*. NOAA Technical Memorandum GLERL-155. Ann Arbor, MI: National Oceanic and Atmospheric Administration, Great Lakes Environmental Research Laboratory. http://www.glerl.noaa.gov/ftp/publications/tech_reports/glerl-155/tm-155.pdf.

Weeks, W. F., P. W. Barnes, D. M. Rearic, and E. Reimnitz. 1983. *Statistical Aspects of Ice Gouging on the Alaskan Shelf of the Beaufort Sea*. CRREL Report 83-21. Hanover, NH: Cold Regions Research and Engineering Laboratory.

Appendix A: Extreme-Value Analysis of Annual Maximum AFDD by Station

Figure A-1. General frequency analytical plot for CUSTER.

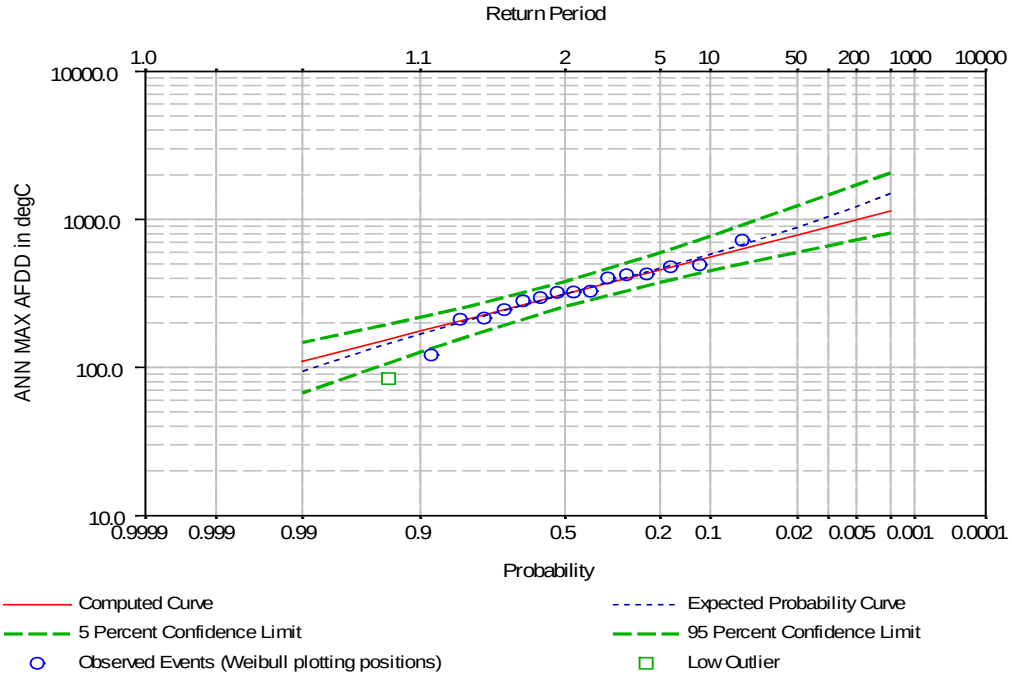

Figure A-2. General frequency analytical plot for DETROIT CITY.

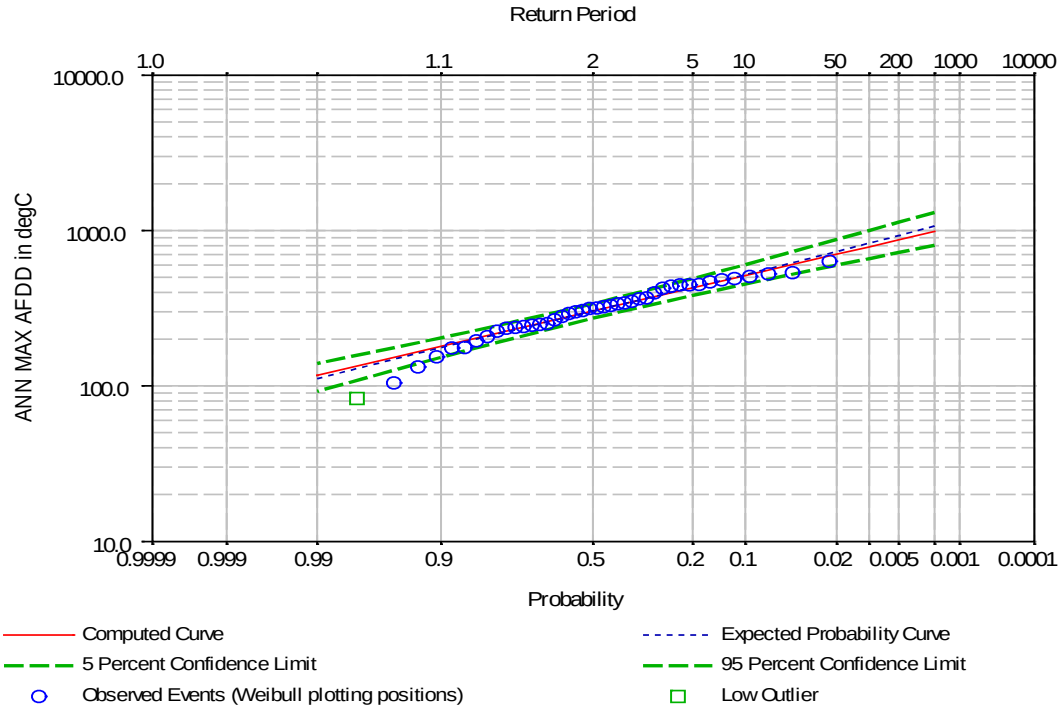

Figure A-3. General frequency analytical plot for DETROIT METROPOLITAN.

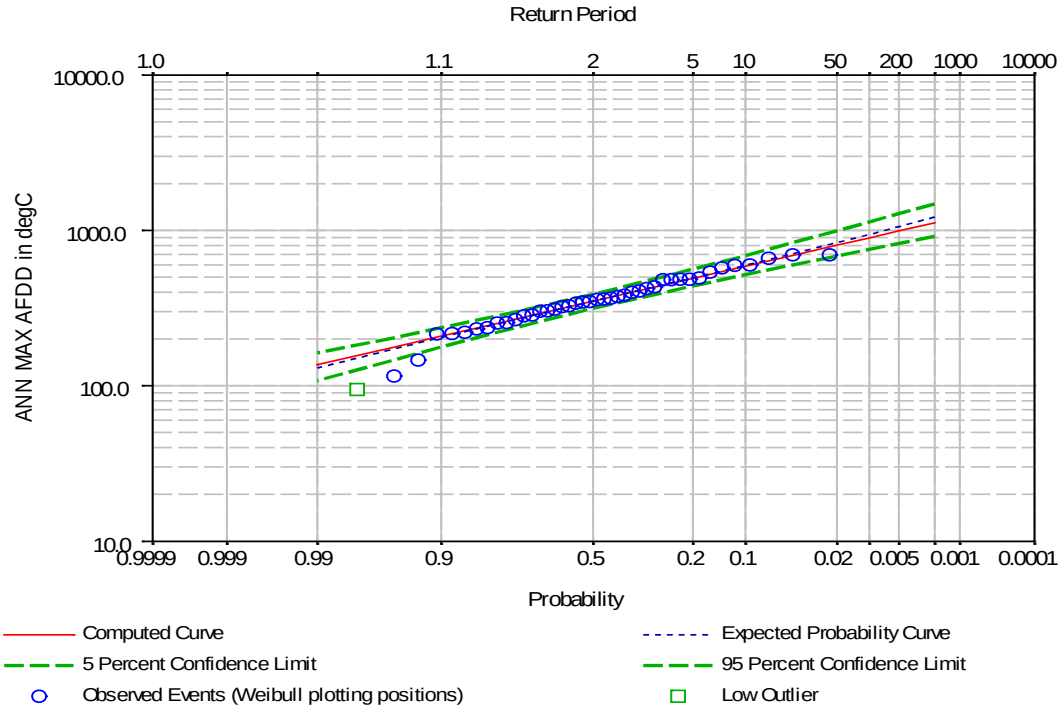

Figure A-4. General frequency analytical plot for GROSSE ISLE MUNI.

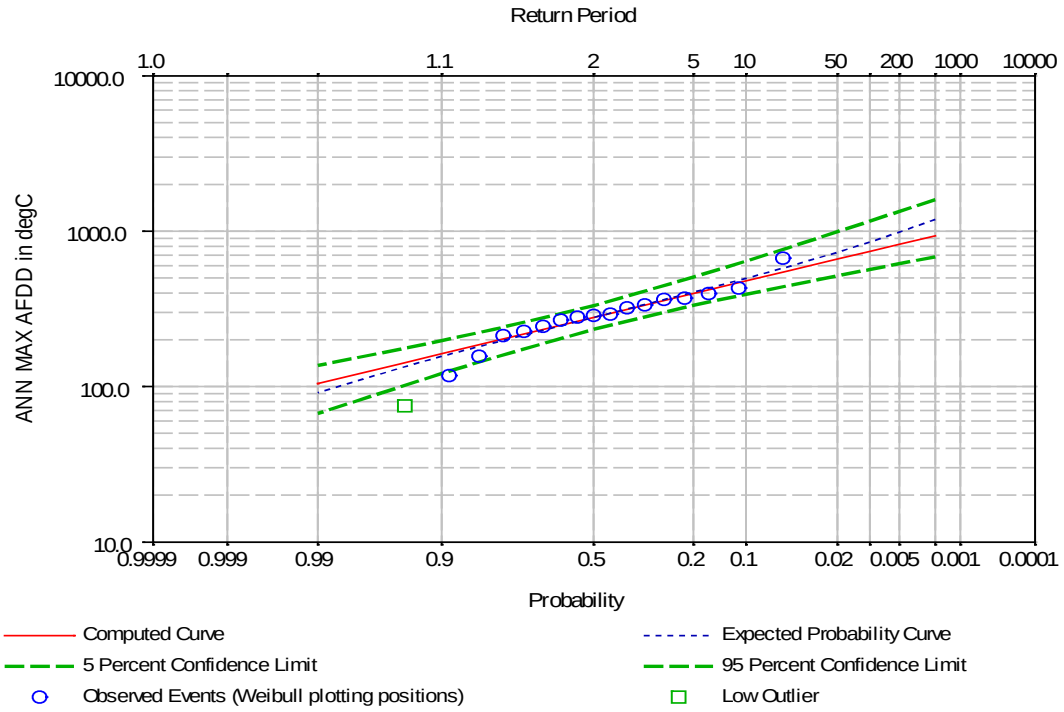

Figure A-5. General frequency analytical plot for OAKLAND CO INTL.

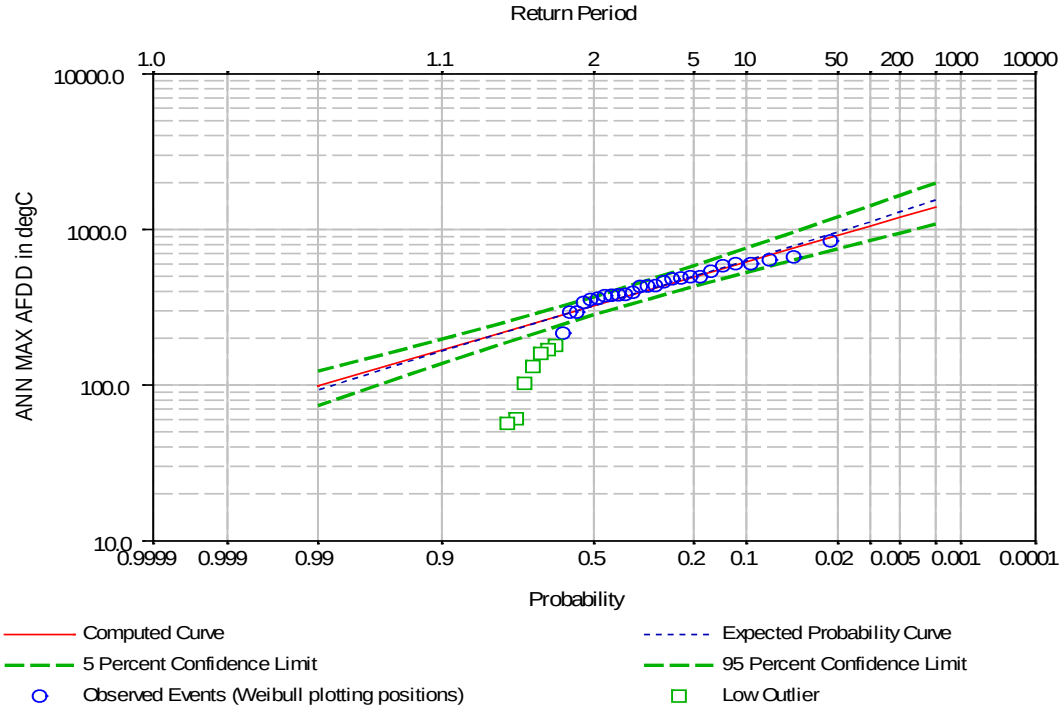

Figure A-6. General frequency analytical plot for SELFRIDGE ANGB.

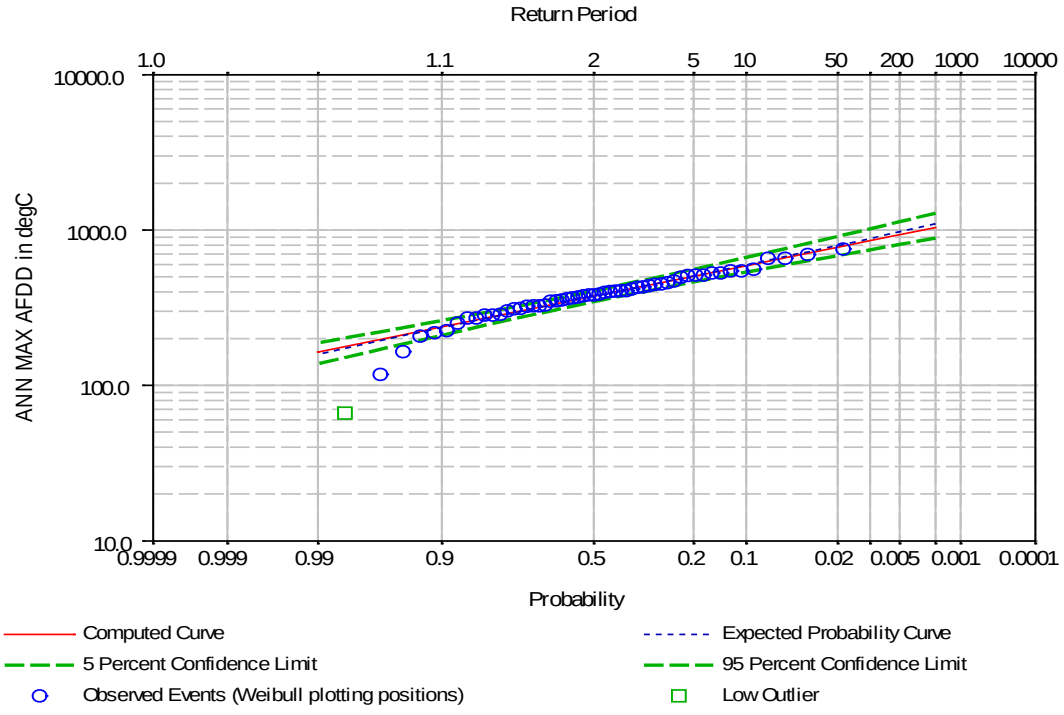

Figure A-7. General frequency analytical plot for WILLOW RUN.

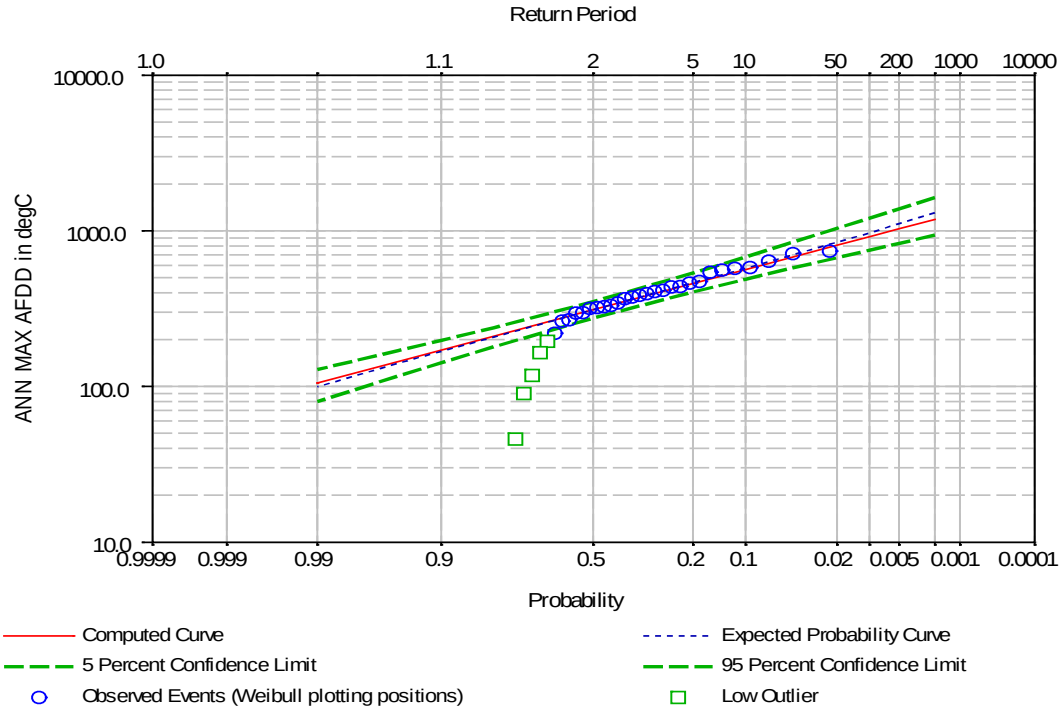

Figure A-8. General frequency analytical plot for CHAUTAUQUA CO DUNKIR.

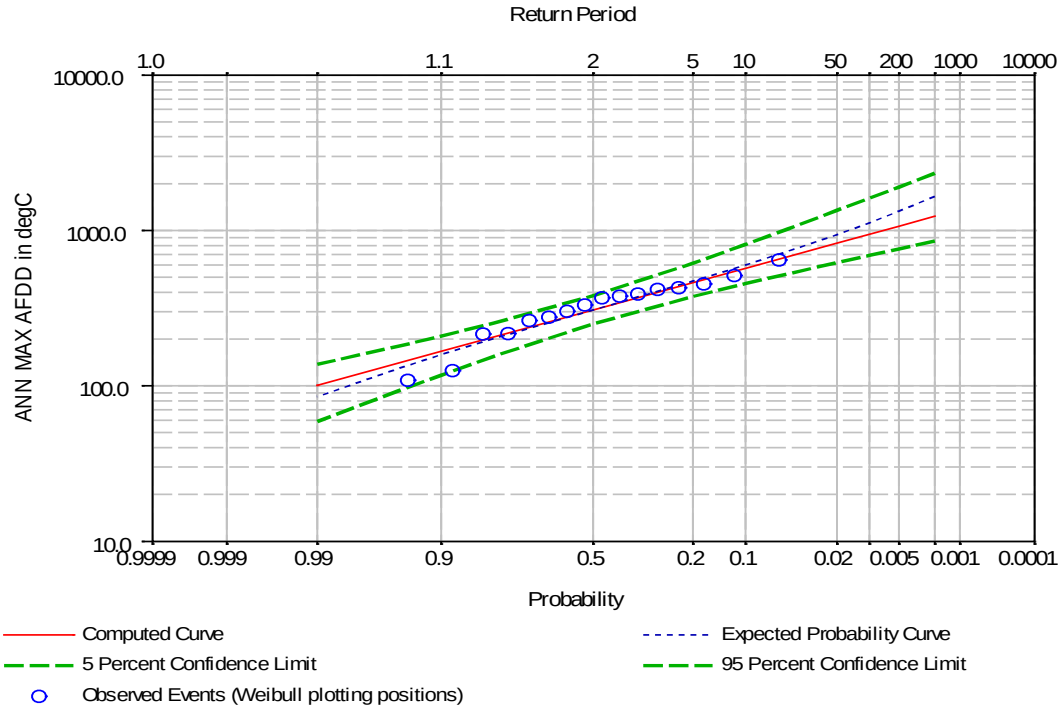

Figure A-9. General frequency analytical plot for DUNKIRK.

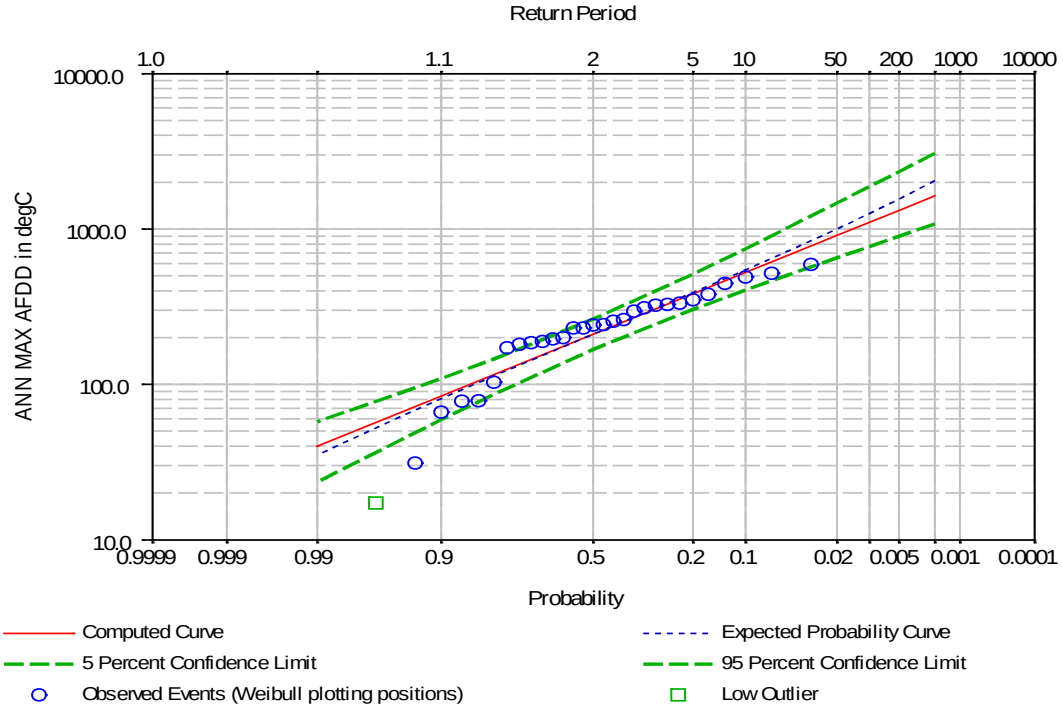

Figure A-10. General frequency analytical plot for GREATER BUFFALO INT.

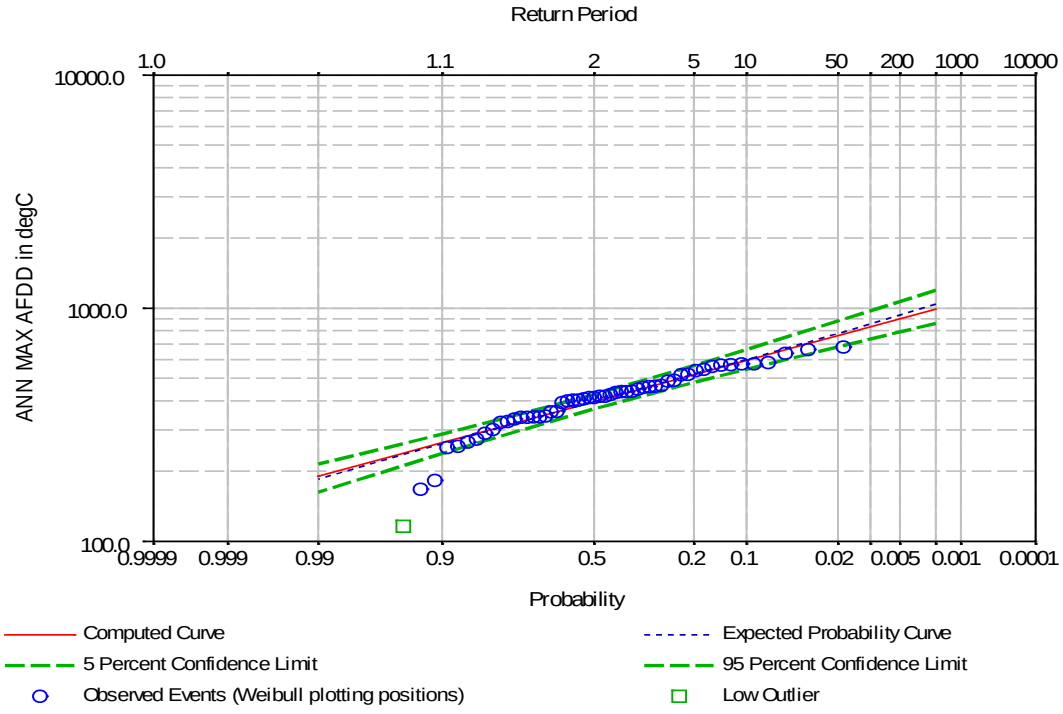

Figure A-11. General frequency analytical plot for AKRON.

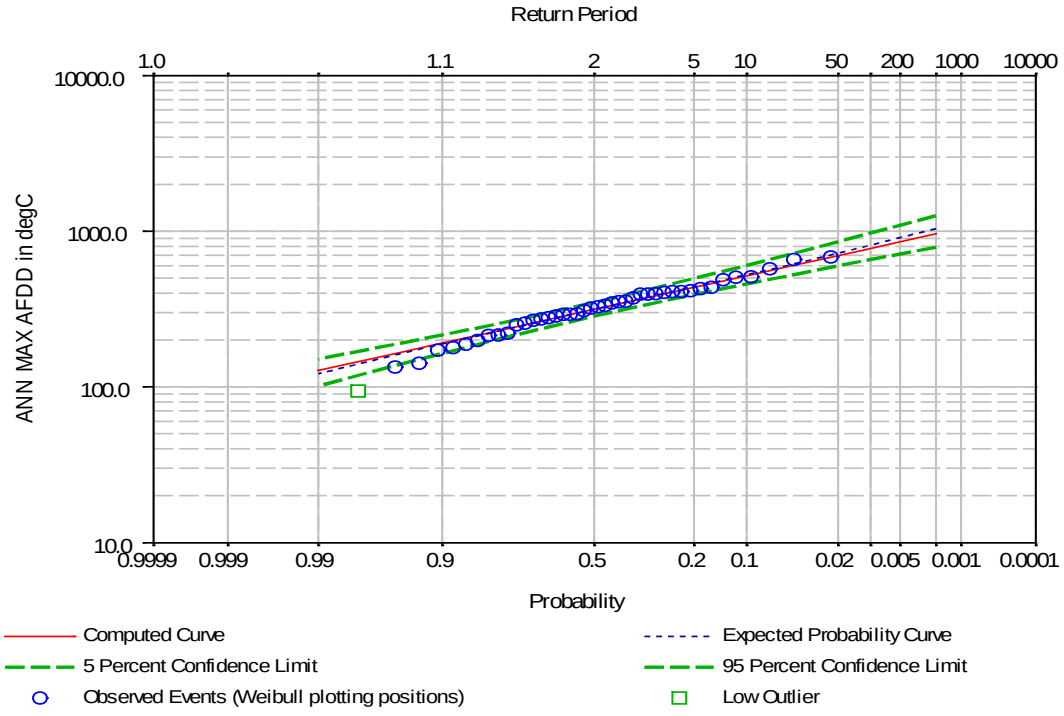

Figure A-12. General frequency analytical plot for AKRON FULTON INTL.

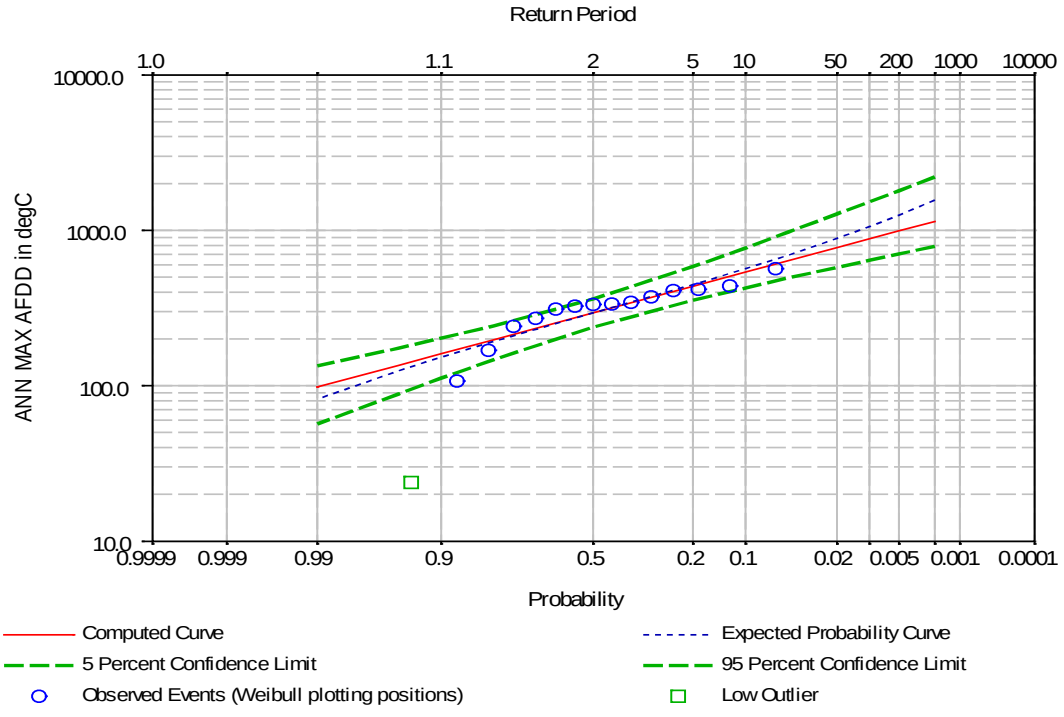

Figure A-13. General frequency analytical plot for CLEVELAND.

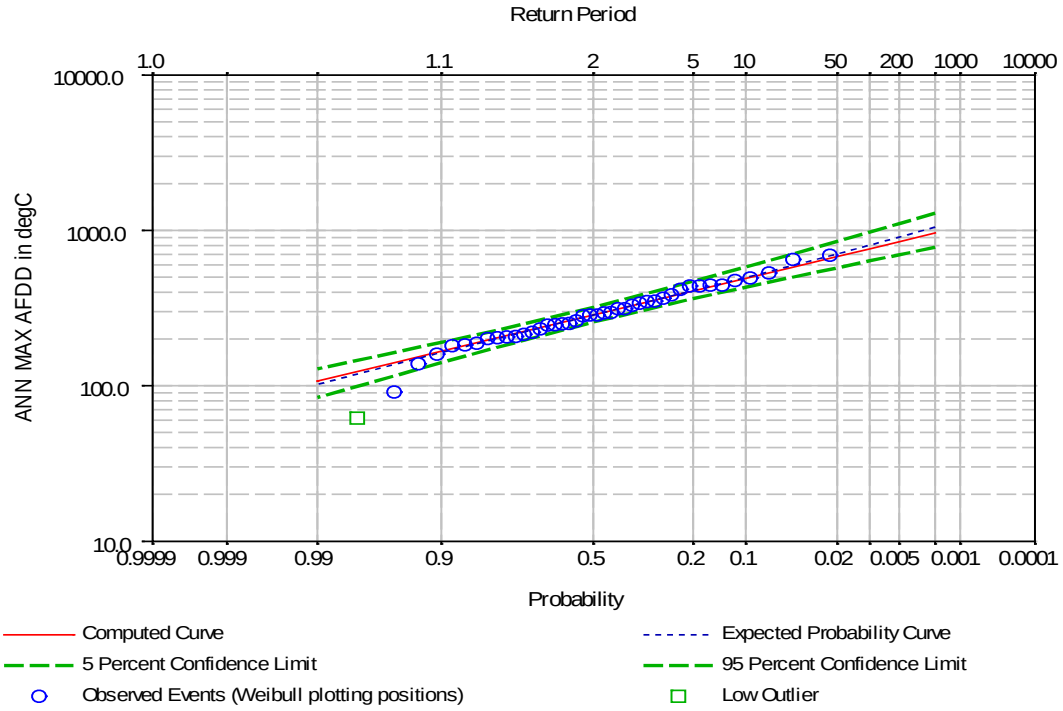

Figure A-14. General frequency analytical plot for SOUTH BASS ISLAND.

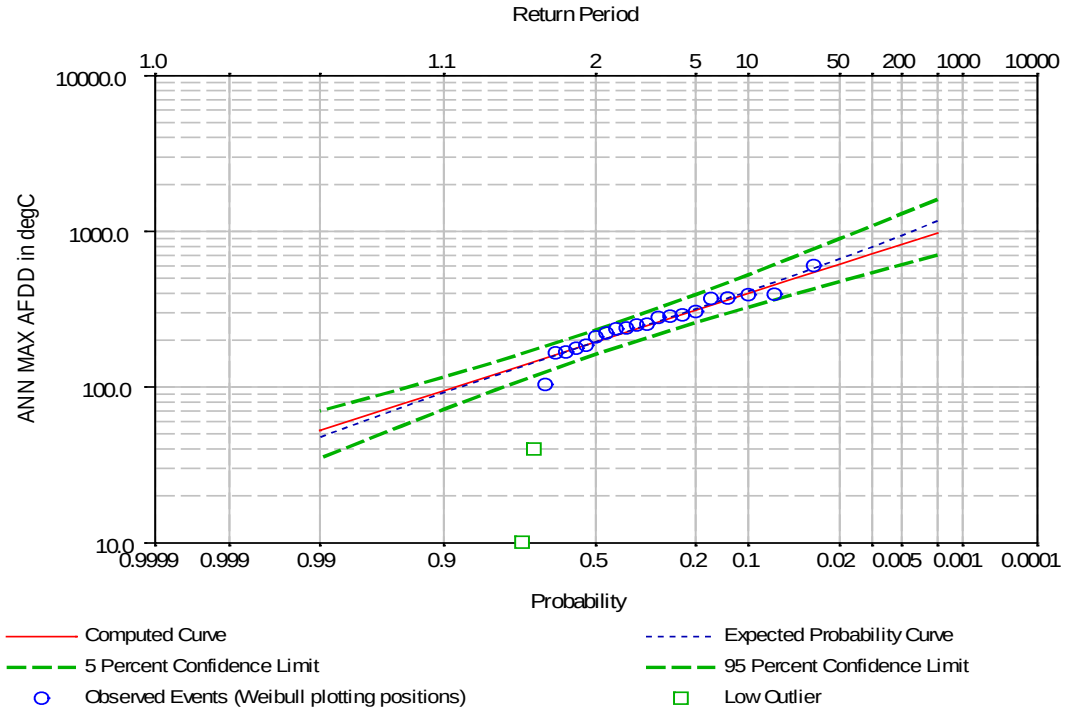

Figure A-15. General frequency analytical plot for TOLEDO EXPRESS.

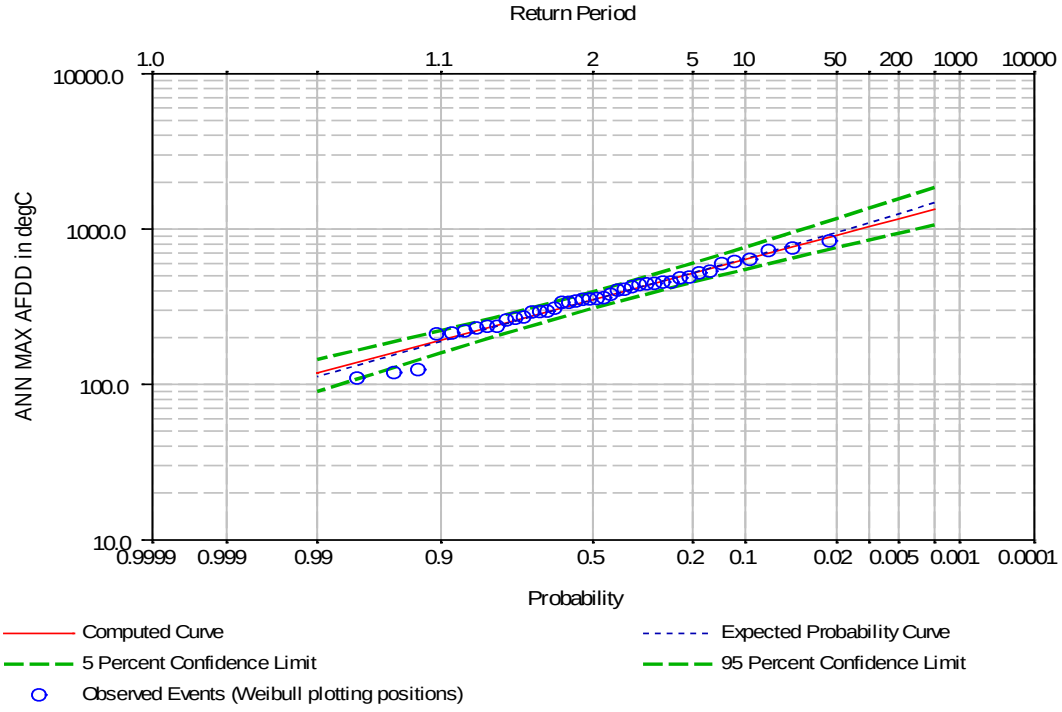

Figure A-16. General frequency analytical plot for YOUNGSTOWN MUNI.

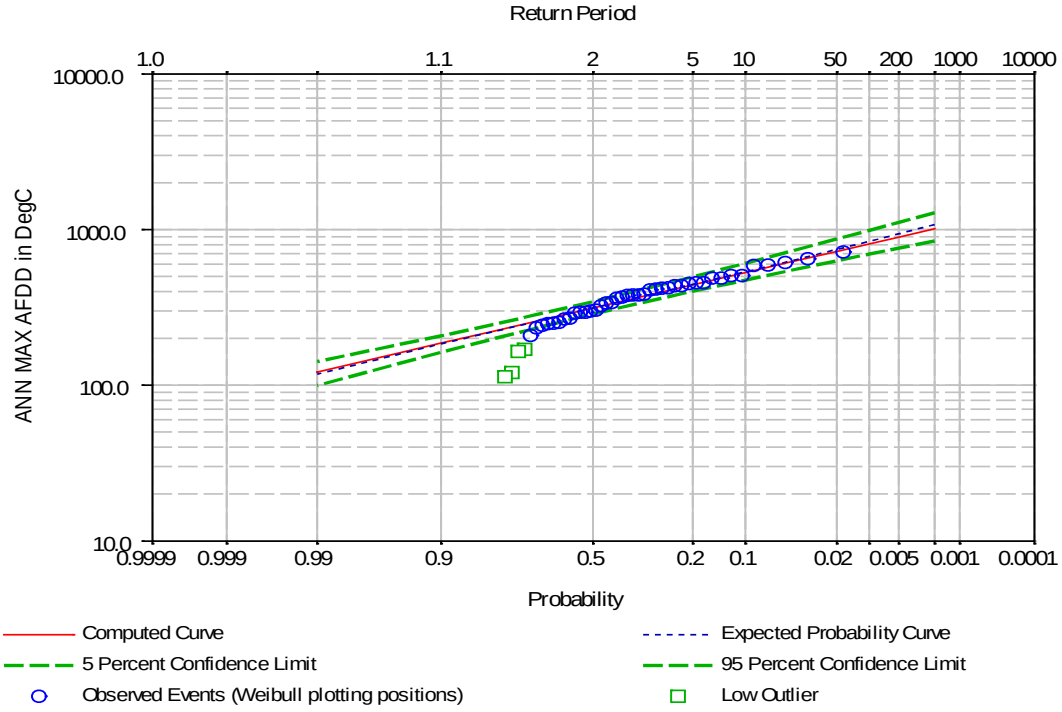

Figure A-17. General frequency analytical plot for HAMILTON AIRPORT.

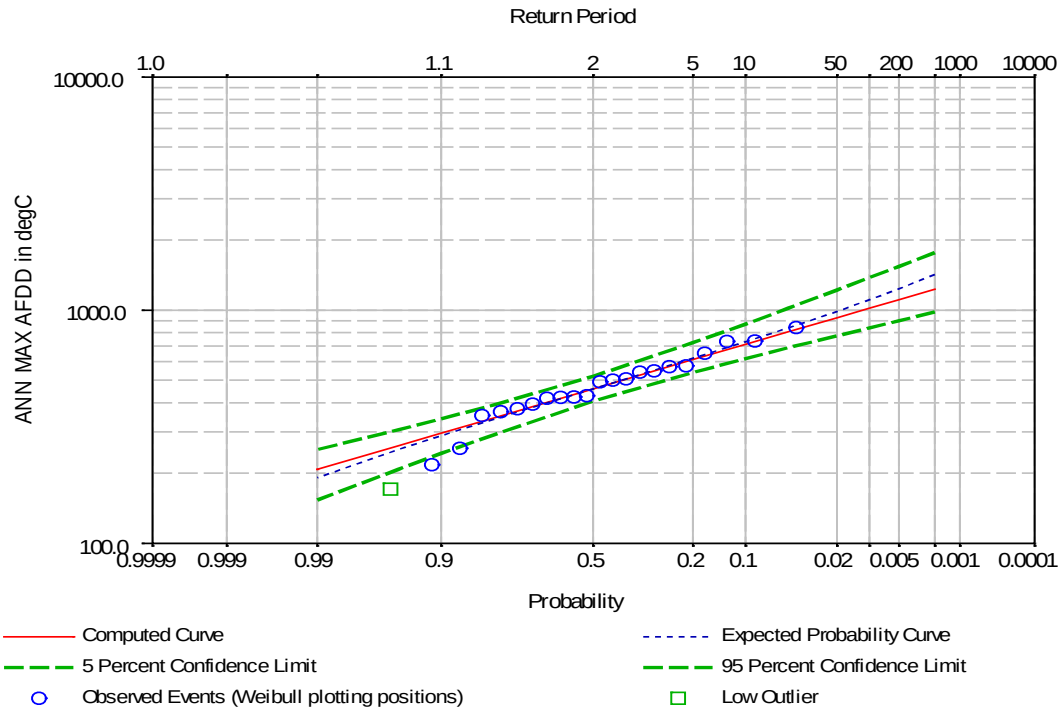

Figure A-18. General frequency analytical plot for HAMILTON RBG CS.

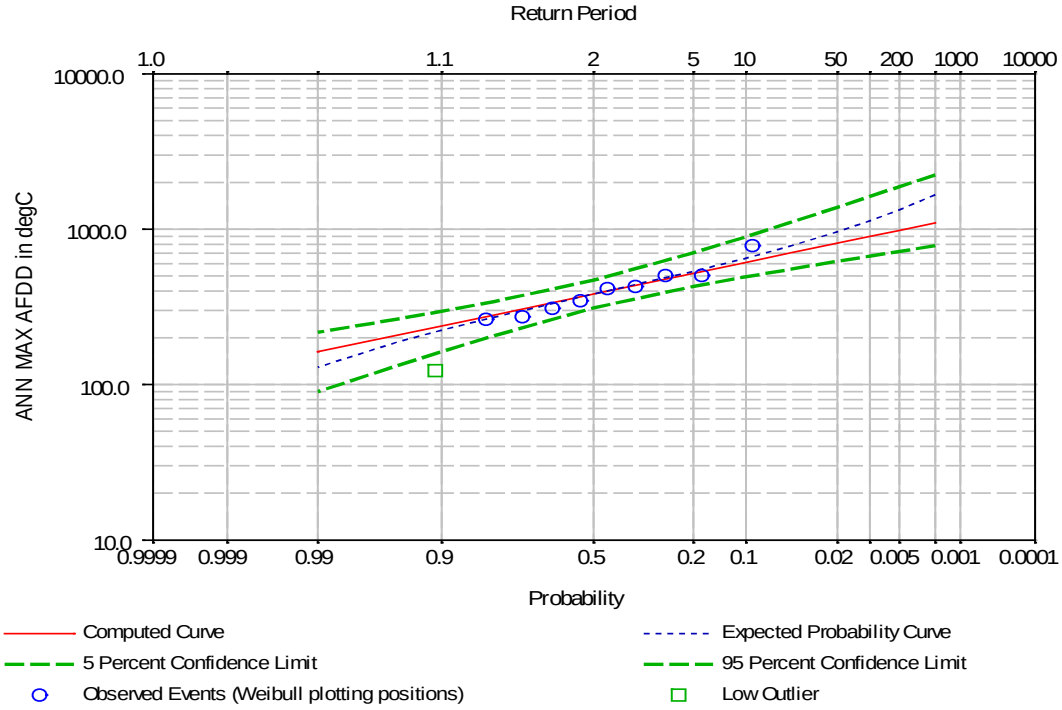

Figure A-19. General frequency analytical plot for KITCHNER WATERLOO.

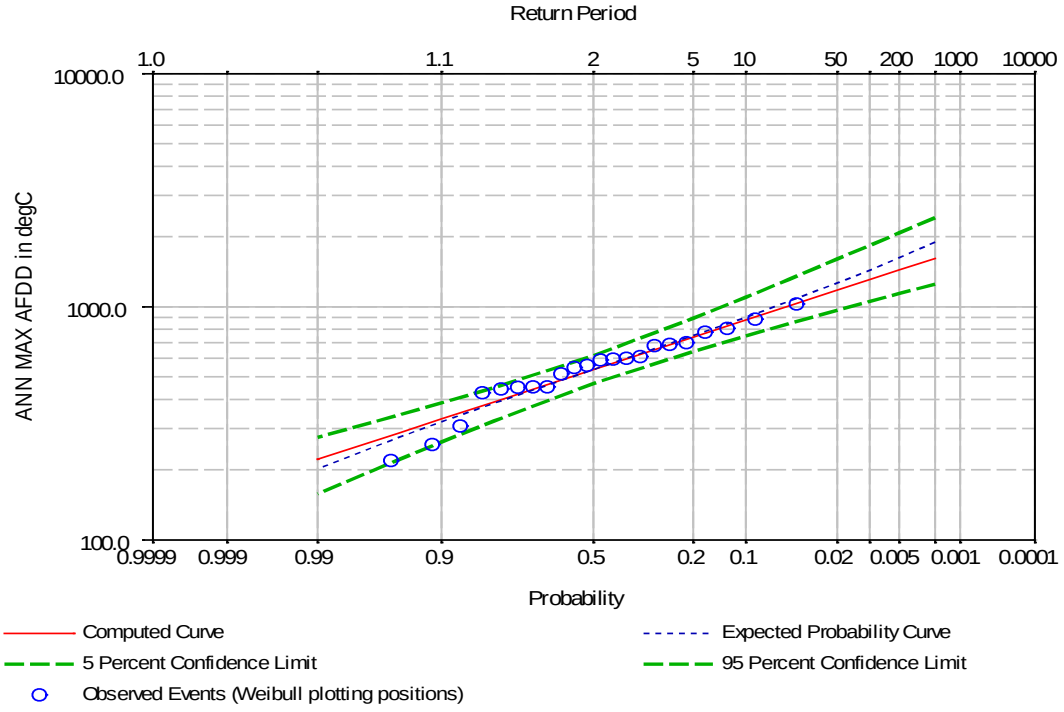

Figure A-20. General frequency analytical plot for NIAGARA DISTRICT.

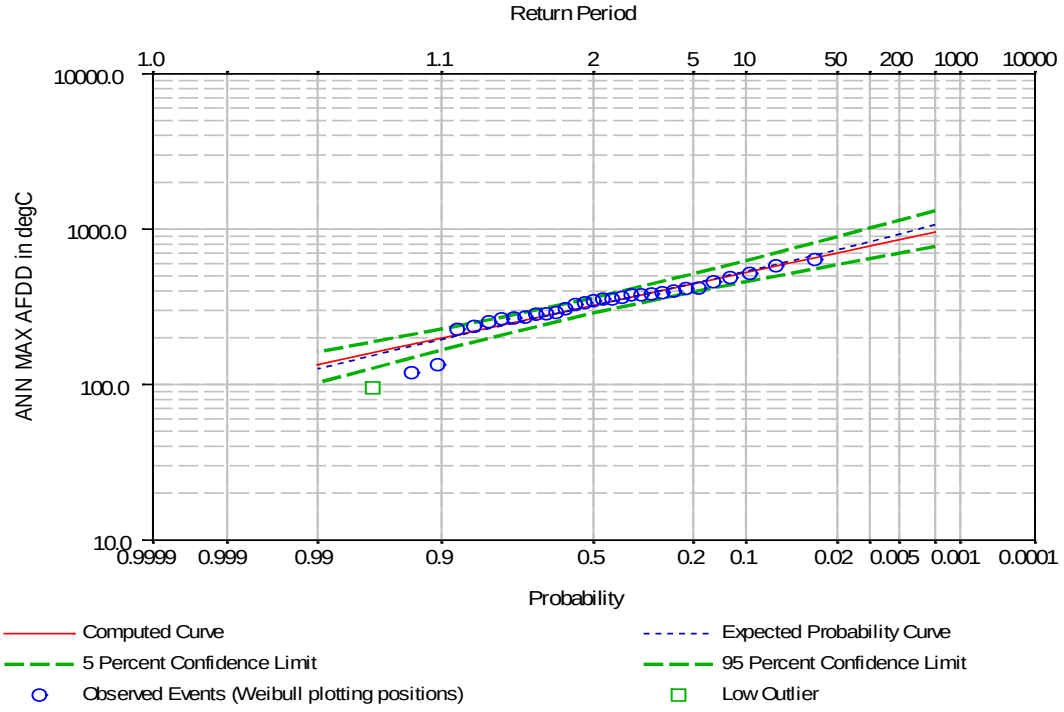

Figure A-21. General frequency analytical plot for ERIE INTL AIRPORT.

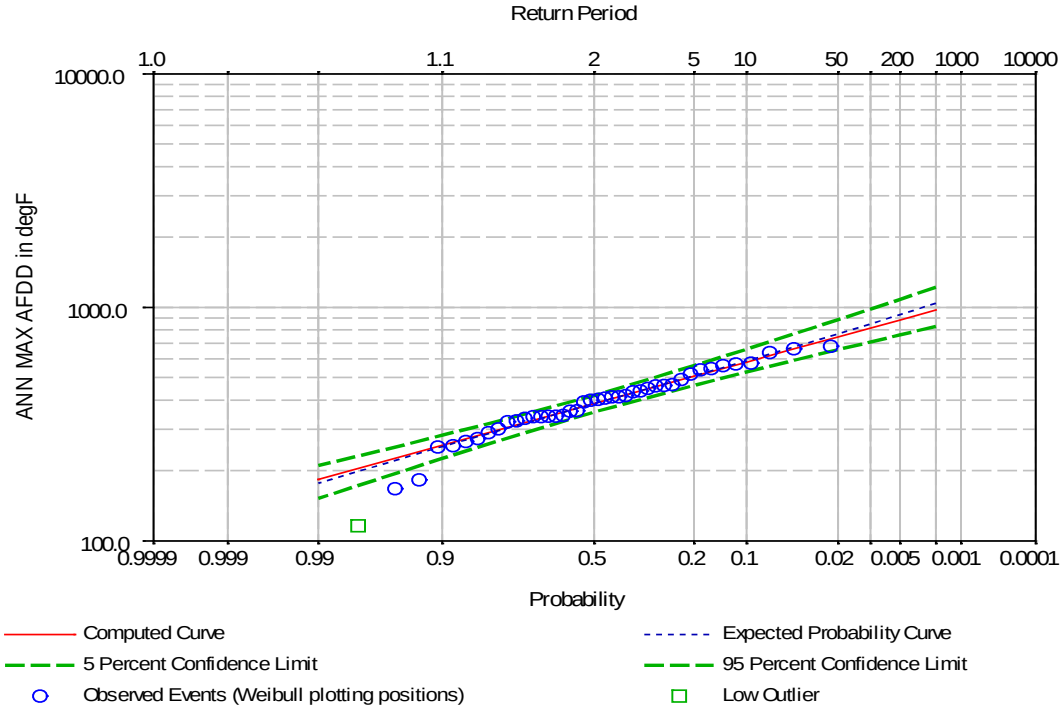

REPORT DOCUMENTATION PAGE

Form Approved
OMB No. 0704-0188

1. REPORT DATE *(DD-MM-YYYY)*	**2. REPORT TYPE**	**3. DATES COVERED** *(From - To)*
April 2016	Technical Report/Final	

4. TITLE AND SUBTITLE

Characterization of the Lake Erie Ice Cover

5a. CONTRACT NUMBER

5b. GRANT NUMBER

5c. PROGRAM ELEMENT NUMBER

6. AUTHOR(S)

Steven F. Daly

5d. PROJECT NUMBER

5e. TASK NUMBER

5f. WORK UNIT NUMBER

7. PERFORMING ORGANIZATION NAME(S) AND ADDRESS(ES)

U.S. Army Engineer Research and Development Center (ERDC)
Cold Regions Research and Engineering Laboratory (CRREL)
72 Lyme Road
Hanover, NH 03755-1290

8. PERFORMING ORGANIZATION REPORT NUMBER

ERDC/CRREL TR-16-5

9. SPONSORING / MONITORING AGENCY NAME(S) AND ADDRESS(ES)

Lake Erie Energy Development Corporation (LEEDCo)
Cleveland, OH

10. SPONSOR/MONITOR'S ACRONYM(S)

LEEDCo

11. SPONSOR/MONITOR'S REPORT NUMBER(S)

12. DISTRIBUTION / AVAILABILITY STATEMENT

Approved for public release; distribution is unlimited.

13. SUPPLEMENTARY NOTES

14. ABSTRACT

The developing offshore wind energy industry in Northern Ohio is looking to place wind turbines in Lake Erie. The floating lake ice that forms in Lake Erie each winter is a very important consideration for the design of the wind-turbine towers and for the foundations sited in the lake.

This report uses historical meteorological and surface-ice thickness observations, 41 years of ice chart information, and lake-bed surveys of ice scours to estimate the characteristics of the Lake Erie ice cover important to the design of offshore wind-turbine towers. These characteristics include the expected thickness of the ice cover due to thermal growth, the historical spatial and temporal distribution of the ice cover throughout the winter season; and the estimated consolidated layer thickness and maximum keel depths of ice ridges formed in the lake. The report also describes the results of an innovative satellite-based synthetic aperture radar survey that included multi-temporal acquisitions of the lake ice cover during the winter of 2014–15. A stationary linear feature was evident in a time series of three spatially overlapping images, suggesting a grounded ice ridge. At that time of this publication, this is the first satellite-based evidence of ice ridges in Lake Erie.

15. SUBJECT TERMS

Ice cover
Ice on rivers, lakes, etc.
Ice ridges
Lake Erie
Meteorology
Offshore wind farms
Remote sensing
Wind turbines

16. SECURITY CLASSIFICATION OF:			**17. LIMITATION OF ABSTRACT**	**18. NUMBER OF PAGES**	**19a. NAME OF RESPONSIBLE PERSON**
a. REPORT	**b. ABSTRACT**	**c. THIS PAGE**			**19b. TELEPHONE NUMBER** *(include area code)*
Unclassified	Unclassified	Unclassified	SAR	100	